ESC-TR-2005-055

Technical Report
TR-1101

Capon and Bartlett Beamforming: Threshold Effect in Direction-of-Arrival Estimation Error and On the Probability of Resolution

C.D. Richmond

16 May 2005

Lincoln Laboratory
MASSACHUSETTS INSTITUTE OF TECHNOLOGY
LEXINGTON, MASSACHUSETTS

Prepared for the Defense Advanced Research Projects Agency under Air Force Contract F19628-00-C-0002.

This report is based on studies performed at Lincoln Laboratory, a center for research operated by Massachusetts Institute of Technology. This work was sponsored by the Defense Advanced Research Projects Agency, ATO, under Air Force Contract F19628-00-C-0002.

The ESC Public Affairs Office has reviewed this report, and it is releasable to the National Technical Information Service, where it will be available to the general public, including foreign nationals.

This technical report has been reviewed and is approved for publication.

FOR THE COMMANDER

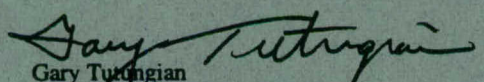

Gary Tutungian
Administrative Contracting Officer
Plans and Programs Directorate
Contracted Support Management

Massachusetts Institute of Technology
Lincoln Laboratory

Capon and Bartlett Beamforming: Threshold Effect in Direction-of-Arrival Estimation Error and On the Probability of Resolution

C.D. Richmond
Group 103

Technical Report 1101

16 May 2005

Lexington Massachusetts

ABSTRACT

Below a specific threshold signal-to-noise ratio (SNR), the mean squared error (MSE) performance of signal direction-of-arrival (DOA) estimates derived from the Capon algorithm degrades swiftly. Prediction of this threshold SNR point is of practical significance for robust system design and analysis. The exact pairwise error probabilities for the Capon (and Bartlett) algorithm are derived herein, given by simple finite sums involving no numerical integration, include finite sample effects, and hold for an arbitrary colored data covariance. An accurate large sample approximation of these error probabilities in terms of the well tabulated complementary error function is also provided. Via an adaptation of an interval error-based method, these error probabilities, along with the local error MSE predictions of Vaidyanathan and Buckley, facilitate accurate prediction of the Capon threshold region DOA MSE performance for an arbitrary number of well separated sources, circumventing the need for numerous Monte Carlo simulations. A large sample closed form approximation for the Capon (and Bartlett) threshold SNR is provided for uniform linear arrays. A new exact two-point measure of the Capon probability of resolution, that includes the deleterious effects of signal model mismatch, is a serendipitous by-product of this analysis that predicts the SNRs required for closely spaced sources to be mutually resolvable by the Capon algorithm. Lastly, a new general strategy is provided for obtaining accurate MSE predictions that account for signal model mismatch.

ACKNOWLEDGMENTS

My thanks to Dr. Wen Xu, Prof. Arthur B. Baggeroer, Prof. Kristine Bell, and Prof. Donald Tufts for initiating my interest in the general area of threshold region mean squared error analysis of nonlinear parameter estimation. Consideration of the class of adaptive estimation problems including maximum-likelihood estimation and the Capon algorithm that find routine use in space-time adaptive processing application areas such as radar and sonar proved a fruitful venture. While a wealth of literature presently exists in the area of adaptive detection performance analysis, the area of adaptive estimation performance analysis has been less explored.

Thanks to Dr. Allan O. Steinhardt, Prof. Donald Tufts, Dr. Harry Cox, and anonymous reviewers for their insightful feedback that has improved the presentation of this material. A thanks to Dr. Jim Ward for support and encouraging documentation in the form of a technical report, and Dr. Nigel Lee for providing useful feedback.

TABLE OF CONTENTS

LIST OF ILLUSTRATIONS

1. INTRODUCTION

The threshold region mean squared error (MSE) performance of angle estimates derived from the Capon algorithm, *a.k.a* the minimum variance distortionless response (MVDR) spectral estimator, is the primary subject of this report. The classical Bartlett algorithm wherein an angle estimate is obtained via a smoothed *periodogram* is a closely related approach whose analysis shall be developed in parallel. The Capon algorithm can be described as a *high-resolution*, data adaptive, nonparametric approach to direction of arrival (DOA) estimation [15, 17, 18, 33, 29, 11, 52, 61], whereas the Bartlett algorithm is a classical, nonparametric, conventional beamforming approach [6, 7, 14, 29, 52]. The parallel development given herein is motivated by the similarities involved in the analysis as well as the contrast provided by use of conventional beamforming performance as a reference point for super-resolution approaches. The angle estimates are obtained as the arguments of the largest peaks of an estimated power spectrum over spatial frequency or angle. Similar to maximum-likelihood (ML) estimation, the Capon and Bartlett algorithms are beamscan type algorithms involving a nonlinear search of a data dependent objective search function (OSF). Parameter estimates derived from nonlinear searches often exhibit a *threshold effect* in MSE performance [66, 59, 43, 65]. Below a specific signal-to-noise ratio (SNR) called the estimation threshold point, the MSE departs from an often well-behaved (inversely proportional to SNR) asymptotic MSE performance and rises rapidly. It rises until it reaches a maximum that at times can be well approximated by the worst case variance, *i.e.*, that of an estimate that is uniformly distributed over the angle search domain. The SNR at which the MSE performance achieves this level of futility is called the no information point. Figure 1 illustrates this composite MSE performance typical of nonlinear estimation schemes. Three distinct regions of MSE performance are evident: no information (as SNR$\rightarrow$ 0), threshold (or ambiguity), and asymptotic (as SNR$\rightarrow \infty$). The departure of the MSE curve from the asymptotic performance as the SNR decreases below the threshold point is due to *global errors* caused by the presence of false peaks (sidelobes) in the underlying ambiguity function[1]. Each scan over the angle search domain of interest of the OSF produces a realization of a stochastic process whose statistical behavior ultimately determines the accuracy of the angle estimates. The ambiguity function has a strong influence on the character and nature of this non-Gaussian, nonstationary stochastic process, especially in the vicinity of the threshold region. The composite MSE behavior shown in Figure 1 is typical of nonlinear ML estimation [59, 60], but likewise occurs with the Capon and Bartlett DOA estimators. Although the threshold effect of the Capon algorithm has been observed in practice [61], accurate prediction of the composite MSE performance curve is an open problem. Because the Capon algorithm is a high-resolution approach, significant beamsplit ratios (BSR) are possible in the threshold region, making its performance prediction in this region of practical interest. The goal of this analysis is to provide accurate prediction of the threshold SNR point for angle estimates derived from the Capon algorithm, as well as prediction of the threshold region of the MSE curve, accounting for finite sample effects [16, 35], and colored noise. Signal model mismatch is known to be a formidable practicality to realizing

[1]The ambiguity function for the Capon estimator is obtained by evaluating the OSF over the angle range of interest, but using the true data covariance in place of the usual estimated data covariance. Although an ambiguity function is classically defined as the deterministic signal component of the output of a linear matched filter response [66, 46, 44, 60], it is appropriate to define the ambiguity function of the Capon algorithm as stated, given the stochastic nature of the signal models considered herein.

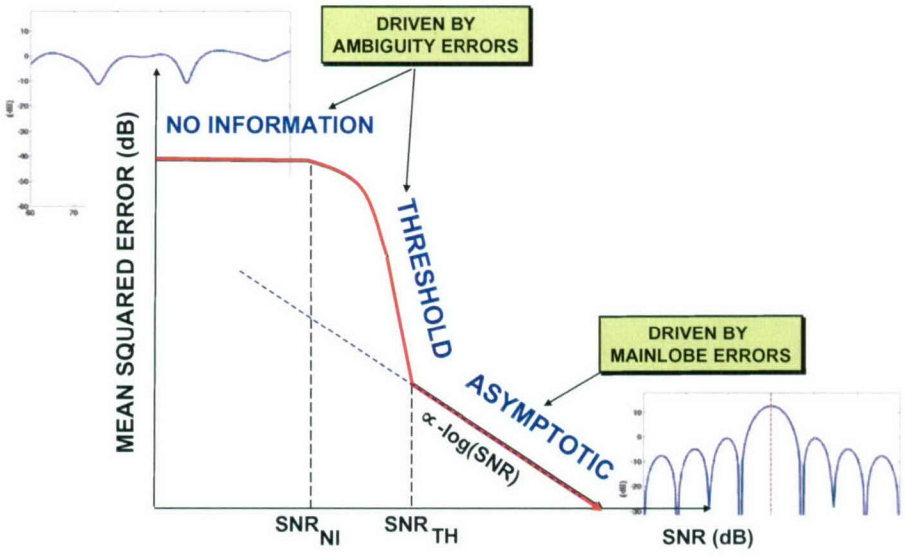

Figure 1. Typical composite MSE curve for nonlinear parameter estimation.

the full potential of super-resolution approaches [18, 26, 63, 64]. Thus, some consideration is given herein to account for its presence in these threshold region MSE predictions.

A classical method of MSE approximation, referred to herein as the method of interval errors (MIE), was introduced by Van Trees [59] and provides a means of predicting threshold region performance of nonlinear estimation techniques. MIE (and its variants) is a well established approach that has been shown to provide accurate MSE prediction of ML estimation and related nonlinear techniques well into the estimation threshold region (see discussion in Section 2). Although MIE is well established, obtaining the components necessary to apply this approach to a specific algorithm can be quite nontrivial. Indeed, the successful application of MIE requires good approximations of two quantities: (i) interval error probabilities, and (ii) the asymptotic MSE performance. Both of these quantities are algorithm dependent. The interval error probabilities quantify the likelihood that the estimator derives its signal parameter estimate from an interval (local neighborhood) of the search domain dominated by a false peak of the ambiguity function, as opposed to the local interval containing the true peak (global maximum). These probabilities are often well approximated via the Union Bound in conjunction with good approximations of pairwise error probabilities. Exact pairwise error probabilities for the Capon (and Bartlett) estimator are derived herein that hold for an arbitrary colored data covariance and include finite sample support effects. The Cramér-Rao Bound (CRB) often serves as an adequate approximation of the asymptotic local error MSE perfor-

mance of ML estimation due to its well established properties regarding efficiency [59]. Although the Capon estimator is not asymptotically efficient [61], its asymptotic (in SNR and large sample support) local error MSE performance has been studied extensively. Stoica et al. [51] established the theoretical large sample MSE performance of the Capon estimator as well as an improved Capon estimator in the context of DOA estimation. Vaidyanathan and Buckley (VB) [57, 58] independently provided theoretical predictions of this MSE performance that includes the effects of finite training and sensitivity to random perturbations of the assumed signal model. Hawkes and Nehorai (HN) [21] have extended these results to the estimation of vector signal parameters and include a parallel theoretical development for the Bartlett spectral estimator. The MSE predictions of VB that capture finite sample effects shall be used herein for the Capon algorithm, and those of HN shall be used for the Bartlett algorithm.

Signal modeling errors are inevitable in several application areas. Assessing the impact of such errors on the accuracy of DOA estimates is of practical concern. A new strategy is proposed for applying MIE to cases involving signal model match. It consists of a modification of this classic technique. The proposed strategy is based primarily on the fundamental nature of nonlinear searches driven by multimodal ambiguity functions, and it represents a unique generalization of this classic approach.

A serendipitous by-product of this present threshold region analysis is the definition of a new exact two-point measure of the Capon probability of resolution that provides accurate prediction of the SNRs required for closely spaced sources to be mutually resolvable. It is obtained via a modified pairwise error probability calculation, holds for an arbitrary colored data covariance, and includes finite sample effects. This resolution measure is parameterized by the true data covariance and choice of scanning vectors. It, therefore, can account for the presence of signal model mismatch, allowing for sensitivity analyses of signal modeling errors [20, 64]. The approach taken herein leads to an exact probability density function (pdf) for the ratio of two Capon (and Bartlett) power spectral estimates, from which the error probabilities easily follow.

This present analysis provides two very useful results in relation to the asymptotic local error MSE approximations. First, for signals that are spaced by more than a beamwidth, this analysis provides accurate prediction of the threshold SNR point, thus indicating the region of SNRs for which these asymptotic MSE approximations are valid. Second, for closely spaced sources, the proposed two-point measure of the Capon algorithm probability of resolution lower bounds the threshold SNR [25] above which the asymptotic MSE approximations are valid.

This technical report is organized as follows. Section 2 summarizes the contributions of early pioneers of threshold region MSE analysis, and reviews recent activity in this area of research. Section 3 gives brief descriptions of the Capon and Bartlett algorithms, summarizes known results on their large sample local error MSE performance prediction, and establishes the notational convention. Section 4 describes the MIE technique of MSE prediction, its adaptation to the Capon and Bartlett algorithms for well separated sources, and it includes a stepwise summary for the computation of the necessary pairwise error probabilities. Section 5 proposes a method of direct closed form approximation for the Capon (and Bartlett) algorithm large sample threshold SNR for the canonical and theoretically fundamental case of a single planwave signal in white noise. Section 6 proposes a two-point measure of the probability of resolution for the Capon (and Bartlett) algorithm that

can be applied to the case of closely spaced sources. Section 7 considers a direct calculation of the Capon algorithm resolution SNR (sometimes called the detection SNR [25]) required to resolve sources with a specified level of confidence. Section 8 describes a new generalization of MIE that encompasses the possibility of signal model mismatch. Section 9 provides several numerical results corroborating the success and demonstrating the utility of these predictions. Conclusions are given in Section 10. Appendices are provided detailing the derivation of the required pairwise error probabilities and exact distributions of the ratio of power estimates. MATLAB code is also provided for the threshold region MSE prediction of the canonical case of a single planewave signal in white noise for the interested reader.

2. THE THRESHOLD EFFECT: A HISTORICAL PERSPECTIVE AND REVIEW OF RELATED WORK

The threshold effect is in essence a rapid degradation in system performance observed when the signal level falls below a specific signal-to-noise ratio (SNR) referred to as the threshold. Historically such an effect has been observed for over half a century in the performance of communication systems that employ data modulation schemes such as pulse code modulation (PCM) [45] or phase/frequency modulation (FM) [32]. These schemes, coupled with a system designer's desire for efficiency that inevitably leads to a minimum power requirement, brings threshold region system performance to the forefront of communication systems analysis. Transmission of binary digits (called bits) obtained from a coding strategy that converts useful information (speech/voice, for example) into a form robust for efficient data transmission over a noisy channel is the staple of all communication systems. These bitstreams are often decomposed into sub-bitstreams that are mapped into one of several symbols of a constellation of say M possible symbols. The job of the receiver is to determine which symbol was transmitted over the channel in the presence of noise. A communication system, therefore, has as one of its most fundamental tasks that of M-ary detection, *i.e.*, the testing of multiple hypotheses. Correct detection of each transmitted symbol obviously permits the correct synthesis of the original bitstream, and ultimately intelligible reconstruction of the original transmitted information. When the SNR falls below the threshold, incorrect symbol detection errors can corrupt the bitstream making the received demodulated waveform and message (speech, for example) unintelligible. Shannon referred to this threshold SNR as the *threshold of intelligibility* [45] and offered a very interesting explanation for its presence. His explanation derives from a dimension theoretical interpretation of coding theory that suggests that folds (or ambiguities) in the signal space are an inevitable topological consequence of mapping (or coding) a higher dimensional signal into a lower dimensional space or vice versa when the low-dimensional signal is designed to fill the high dimensional space. *Shannon attributes the threshold effect of communication systems to the presence of these folds/ambiguities, much in the same way that the observed threshold effect in the MSE performance of nonlinear parameter estimation schemes is attributed to the presence of subsidiary multiple maxima in the underlying ambiguity function associated with the OSF.*

Woodward [66] draws this parallel between communication theory and nonlinear parameter estimation. He considers the classic range/delay estimation problem encountered in Radar applications and describes in lucid detail the performance accuracy of such estimates. Woodward defines the ambiguity function in the classical sense as the signal component of the optimal matched filter output and describes its impact in the presence of noise on the accuracy of range estimates for the high, moderate, and low SNR cases. His analysis identifies three distinct regions of performance as SNR is varied[2], and he offers an interesting interpretation of the threshold effects in range estimation from the perspective of Shannon's thesis (see p. 90 of [66]); namely, the transmitted waveform that carries the information is a multidimensional quantity, whereas the information it carries (the target range) is one-dimensional. Thus, one can viably interpret the waveform as a multidimensional encoding of the original message (range) that is one-dimensional. Similarly, one

[2] Although Woodward did not name the regions, they are referred to today as the asymptotic, threshold/ambiguity, and no information regions.

can interpret the range estimate as a one-dimensional output of the demodulation/decoding of a higher dimensional input (the waveform).

The interpretation of the threshold effect in DOA estimation error from the perspective of Shannon's thesis is rather transparent in light of Woodward's work, but noteworthy nonetheless. The relative phase from sensor-to-sensor of the signal component (known as the signal steering vector, array response vector, or system function vector, etc.) can be interpreted as a multidimensional encoding of a one-dimensional message (the signal's arrival angle). The same interpretation applies to matched field processing, for example, where the low-dimensional encoded message would be the source range and depth.

Van Trees [59] discusses the threshold effect in the context of classical estimation theory. This discussion is embedded primarily in an example problem (Example 2 of Section 4.2.3 Nonlinear Estimation), but provides a general strategy for predicting MSE performance of nonlinear estimation schemes when local bounds like the CRB are no longer useful. The example problem deals with ML estimation of waveform parameters where the waveforms are those of a nonlinear pulse frequency modulation scheme, and the general strategy proposed for threshold region MSE prediction is referred to herein as MIE. A detailed description of MIE shall be deferred to Section 4 of this report, but the short description is that it builds on a judicious decomposition of the integral for the MSE of the parameter estimate. Van Trees approximated the necessary interval error probabilities with standard asymptotics and use of well known bounds on the error function.

Rife and Boorstyn (RB) [43] build on Van Trees' approach to predict the threshold region performance of a Discrete Fourier Transform (DFT)-based approximate implementation of an ML estimator. RB considers the estimation of the frequency of a single pure sinusoid in additive white Gaussian noise (AWGN) where the sinusoid is assumed deterministic (and therefore represented in the mean of the distribution). True ML requires a full search over a continuous interval of frequencies. RB considers a DFT-based approach that restricts the ML continuous search to a finite set of discrete sample points. When sampled at Nyquist, the DFT samples the mainlobe of the ambiguity function (a sinc in this case), and the zeros of the ambiguity function in the sidelobe region. Thus, RB considers the impact of restricting the ML search to discrete sampling of the mainlobe and the zeros of the ambiguity function. Since the DFT bins corresponding to the zeros of the ambiguity function are orthogonal to the mainlobe, the analysis of RB (derivation of the interval error probabilities, or outlier probabilities as RB refers to them) simplifies significantly. This landmark paper popularized Van Trees' MIE approach to below threshold MSE prediction.

Steinhardt and Bretherton [48] took the analysis of RB two steps further by (i) simplifying the expressions for the error probabilities, and (ii) providing for what appears to be the first time a method for computing directly in closed form the threshold SNR of the RB analysis. Direct calculation of the threshold SNR simply means that an initial prediction of the MSE curve as a function of SNR (from which the threshold SNR is easily determined) is bypassed.

Tufts, Kot, and Vaccaro (TKV) [54, 55] developed a procedure for computing the threshold SNRs for the estimation of the frequencies of multiple sinusoids by linear prediction. Their procedure can be viewed as a variant of MIE. This creative analysis appears to be the first to recognize the general applicability of MIE to a large class of nonlinear estimation schemes. It is also the first

to jointly quantify the below threshold SNR performance of the estimation of multiple sinusoids. As mentioned in the introduction, application of MIE requires good approximation of two quantities: (i) the asymptotic MSE of the algorithm, and (ii) the interval error probabilities. TKV obtained the asymptotic MSE of linear prediction by applying a matrix perturbation analysis to essentially approximate the Taylor's series of the OSF. The linear and quadratic terms are retained to compute the desired local error MSE of the parameter estimates. TKV approximated the required error probabilities by first defining a useful upperbound on the desired probability that is much easier to work with analytically, and secondly assuming the essential random variables involved in the error event are well approximated as Gaussian. The latter assumption allows use of the well tabulated error function. The procedure defined by TKV is classified herein as a variant of MIE because no semblance of intervals of error are ever defined. The recognition of the decomposition of the total MSE as the sum of two contributions (global errors and local errors), as given in equation (127) on p. 282 of [59], but repeated in a form similar to that used in RB [43], however, is present in their work.

An interesting analysis related to TKV is the work of Kaveh and Wang (KW) [25] that focuses on the low SNR performance of the MUltiple SIgnal Classification (MUSIC) algorithm [4, 52, 61] and the minimum-norm (min-norm) algorithm. These are subspace based algorithms that exploit the singular value decomposition (SVD) as does the linear prediction algorithm examined by TKV. KW focuses on quantifying how well both algorithms detect (estimate the number of planewaves), estimate the signal subspace, and resolve closely spaced sources. KW approximates the probability of resolution and uses this as a lower bound on the actual threshold SNR for closely spaced sources. KW primarily builds upon well known asymptotic results on the statistics of the eigenvectors and eigenvalues of a complex Wishart random matrix to quantify their desired performance measures.

The recent work of Xu et al. [67]–[71] that considers source localization error performance of MFP methods in underwater acoustic environments, the work of Athley [2, 3] that considers the ML DOA estimation of multiple planewave signals in white noise, and that of Boyer et al. [12, 13] that also considers the ML DOA estimation of planewaves in white noise, extend the work of [43] in several ways. First, the restriction that the ML search be limited to DFT bins sampled at Nyquist is relaxed. This leads to performance that better approximates true ML, but it likewise complicates the calculation of the interval error probabilities because the sidelobes of the ambiguity function and the mainlobe are statistically dependent in general; second, the signal model is no longer restricted to be a sinusoid (or planewave); and third, analysis was extended to include stochastic signal models (signal component represented in the covariance of the distribution). Richmond [37] has recently extended these analyses to ML signal parameter estimation within an adaptive array context.

Before closing this section, it is worthwhile to point out that researchers have considered Bayesian bounds to address the contribution of global errors to the overall MSE of ML. Bounds receiving the most attention include the Ziv-Zakai bound (ZZB), Bayesian CRB [59], Barankin bound [36], and the Weiss-Weinstein bound. Recent work has extended the theory of ZZBs to include vector parameters [8, 9]. The Bayesian framework is attractive as its applicability is not limited to unbiased estimators, and it provides a viable means of including contributions of global

errors to the overall MSE[3]. Loosely speaking, the nature of the ML search is effectively mimicked by these bounds by randomizing the signal parameter of interest, *e.g.*, the signal's angle of arrival becomes a random variable with a known distribution. This is done, however, at the expense of the classical assumption of ML theory that the unknown parameters are deterministic. The ability to provide system performance prediction for a specific parameter value or given set of parameter values is a desired characteristic of a performance bound. Indeed, the non-Bayesian CRB has enjoyed much popularity in practice as a system design tool, in part because it provides such flexibility. This flexibility is not offered by Bayesian bounds by construction. In addition, Bayesian bounds are often computationally expensive, do not easily support inclusion of the effects of estimating nuisance parameters (like an unknown data covariance matrix), and at best predict the performance of ML estimation. MIE in contrast is an approach to MSE prediction that is algorithm specific, maintains the assumption that parameters are deterministic yet unknown, and can support the presence of nuisance parameter, although the analyses can be nontrivial.

[3]Extensions of classical local bounds to biased estimators do exist. Their use, however, is strictly limited in that good knowledge of the bias is required in order to compute the bound [59].

3. THE CAPON AND BARTLETT ALGORITHMS FOR DOA ESTIMATION

3.1 The Spectral Estimation Problem

The Capon and Bartlett algorithms are well known, and their performance has been studied extensively. The goal of this section is to establish notation and to briefly summarize the algorithms and known results on their large sample local error MSE performance.

The fundamental problem of spectral estimation can be stated as follows: Given a finite length data record, *i.e.*, a sample function of a random process that is at least wide sense stationary observed over some finite interval of time, estimate the power distribution over frequency. The Capon and Bartlett algorithms represent filterbank approaches to this classic problem. Although originally posed for time series analysis where frequency refers to temporal frequency, the power spectrum of interest for the DOA estimation problem is with respect to spatial frequency or angle. To this end, data is obtained from an array of N sensors distributed in space. Each data observation taken across the array (called a spatial snapshot) is modeled as an $N \times 1$ zero mean complex Gaussian vector[4] with representation $\mathbf{x} = S\mathbf{v}(\theta) + \mathbf{n}$ where the array response of the signal of interest associated with DOA parameter θ is given by $\mathbf{v}(\theta)$, and its complex amplitude is Gaussian distributed such that $S \sim \mathcal{CN}_1(0, \sigma_S^2)$, and the colored noise[5] is denoted by $\mathbf{n}$ having covariance $E\{\mathbf{n}\mathbf{n}^H\} = \mathbf{R}_N$, where $E\{\cdot\}$ denotes the statistical expectation. Note that $E\{\mathbf{x}\} = \mathbf{0}$ and that $E\{\mathbf{x}\mathbf{x}^H\} = \mathbf{R} = \mathbf{R}_N + \sigma_S^2\mathbf{v}(\theta)\mathbf{v}^H(\theta)$. A finite set of L array observations is accrued over time and assembled in a data matrix: $\mathbf{X} = [\mathbf{x}(1)|\mathbf{x}(2)|\cdots|\mathbf{x}(L)]$, where $\mathbf{x}(l) \sim \mathcal{CN}_N(\mathbf{0}, \mathbf{R})$, $l = 1, 2, \ldots, L$. These snapshots often represent measurements of the narrowband spatial complex envelope whose real and imaginary parts are respectively composed of the in-phase and quadrature component of demodulated data. The spatial snapshots are used to form the unnormalized data spatial covariance estimate $\widehat{\mathbf{R}} = \mathbf{X}\mathbf{X}^H$ from which the Capon and Bartlett algorithms generate power spectral estimates.

The Capon and Bartlett DOA angle estimates are obtained as the arguments of the largest peaks of the estimated spatial power spectra. If $P(\theta)$ represents the estimated spectrum as a function of angle, then the maximum output provides an estimate of the signal power σ_S^2, and the signal DOA estimate is given by the scan value of θ that achieves this maximum; namely,

$$\widehat{\theta} = \arg\max_{\theta} P(\theta) \tag{1}$$

(assuming a single signal is present). It shall be assumed that K signals are present in the data, and that the Capon/Bartlett parameter estimates $\widehat{\theta}_k$, $k = 1, 2, \ldots, K$ are obtained as the arguments of

[4]The notational convention adopted is as follows: italics indicates a scalar quantity, as in A; lower case boldface indicates a vector quantity, as in $\mathbf{a}$; upper case boldface indicates a matrix quantity, as in $\mathbf{A}$. The n-th row and m-th column of matrix $\mathbf{A}$ will be indicated by $[\mathbf{A}]_{n,m}$. Variables will be assumed complex in general, but some will be real (obvious from context). $\mathrm{Re}(A)$ is the real part of A and $\mathrm{Im}(A)$ is the imaginary part. The complex conjugation of a quantity is indicated by a superscript $*$ as in A^*. The matrix transpose is indicated by a superscript T as in $\mathbf{A}^T$, and the complex conjugate plus matrix transpose is indicated by a superscript H as in $\mathbf{A}^H = (\mathbf{A}^T)^*$.

[5]It is assumed that the colored noise does not contain any low rank directional signals in the search domain, since the total number of signals in search space is assumed known.

the K largest peaks of $P(\theta)$.

3.2 The Bartlett Algorithm: A Conventional Beamforming Approach

Bartlett recognized the inherent tradeoff between resolution and variability in the *periodogram* (Fourier Transform of a sample data record) spectral estimate and recommended averaging over shorter time Fourier Transforms as a means of reducing the high variance at the expense of some resolving capacity. The Bartlett algorithm estimates power spectra over angle by averaging the power out of a bank of conventional spatial filters (beamformers). Each conventional spatial filter is a crude narrowband (in spatial frequency) filter tuned to and centered on a specific angle of interest. The output of each filter is power averaged over time, and with proper normalization provides an estimate of the true underlying power spectral density such that when integrated over the spatial frequency band of interest its area provides an estimate of the power of the random process contained in that band. The resulting spectra plotted as a function of the filter center frequency produces what is classically referred to as a *smoothed periodogram.*

Specifically, let the conventional beamforming weight steered to angle θ for an array with element spatial locations $\mathbf{z}_n$, $n = 1, 2, \ldots, N$ be given by $\mathbf{v}(\theta) = [e^{j\mathbf{k}_\theta^T \mathbf{z}_1}, e^{j\mathbf{k}_\theta^T \mathbf{z}_2}, \ldots, e^{j\mathbf{k}_\theta^T \mathbf{z}_N}]^T$,where $\mathbf{k}_\theta = (2\pi/\lambda)\mathbf{a}(\theta)$ is the wavenumber vector, $\mathbf{a}(\theta)$ is the 3×1 unit vector pointing in the assumed direction of field propagation, $\lambda = c/f$ is the wavelength at temporal frequency f, and c is the wave propagation speed. Note that for a uniform linear array (ULA), this spatial filter weight can be easily implemented with the Fast Fourier Transform (FFT). The Bartlett spectral estimate evaluated at spatial frequency (or angle) θ is given by

$$P_{Bartlett}(\theta) = \frac{1}{L} \sum_{l=1}^{L} \left| \mathbf{v}^H(\theta)\mathbf{x}(l) \right|^2 = \frac{1}{L} \cdot \mathbf{v}^H(\theta)\widehat{\mathbf{R}}\mathbf{v}(\theta) \tag{2}$$

and its ambiguity function is defined as $\psi_{Bartlett}(\theta) \stackrel{\triangle}{=} \mathbf{v}^H(\theta)\mathbf{R}\mathbf{v}(\theta)$.

3.3 The Capon Algorithm: An Adaptive Beamforming Approach

Capon recognized that conventional filterbank techniques for spectral estimation rely too heavily upon the passband and stopband properties of a Fourier Transform frequency bin filter; namely, the FFT bin has a frequency response given by a sinc function. Taper design has been exploited to reduce sidelobes (and leakage), at the expense of a wider mainlobe (and reduced resolution) [29, 52]. When multiple signals are present, sidelobe leakage and mutual signal interference can introduce biases in DOA estimates obtained via conventional techniques like the Bartlett algorithm (see Section 9). Capon proposed designing these filters optimally; namely, a linear narrowband filter designed to pass the desired signal undistorted, while minimizing the power from all other spatial frequency bands (and thus, other sources of interference). Formally, the following constrained optimization problem for the filter weight $\mathbf{w}$ was suggested

$$\min_{\mathbf{w}} \mathbf{w}^H\mathbf{R}\mathbf{w} \text{ such that } \mathbf{w}^H\mathbf{v}(\theta) = 1 \Longrightarrow \mathbf{w}_{MVDR} = \frac{\mathbf{R}^{-1}\mathbf{v}(\theta)}{\mathbf{v}^H(\theta)\mathbf{R}^{-1}\mathbf{v}(\theta)}, \tag{3}$$

that yields the well known MVDR filter as its solution. Note that the optimal filter weight depends on the data covariance matrix $\mathbf{R}$. This filter is often interpreted in the classical sense as a data-dependent taper [15, 17]. By construction, this optimal filter will cancel all spatially coherent energy from all directions other than the scan direction θ. The filter output $\mathbf{w}_{MVDR}^H \mathbf{x}$ likewise provides the ML estimate of the complex signal amplitude S [33, 49, 39, 31]. The average output power is given by

$$E\left\{\left|\mathbf{w}_{MVDR}^H \mathbf{x}\right|^2\right\} = \frac{1}{\mathbf{v}^H(\theta)\mathbf{R}^{-1}\mathbf{v}(\theta)} \stackrel{\triangle}{=} \psi_{Capon}(\theta) = \frac{1}{\mathbf{v}^H(\theta)\mathbf{R}_N^{-1}\mathbf{v}(\theta)} + \sigma_S^2 \tag{4}$$

where the Capon ambiguity function $\psi_{Capon}(\theta)$ has been defined. The last equality in (4) holds only when the signal array response in $\mathbf{R}$ perfectly matches that used to form the weight vector $\mathbf{w}_{MVDR}$, and when $\mathbf{R}$ is perfectly known. Capon, therefore, reasoned that for large enough sample support, an estimate of the covariance $\mathbf{R}$ can be used with (4) to estimate the signal power σ_S^2 and the corresponding signal parameter θ (or set of signal parameters $\boldsymbol{\theta} = [\theta_{1,1}, \theta_{1,2}, \ldots, \theta_{1,A}]^T$ as in [15, 21, 24]). Using the covariance estimate $\widehat{\mathbf{R}} = \mathbf{X}\mathbf{X}^H$, Capon proposed the following power spectral estimator

$$P_{Capon}(\theta) = \frac{1}{L-N+1} \cdot \frac{1}{\mathbf{v}^H(\theta)\widehat{\mathbf{R}}^{-1}\mathbf{v}(\theta)}. \tag{5}$$

$P_{Capon}(\theta)$ can be further normalized to ensure that it is a true power spectral density [29, 52].

3.4 Asymptotic Local Error MSE Performance

Consider the case of a single planewave signal in AWGN and note that at high enough SNRs, namely, those above the threshold SNR, the angle search indicated in (1) will result in a DOA estimate obtained from the local neighborhood of the true global maximum of the ambiguity function with near probability 1. At such SNRs it is possible to characterize the average error or jitter in DOA estimates about the true value by exploiting Taylor's theorem. For ML estimation of DOAs, this jitter error is characterized by the CRB (it will be demonstrated in Section 9 that the Bartlett algorithm in fact produces the ML DOA estimate for the single signal case in white noise). The same ideas hold in the multiple signal case, where the estimate of the k-th signal angle will be obtained from the local neighborhood of the k-th largest peak of the ambiguity function with near probability 1 (assuming all signals have large SNRs). The following sections describe the fundamental results of analyses that compute this jitter error, *i.e.*, the asymptotic local error MSE of the DOA estimate of the k-th signal.

It will be assumed in this section that for well separated (by at least a beamwidth) signals, SNRs exceed estimation threshold, and that for closely spaced signals, SNRs are large enough for all signals to be mutually resolved with zero probability of intersource errors. In addition, it is assumed that no pairs of perfectly coherent signals are present (coherent sources are not resolvable with the Capon algorithm [61]), and that the total number of signals present in the data is known[6].

[6]Subspace rank (model order) determination is an important topic and active area of research, but will not be pursued herein.

3.4.1 Bartlett Algorithm

Hawkes and Nehorai (HN) [21] developed the theory based on Taylor's theorem for predicting the asymptotic local error MSE performance of DOA estimates derived from the Bartlett spectral estimator. To summarize the results of HN, let θ_k, $k = 1, 2, \ldots, K$ represent the true DOA angle values of the K signals present in the data. Let $\tilde{\theta}_k$, $k = 1, 2, \ldots, K$ represent the asymptotic ($L \to \infty$) estimates of these K angles, *i.e.*, the locations of the K largest peaks of the ambiguity function $\psi_{Bartlett}(\theta)$ (that are not necessarily equal to θ_k for all SNR). The MSE is the sum of the bias squared and variance. Thus, the MSE of the estimate $\widehat{\theta}_k$ is given by

$$E\left\{\left(\widehat{\theta}_k - \theta_k\right)^2\right\} = \left[E\left\{\left(\widehat{\theta}_k - \theta_k\right)\right\}\right]^2 + E\left\{\left(\widehat{\theta}_k - \tilde{\theta}_k\right)^2\right\} \tag{6}$$

where the bias can be written

$$E\left\{\widehat{\theta}_k - \theta_k\right\} = E\left\{\widehat{\theta}_k - \tilde{\theta}_k\right\} + \left(\tilde{\theta}_k - \theta_k\right). \tag{7}$$

HN derived expressions for the asymptotic bias and variance needed to approximate the MSE in (6). Denote the first three derivatives of the array response with respect to the scan variable θ, respectively, as

$$\dot{\mathbf{v}}(\theta) \stackrel{\triangle}{=} \frac{d\mathbf{v}(\theta)}{d\theta}, \quad \ddot{\mathbf{v}}(\theta) \stackrel{\triangle}{=} \frac{d^2\mathbf{v}(\theta)}{d\theta^2}, \quad \dddot{\mathbf{v}}(\theta) \stackrel{\triangle}{=} \frac{d^3\mathbf{v}(\theta)}{d\theta^3}. \tag{8}$$

As mentioned in [21], the additional bias term for the Bartlett DOA estimate is negligible in most cases, *i.e.*, $E\{\widehat{\theta}_k - \tilde{\theta}_k\} \simeq 0$. When the asymptotic bias is small and nonzero, it can be approximated via

$$\left(\tilde{\theta}_k - \theta_k\right) \simeq \frac{-\mathrm{Re}\left[\dot{\mathbf{v}}^H(\theta_k)\mathbf{R}\mathbf{v}(\theta_k)\right]}{\mathrm{Re}\left[\dot{\mathbf{v}}^H(\theta_k)\mathbf{R}\dot{\mathbf{v}}(\theta_k) + \mathbf{v}^H(\theta_k)\mathbf{R}\ddot{\mathbf{v}}(\theta_k)\right]}. \tag{9}$$

If the bias is large, then (9) can be grossly inaccurate. The bias, however, can always be easily inferred directly from the location of the true k-th peak of the ambiguity function $\psi_{Bartlett}(\theta)$, relative to the true k-th signal angle. The asymptotic variance is given by

$$E\left\{\left(\widehat{\theta}_k - \tilde{\theta}_k\right)^2\right\} \simeq \frac{1}{2L} \frac{\mathrm{Re}\left[\mathbf{v}^H(\tilde{\theta}_k)\mathbf{R}\mathbf{v}(\tilde{\theta}_k)\dot{\mathbf{v}}^H(\tilde{\theta}_k)\mathbf{R}\dot{\mathbf{v}}(\tilde{\theta}_k) - \dot{\mathbf{v}}^H(\tilde{\theta}_k)\mathbf{R}\mathbf{v}(\tilde{\theta}_k)\mathbf{v}^H(\tilde{\theta}_k)\mathbf{R}\dot{\mathbf{v}}(\tilde{\theta}_k)\right]}{\mathrm{Re}\left[\dot{\mathbf{v}}^H(\tilde{\theta}_k)\mathbf{R}\dot{\mathbf{v}}(\tilde{\theta}_k) + \mathbf{v}^H(\tilde{\theta}_k)\mathbf{R}\ddot{\mathbf{v}}(\tilde{\theta}_k)\right]^2}. \tag{10}$$

The total asymptotic local error MSE approximation obtained for the Bartlett DOA estimates using (6)–(10) shall be herein denoted by $\sigma^2_{HN}(\theta_k)$.

3.4.2 Capon Algorithm

The large sample ($L \gg N$) asymptotic local error MSE performance of the Capon signal parameter estimator has been theoretically analyzed by several authors. Stoica et al. [51], VB [57], and HN [21] exploit Taylor's theorem and complex gradient methods to approximate the MSE.

VB provides an additional bias term via a second order Taylor series expansion that is intended to further capture finite sample effects and therefore a broader range of values for L and SNR.

To summarize the results of VB, let θ_k, $k = 1, 2, \ldots, K$ represent the true parameter values of the K signals present in the data. Let $\tilde{\theta}_k$, $k = 1, 2, \ldots, K$ represent the asymptotic ($L \to \infty$) estimates of these K parameters, *i.e.*, the locations of the K largest peaks of the ambiguity function $\psi_{Capon}(\theta)$ (that are not necessarily equal to θ_k for all SNR). The MSE of the estimate $\widehat{\theta}_k$ is given in form by (6) with bias given by (7). Recalling the derivatives given in (8), define the function $f_{Capon}(\theta)$ and denote its second and third order derivatives, respectively, as

$$\begin{aligned} f_{Capon}(\theta) &= \mathbf{v}^H(\theta)\mathbf{R}^{-1}\mathbf{v}(\theta) = 1/\psi_{Capon}(\theta) \\ \ddot{f}_{Capon}(\theta) &= 2\mathrm{Re}\left[\dot{\mathbf{v}}^H(\theta)\mathbf{R}^{-1}\dot{\mathbf{v}}(\theta) + \mathbf{v}^H(\theta)\mathbf{R}^{-1}\ddot{\mathbf{v}}(\theta)\right] \\ \dddot{f}_{Capon}(\theta) &= 2\mathrm{Re}\left[3\dot{\mathbf{v}}^H(\theta)\mathbf{R}^{-1}\ddot{\mathbf{v}}(\theta) + \mathbf{v}^H(\theta)\mathbf{R}^{-1}\,\dddot{\mathbf{v}}(\theta)\right] \end{aligned} \tag{11}$$

and define the matrix $\mathbf{B}(\tilde{\theta}_k)$ as

$$\mathbf{B}(\tilde{\theta}_k) = \dot{\mathbf{v}}(\tilde{\theta}_k)\mathbf{v}^H(\tilde{\theta}_k) + \mathbf{v}(\tilde{\theta}_k)\dot{\mathbf{v}}^H(\tilde{\theta}_k). \tag{12}$$

The following expressions for the bias and asymptotic variance of the Capon algorithm signal parameter estimates were derived by VB [57]:

$$\left(\tilde{\theta}_k - \theta_k\right) \simeq \frac{-\mathrm{Re}\left[\dot{\mathbf{v}}^H(\theta_k)\mathbf{R}^{-1}\mathbf{v}(\theta_k)\right]}{\mathrm{Re}\left[\dot{\mathbf{v}}^H(\theta_k)\mathbf{R}^{-1}\dot{\mathbf{v}}(\theta_k) + \mathbf{v}^H(\theta_k)\mathbf{R}^{-1}\ddot{\mathbf{v}}(\theta_k)\right]}$$

$$\begin{aligned} E\left\{\left(\widehat{\theta}_k - \tilde{\theta}_k\right)\right\} \simeq \left[\frac{2(L-N)}{(L-N-1)(L-N+1)}\right] & \frac{\mathrm{Re}\left[\mathbf{v}^H(\tilde{\theta}_k)\mathbf{R}^{-1}\mathbf{B}(\tilde{\theta}_k)\mathbf{R}^{-1}\ddot{\mathbf{v}}(\tilde{\theta}_k)\right]}{[\ddot{f}_{Capon}(\tilde{\theta}_k)]^2} \\ & -\frac{\dddot{f}_{Capon}(\tilde{\theta}_k)}{2\ddot{f}_{Capon}(\tilde{\theta}_k)} \cdot E\{(\widehat{\theta}_k - \tilde{\theta}_k)^2\} \end{aligned} \tag{13}$$

$$E\left\{\left(\widehat{\theta}_k - \tilde{\theta}_k\right)^2\right\} \simeq \left[\frac{2(L-N)}{(L-N-1)(L-N+1)}\right] \frac{\mathrm{Re}\left[\mathbf{v}^H(\tilde{\theta}_k)\mathbf{R}^{-1}\mathbf{B}(\tilde{\theta}_k)\mathbf{R}^{-1}\dot{\mathbf{v}}(\tilde{\theta}_k)\right]}{[\ddot{f}_{Capon}(\tilde{\theta}_k)]^2}. \tag{14}$$

The Capon large sample MSE is obtained by using relations (11)–(14) in the expression for MSE (6)–(7). This MSE approximation[7] shall be herein denoted by the symbol $\sigma^2_{VB}(\theta_k)$.

Note in general that both MSE approximations, $\sigma^2_{HN}(\theta_k)$ for the Bartlett algorithm and $\sigma^2_{VB}(\theta_k)$ for the Capon algorithm, are functions of the array geometry, number of sensors N, sample support L, true data covariance $\mathbf{R}$ (includes colored noise and true array manifold of signals), assumed scanning vectors $\mathbf{v}(\theta)$, and SNRs. Thus, the asymptotic MSE performance can be explored versus combination of these parameters.

[7] It was observed in this analysis that the additional bias term was often negligible (as mentioned in [21]). It was likewise found that the approximate bias expression given by the first equation in (13) can be grossly inaccurate when the bias is large. A reliable estimate of the bias $(\tilde{\theta}_k - \theta_k)$, however, is easily inferred directly from the location of the peak of the ambiguity function $\psi_{Capon}(\theta)$ relative to the true signal parameter value θ_k.

4. AN INTERVAL ERROR-BASED METHOD OF THRESHOLD REGION MEAN SQUARED ERROR PREDICTION

This section describes the method of interval errors (MIE) for MSE prediction and its adaptation to the Capon (and Bartlett) algorithm. Application of MIE to the single signal case ($K = 1$) is restricted to estimation scenarios that are at least asymptotically (SNR$\rightarrow \infty$) well-posed estimation problems, consisting of ambiguity functions that possess a unique global maximum over the signal parameter search space. While this technique can be used for arbitrary array configurations and signal models (more general than planewaves), it cannot predict performance when the ambiguity function does not possess a unique global maximum over the parameter search domain at least for very large SNRs. Extension of MIE to the multisignal case ($K > 1$) requires that the ambiguity function possess K unique local maxima due to the K sources.

The following discussion assumes that no signal modeling errors are present. Mismatch will be considered in Section 8. MIE is first described for the case of a single source present. Its extension to multiple sources is described subsequently. The steps for computing the required pairwise error probabilities for both the Capon estimator and the Bartlett are then summarized. Simple large sample approximations of these pairwise error probabilities based on the complementary error function are derived in Section 4.2.1.

The following discussion focuses on the Capon algorithm. The parallel application to the Bartlett algorithm is transparent; however, a summary of the analogous results is provided at this section's end.

4.1 Method of Interval Errors

MIE builds upon the two regions of the composite MSE curve of Figure 1 that are given by the asymptotes of the SNR; namely, the no information (SNR$\rightarrow$ 0) and asymptotic (SNR$\rightarrow \infty$) regions. Define the conditioning event

$$\mathcal{A} = \{\text{True source parameters are } \theta_k, k = 1, 2, \ldots, K\}. \tag{15}$$

MIE decomposes the MSE expression into two components: "no interval errors" (NIE) and "interval errors" (IE)

$$\begin{aligned} E\left\{\left(\widehat{\theta}_k - \theta_k\right)^2 \middle| \mathcal{A}\right\} &= \int p_{\widehat{\theta}_k}\left(\widehat{\theta}_k = \theta_0 \middle| \mathcal{A}\right)(\theta_0 - \theta_k)^2 \, d\theta_0 \\ = \Pr(\text{NIE} \mid \mathcal{A})\, E\left\{\left(\widehat{\theta}_k - \theta_k\right)^2 \middle| \text{NIE}, \mathcal{A}\right\} &+ \Pr(\text{IE} \mid \mathcal{A})\, E\left\{\left(\widehat{\theta}_k - \theta_k\right)^2 \middle| \text{IE}, \mathcal{A}\right\} \end{aligned} \tag{16}$$

(see equation (127) on p. 282 of [59]). The parameter search space, *i.e.*, the scanning domain for θ, is divided into disjoint mutually exclusive intervals based on the characteristics of underlying ambiguity function $\psi_{Capon}(\theta)$ that innately drives the character of the stochastic process generated by the OSF $P_{Capon}(\theta)$ on each scan. Note from (4) that $\psi_{Capon}(\theta)$ depends on $\mathbf{R}$, and is a function of the K SNRs of the K signals present. Consequently, *this SNR dependence can affect the interval*

choice and must be accounted for in general. When the SNR dependence is weak however, then a single choice of intervals will suffice for all SNRs with no need to adjust. For the presentation that follows, weak dependence is assumed.[8] The ambiguity function used for interval selection is obtained from an arbitrary choice of some high value of SNR.

4.1.1 Single Source, $K = 1$

A large enough SNR (how large is scenario dependent) leads to an ambiguity function with a dominant peak located at the true parameter value, say θ_1, and several false peaks located elsewhere within the domain of interest. An example ambiguity function is illustrated in Figure 2. MIE divides the parameter search space into disjoint neighborhoods or intervals around all local maxima of the ambiguity function $\psi_{Capon}(\theta)$, and interprets the resulting MSE in terms of these intervals. When signal parameter estimates fall inside the interval containing the global maximum θ_1, then it is said that "no interval errors" have occurred. Such estimates result in the smallest contributions to the MSE, often referred to as *local errors* (jitter errors). This NIE component represents the contribution dominating the MSE within the asymptotically high SNR regime. When considering ML estimation, for example, the CRB is often a good predictor of the ML MSE performance in this region, describing the small perturbations or jitter in the resulting signal parameter estimate as the ML search resides with near probability 1 in a small neighborhood of the true peak of the ambiguity function. *The large sample MSE approximation obtained via $\sigma^2_{VB}(\theta_1)$ (as defined in Section 3.4.2) for signal parameter estimates derived from the Capon algorithm will be used to describe this NIE component contribution to the overall MSE.* This is appropriate by virtue of Taylor's theorem upon which $\sigma^2_{VB}(\theta_1)$ is based. The truncated Taylor series approximates the local behavior of the Capon OSF about the point of expansion θ_1.

When signal parameter estimates fall outside the interval consisting of the local neighborhood around the global maximum of $\psi_{Capon}(\theta)$ located at θ_1, then it is said that an "interval error" has occurred. Such estimates result in the largest contributions to the MSE, contributing what are referred to as *global errors.* This IE component results as a consequence of the Capon algorithm choosing maxima of the OSF that can be traced to false peaks (those local maxima not corresponding to θ_1) of the underlying ambiguity function. This component dominates in the low to very low SNR regimes and must be approximated numerically. An adequate approximation can be obtained by exploiting a property that is characteristic of nonlinear estimation schemes consisting of an OSF driven by an underlying multimodal ambiguity function; namely, that the pdf of the resulting signal parameter estimate tends to aggregate its density in parameter space θ around the local maxima of the multimodal ambiguity function, especially at SNRs in the vicinity of the estimation threshold region (see histogram in Figure 2 that corresponds to the ambiguity function shown to its left; also, see analogous histograms for MUSIC in Figure 9.30, p. 1199 of [61], for example). Consequently, the continuous pdf of the Capon signal parameter estimate can be well approximated by a discrete probability mass function (pmf) (or a finite set of Dirac delta functions in continuous parameter space), where the masses (or delta function areas) are given by interval error probabilities. Specifically, let all local maxima of the ambiguity function $\psi_{Capon}(\theta)$ within the

[8] This assumption is well satisfied for well separated signals in white noise. Colored noise and/or closely spaced signals can require that this dependence be accounted for (see [30], for example).

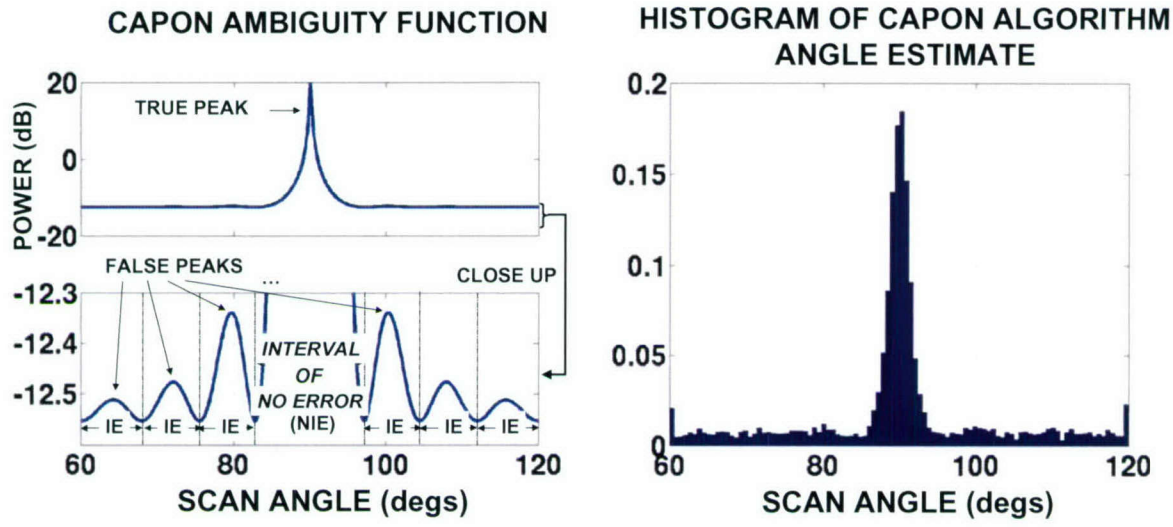

Figure 2. Example Capon ambiguity function and histogram with true signal at $\theta_1 = 90$ degrees.

signal parameter domain of interest when evaluated at a sufficiently large SNR (large enough such that the true peak is evident and located at θ_1) be given by the finite set $\mathcal{M}_1 = \{\theta \,|\, \theta_1, \theta_2, \ldots, \theta_M\}$, where θ_1 is the global maximum location and θ_k for $k = 2, 3, \ldots, M$ are all other local maxima; with this discretization one can effectively approximate the continuous scanning search over an infinite number of possible outcomes with a M-ary hypothesis testing over a finite number of possible estimates. The total MSE for this Capon parameter estimate can be approximated by[9]

$$E\left\{\left(\widehat{\theta}_1 - \theta_1\right)^2 \middle| \mathcal{A}\right\} \simeq \left[1 - \sum_{m=2}^{M} p\left(\widehat{\theta}_1 = \theta_m \middle| \mathcal{A}\right)\right] \cdot \sigma_{VB}^2(\theta_1) + \sum_{m=2}^{M} p\left(\widehat{\theta}_1 = \theta_m \middle| \mathcal{A}\right)(\theta_m - \theta_1)^2 \tag{17}$$

where the NIE component is described by the results of VB, and the IE component has been discretized. The interval error probability $p\left(\widehat{\theta}_1 = \theta_m \middle| \mathcal{A}\right)$ represents the likelihood of the Capon search algorithm choosing the false peak located at $\theta = \theta_m$ as an estimate, when the true signal is located at parameter value $\theta = \theta_1$. Technically speaking, the interval error probability is obtained by integrating the pdf of the parameter estimate over the error interval. Since the pdf is unknown, the approximation in (17) focuses on the single point in each interval most likely to contend with the global maximum at θ_1; namely, the local maximum contained in each interval. This single point

[9] Although negligible in the threshold region, the following adjustment to the local error contribution is often necessary in the no information region due to the approximate nature of the calculation: $\left\{1 - \min\left[1, \sum_{m=2}^{M} p\left(\widehat{\theta}_1 = \theta_m \middle| \mathcal{A}\right)\right]\right\} \cdot \sigma_{VB}^2(\theta_1)$.

dominates the interval error probability for SNRs in the vicinity of the threshold region. *These interval error probabilities are sample support and SNR dependent in general, and essentially weight the transition of the MSE from the asymptotic in low SNR region (no information region) to the asymptotic in high SNR region (described by VB approximation);* thus, producing the threshold or ambiguity region of the MSE curve as SNR is varied. An estimate of the estimation threshold SNR is easily obtained from the predicted MSE curve.

4.1.2 Multiple Sources, $K \geq 1$

Now assume arbitrary $K \geq 1$; in addition assume that these K signals are separated by at least a beamwidth (consideration of closely spaced sources shall be given in Section 6). The extension of MIE to multiple sources is accomplished by expanding the NIE set to include all local neighborhoods of the K peaks in the ambiguity function due to the K sources present. As in the previous section, *the large sample local error MSE approximation obtained via $\sigma^2_{VB}(\theta_k)$ will be used to describe the NIE component contribution to the over MSE of the k-th source parameter estimate.*

Let all local maxima of the ambiguity function $\psi_{Capon}(\theta)$ within the signal parameter domain of interest when evaluated at K large SNRs (large enough such that[10] $\tilde{\theta}_k = \theta_k$, $k = 1, 2, \ldots, K$) be given by the finite set $\mathcal{M} = \{\theta \,|\, \theta_1, \theta_2, \ldots, \theta_K, \theta_{K+1}, \ldots, \theta_{K+M-1}\}$, where θ_k for $k = 1, 2, \ldots, K$ represent the peak locations due to the K sources, and θ_k for $k = K+1, K+2, \ldots, K+M-1$ represent all other local maxima. Local errors for the k-th source will originate from the local neighborhood of the θ_k peak of the ambiguity function. Thus, signal parameter estimates falling within the local neighborhood of the ambiguity function about the parameter value θ_k will be classified as NIE events. Global errors for the k-th source can originate from all nonsource intervals, *i.e.*, intervals centered about local maxima θ_k for $k > K$. Intersource errors, for example, error contributions to the MSE of the parameter for source $k = k_1$ due to source $k = k_2 \neq k_1$, are very unlikely to occur because the sources are assumed separated by at least a beamwidth.[11] Consider the k-th source with true parameter value $\theta = \theta_k$. The total MSE for this Capon parameter estimate can be approximated by

$$E\left\{\left(\widehat{\theta}_k - \theta_k\right)^2 \middle| \mathcal{A}\right\} \simeq \left[1 - \sum_{m=K+1}^{K+M-1} p\left(\widehat{\theta}_k = \theta_m \middle| \mathcal{A}\right)\right] \cdot \sigma^2_{VB}(\theta_k) + \sum_{m=K+1}^{K+M-1} p\left(\widehat{\theta}_k = \theta_m \middle| \mathcal{A}\right)(\theta_m - \theta_k)^2 . \tag{18}$$

The interval error probability $p\left(\widehat{\theta}_k = \theta_m \middle| \mathcal{A}\right)$ represents the likelihood of the Capon search algorithm choosing the false peak located at $\theta = \theta_m$ as an estimate for θ_k, when the K true signals are located at parameter values $\theta = \theta_k$, $k = 1, 2, \ldots, K$.

Use of (18) or (17) requires calculation of the interval error probabilities. Exact calculation

[10] Such SNRs will exist provided that no array response mismatch is present, *i.e.*, provided that the array responses used to compute $\psi_{Capon}(\theta)$ match the K array responses existing in the true data covariance $\mathbf{R}$ for θ_k, $k = 1, 2, \ldots, K$.

[11] Intersource errors are not accounted for by the large sample MSE predictions of VB, nor the adaptation of MIE as presented herein, and does not apply to the closely spaced sources case. However, the probability of resolution provided herein should prove instrumental for such future extensions.

is very difficult. Consequently, the Union Bound (UB), which is widely used in Digital Communications to calculate M-ary detection error probabilities for the determination of bit/symbol error rates [5], is employed to simplify the analysis while maintaining an acceptable degree of accuracy. Define the set of M positive integers $\mathcal{N}_k = \{k, K+1, K+2, \ldots, K+M-1\}$. As in [67, 2], note that the interval error probability for the M-ary hypothesis testing problem is given by

$$p\left(\widehat{\theta}_k = \theta_m \middle| \mathcal{A}\right) = 1 - p\left(\widehat{\theta}_k \neq \theta_m \middle| \mathcal{A}\right) = 1 - \Pr\left\{ \bigcup_{\substack{n \in \mathcal{N}_k \\ n \neq m}} \left[P_{Capon}(\theta_n) > P_{Capon}(\theta_m) | \mathcal{A}\right] \right\}$$

where the UB leads to

$$\Pr\left\{ \bigcup_{\substack{n \in \mathcal{N}_k \\ n \neq m}} \left[P_{Capon}(\theta_n) > P_{Capon}(\theta_m) | \mathcal{A}\right] \right\} \leq \sum_{\substack{n \in \mathcal{N}_k \\ n \neq m}} \Pr\left[P_{Capon}(\theta_n) > P_{Capon}(\theta_m) | \mathcal{A}\right]$$

with the upper bound determined by pairwise error probabilities. Methods exist to tighten this bound by expurgating redundant terms from the sum [62, 10]. A simple approach that improves the UB approximation in all cases considered herein is to approximate the sum with the dominant term [5]. This leads to the approximation

$$\begin{aligned} \sum_{\substack{n \in \mathcal{N}_k \\ n \neq m}} \Pr\left[P_{Capon}(\theta_n) > P_{Capon}(\theta_m) | \mathcal{A}\right] &\simeq \Pr\left[P_{Capon}(\theta_k) > P_{Capon}(\theta_m) | \mathcal{A}\right] \\ &= 1 - \Pr\left[P_{Capon}(\theta_m) > P_{Capon}(\theta_k) | \mathcal{A}\right]; \end{aligned} \tag{19}$$

thus, the interval error probabilities are approximated by the dominant pairwise error probability

$$p\left(\widehat{\theta}_k = \theta_m \middle| \mathcal{A}\right) \simeq \Pr\left[P_{Capon}(\theta_m) > P_{Capon}(\theta_k) | \mathcal{A}\right]. \tag{20}$$

This simple approach to approximating the interval error probabilities works remarkably well for the MSE prediction of DOA estimates of planewaves.[12]

To summarize, the goal is to approximate the MSE of the Capon signal parameter estimate for the k-th source via use of (18) that requires calculation of error probabilities $p\left(\widehat{\theta}_k = \theta_m \middle| \mathcal{A}\right)$. These interval error probabilities will be approximated via the dominant term of the UB sum, as in (20). It is found that this modified UB approximation is remarkably accurate in the vicinity of

[12] Initial results [30] demonstrate very good prediction of localization performance of adaptive matched field processing of underwater acoustic field data (often a high multipath environment). Although these initial results are encouraging, better approximation of the exact interval error probabilities should be considered an open problem. The simple approach taken herein is known to break down in the multidimensional parameter case, *i.e.*, when each signal is described by a set of signal parameters $\boldsymbol{\theta}_k = [\theta_{k,1}, \theta_{k,2}, \ldots, \theta_{k,A}]^T$, although the idea of projected ambiguity function has shown promise [67] in repairing this breakdown.

the estimation threshold SNR, but tends to over predict the MSE in the no information region. *Thus, the minimum of (18) and the worse case MSE obtained with an estimate $\widehat{\theta}_k$ that is uniformly distributed over the parameter search space will be chosen as the MSE prediction.*

Regarding the Bartlett algorithm, simply note that the sets of local maxima $\mathcal{M}_1 = \{\theta \,|\, \theta_1, \theta_2, \ldots, \theta_M\}$ and $\mathcal{M} = \{\theta \,|\, \theta_1, \theta_2, \ldots, \theta_K, \theta_{K+1}, \ldots, \theta_{K+M-1}\}$ will be based on ambiguity function $\psi_{Bartlett}(\theta)$. The single source ($K = 1$) and the multiple source ($K > 1$) based MSE for the Bartlett DOA estimates are given, respectively, by the following:

$$\begin{aligned} E\left\{ \left(\widehat{\theta}_1 - \theta_1\right)^2 \middle| \mathcal{A} \right\} \simeq & \left[1 - \sum_{m=2}^{M} p\left(\widehat{\theta}_1 = \theta_m \middle| \mathcal{A}\right) \right] \cdot \sigma^2_{HN}(\theta_1) \\ & + \sum_{m=2}^{M} p\left(\widehat{\theta}_1 = \theta_m \middle| \mathcal{A}\right) (\theta_m - \theta_1)^2 \end{aligned} \tag{21}$$

$$\begin{aligned} E\left\{ \left(\widehat{\theta}_k - \theta_k\right)^2 \middle| \mathcal{A} \right\} \simeq & \left[1 - \sum_{m=K+1}^{K+M-1} p\left(\widehat{\theta}_k = \theta_m \middle| \mathcal{A}\right) \right] \cdot \sigma^2_{HN}(\theta_k) \\ & + \sum_{m=K+1}^{K+M-1} p\left(\widehat{\theta}_k = \theta_m \middle| \mathcal{A}\right) (\theta_m - \theta_k)^2 . \end{aligned} \tag{22}$$

The Bartlett interval error probabilities are approximated by the following pairwise error probability[13]

$$p\left(\widehat{\theta}_k = \theta_m \middle| \mathcal{A}\right) \simeq \Pr\left[P_{Bartlett}(\theta_m) > P_{Bartlett}(\theta_k) | \, \mathcal{A} \right]. \tag{23}$$

The next section summarizes the algorithm for computing the Capon and Bartlett pairwise error probabilities.

4.2 Capon and Bartlett Pairwise Error Probabilities

The Capon statistic evaluated at two test points is given by

$$P_{Capon}(\theta_a) = \frac{1}{L-N+1} \cdot \frac{1}{\mathbf{v}^H(\theta_a)\widehat{\mathbf{R}}^{-1}\mathbf{v}(\theta_a)}, \quad P_{Capon}(\theta_b) = \frac{1}{L-N+1} \cdot \frac{1}{\mathbf{v}^H(\theta_b)\widehat{\mathbf{R}}^{-1}\mathbf{v}(\theta_b)}. \tag{24}$$

The desired pairwise error probabilities are of the form

$$P_e^{Capon}(\theta_a|\theta_b) \stackrel{\triangle}{=} \Pr\left[P_{Capon}(\theta_a) > P_{Capon}(\theta_b) | \, \mathcal{A} \right]. \tag{25}$$

[13] Although no mismatch has been assumed thus far, when $K > 1$ the signal sidelobe interference of multiple signals introduces mismatch effects (biases) with the Bartlett algorithm. The presence of these effects is already accounted for in the HN asymptotic local error MSE term, *i.e.*, the NIE term, but the IE term in theory also requires that the error probabilities be computed with respect to the asymptotic maxima $\tilde{\theta}_k$. The details of extending analysis to the mismatch case is discussed further in Section 8.

The following probabilities are based on the assumption that the array spatial snapshots are independent, identically distributed zero mean complex Gaussian with covariance $\mathbf{R}$. Define the following function

$$\mathcal{F}(x, J) \triangleq \frac{x^J}{(1+x)^{2J-1}} \sum_{k=0}^{J-1} \left(\begin{array}{c} 2J-1 \\ k+J \end{array} \right) \cdot x^k \tag{26}$$

where $\mathcal{F}(x, J)$ is the cdf for a special case of the complex central F statistic; namely, the case when both degrees of freedom are equal (see Appendix C). The algorithm for computing the pairwise error probabilities for the Capon estimator is as follows:

1. Choose the desired covariance parameter $\mathbf{R}$. Although the resulting probabilities hold for any hermitian positive definite (hpd) $\mathbf{R}$, the following form satisfies the conditioning event $\mathcal{A}$:

$$\mathbf{R} = \mathbf{R}_N + \sum_{k=1}^{K} \sigma_{S,k}^2 \cdot \mathbf{v}(\theta_k)\mathbf{v}^H(\theta_k). \tag{27}$$

2. Define parameters $P_+(F), P_-(F)$ and $I_{ab}(F)$ such that:

$$P_{\pm}(F) \triangleq \frac{\mathbf{v}^H(\theta_b)\mathbf{R}^{-1}\mathbf{v}(\theta_b) \pm F\mathbf{v}^H(\theta_a)\mathbf{R}^{-1}\mathbf{v}(\theta_a)}{2} \quad \text{and} \quad I_{ab}(F) \triangleq F\left|\mathbf{v}^H(\theta_a)\mathbf{R}^{-1}\mathbf{v}(\theta_b)\right|^2. \tag{28}$$

   Define the ratio $l_\lambda(F)$ and sign variable $\mathcal{S}_\lambda(F)$:

$$l_\lambda(F) \triangleq -\frac{P_-(F) + \sqrt{P_+^2(F) - I_{ab}(F)}}{P_-(F) - \sqrt{P_+^2(F) - I_{ab}(F)}}; \quad \mathcal{S}_\lambda(F) \triangleq \text{sign}\left[P_-(F) - \sqrt{P_+^2(F) - I_{ab}(F)}\right]. \tag{29}$$

3. The desired exact pairwise error probability for the Capon algorithm is given by

$$\boxed{P_e^{Capon}(\theta_a|\theta_b) = 0.5 \cdot \{1 + \mathcal{S}_\lambda(1)\} - \mathcal{S}_\lambda(1) \cdot \mathcal{F}[l_\lambda(1), L - N + 2].} \tag{30}$$

These pairwise error probabilities conveniently consist of finite sums involving no numerical integration.

The Bartlett statistic evaluated at two test points is given by

$$P_{Bartlett}(\theta_a) = \frac{1}{L} \cdot \mathbf{v}^H(\theta_a)\widehat{\mathbf{R}}\mathbf{v}(\theta_a), \quad P_{Bartlett}(\theta_b) = \frac{1}{L} \cdot \mathbf{v}^H(\theta_b)\widehat{\mathbf{R}}\mathbf{v}(\theta_b). \tag{31}$$

The desired pairwise error probability is given by the following

$$P_e^{Bartlett}(\theta_a|\theta_b) \triangleq \Pr\left[P_{Bartlett}(\theta_a) > P_{Bartlett}(\theta_b)|\,\mathcal{A}\right]. \tag{32}$$

The algorithm for calculation of the Bartlett error probability is exactly the same as the Capon with minor parameter swaps. In particular, the parameter definitions of step 2 should replace $\mathbf{R}^{-1}$ with $\mathbf{R}$, θ_a with θ_b, and θ_b with θ_a, and in step 3 $L - N + 2$ should be replaced with L in (30). The proof of these probabilities is given in Appendix A.

4.2.1 A Simple Large Sample Approximation to Pairwise Error Probabilities

While the finite sum of (30) is simple to compute for small values of $L-N+2$, it can become problematic for large values due to the binomial coefficient. The ratio $l_\lambda(1)$ approaches zero as the SNR increases. Thus, the pairwise error probabilities of the Capon algorithm are given by the tails of the complex F-statistic $F_{L-N+2,L-N+2}$ that are equivalently represented by the tails of an associated complex beta statistic $\beta_{L-N+2,L-N+2}$ (see Proposition C.5 of Appendix C). In particular, let $J = L-N+2$, and note that[14] $F_{J,J} \stackrel{d}{=} -1 + 1/\beta_{J,J}$. Thus, it follows that the probability in the tails can be derived from the relations

$$\Pr\left(F_{J,J} \leq x\right) = \Pr\left(-1 + 1/\beta_{J,J} \leq x\right) = \Pr\left(\beta_{J,J} > \frac{1}{1+x}\right). \tag{33}$$

Note that the pdf of this beta random variable has perfect symmetry in $[0,1]$:

$$P_{\beta_{J,J}}(\beta) \propto [\beta(1-\beta)]^{J-1}. \tag{34}$$

The first and second moments are easily shown to be

$$E\left\{\beta_{J,J}\right\} = \frac{1}{2}, \quad E\left\{\beta_{J,J}^2\right\} = \frac{J+1}{2(2J+1)}. \tag{35}$$

Due to the perfect symmetry of the pdf of this beta statistic, it is reasonable to approximate the beta tails with those of a Gaussian via[15]

$$\Pr\left(F_{J,J} \leq x\right) \simeq \mathcal{Q}\left(\frac{\frac{1}{1+x} - \frac{1}{2}}{\sqrt{\frac{J+1}{2(2J+1)} - \frac{1}{4}}}\right) \tag{36}$$

where $\mathcal{Q}(\cdot)$ is related to the complementary error function. Since this error function is based on the real Gaussian distribution with zero mean and variance of one half, the m standard deviation point in the tail is given by satisfying the equation

$$\frac{\frac{1}{1+x} - \frac{1}{2}}{\sqrt{2}\sqrt{\frac{J+1}{2(2J+1)} - \frac{1}{4}}} = \frac{m}{\sqrt{2}}. \tag{37}$$

Solving for x one obtains the desired threshold for the m standard deviation tail point:

$$\alpha(m,J) \simeq \left[1 - \frac{m}{\sqrt{2J+1}}\right] \Big/ \left[1 + \frac{m}{\sqrt{2J+1}}\right]. \tag{38}$$

[14] If random variable A has the same pdf as random variable B, then they are said to be equal in distribution, and this is denoted by $A \stackrel{d}{=} B$.

[15] The complementary distribution function of the standard Gaussian is denoted by $\mathcal{Q}(\cdot)$. It is related to the well-tabulated error function $\mathrm{erf}(\cdot)$ and complementary error function $\mathrm{erfc}(\cdot)$; namely, $\mathcal{Q}(x) \stackrel{\triangle}{=} \frac{1}{2}\mathrm{erfc}\left(\frac{x}{\sqrt{2}}\right) = \frac{1}{2}\left[1 - \mathrm{erf}\left(\frac{x}{\sqrt{2}}\right)\right] = \frac{1}{\sqrt{2\pi}}\int_x^\infty e^{-t^2/2}dt$. See [1, 5] for more details.

This tail threshold will be of use in Section 5. Equation (36) leads to the following large sample approximation of the Capon algorithm pairwise error probabilities:

$$P_e^{Capon}(\theta_a|\theta_b) \simeq 0.5 \cdot \{1 + \mathcal{S}_\lambda(1)\} - \mathcal{S}_\lambda(1) \cdot \mathcal{Q}\left(\frac{\frac{1}{1+l_\lambda(1)} - \frac{1}{2}}{\sqrt{\frac{L-N+3}{2[2(L-N+2)+1]} - \frac{1}{4}}} \right). \tag{39}$$

Equation (36) similarly leads to the following large sample approximation of the Bartlett algorithm pairwise error probabilities:

$$P_e^{Bartlett}(\theta_a|\theta_b) \simeq 0.5 \cdot \{1 + \mathcal{S}_\lambda(1)\} - \mathcal{S}_\lambda(1) \cdot \mathcal{Q}\left(\frac{\frac{1}{1+l_\lambda(1)} - \frac{1}{2}}{\sqrt{\frac{L+1}{2(2L+1)} - \frac{1}{4}}} \right) \tag{40}$$

where for the Bartlett algorithm $J = L$ and the aforementioned parameter swaps have been assumed. These approximations work well for large values of the degrees of freedom parameter (good for $J > 40$ approximately), and can be valuable for system design and analysis, since the tail probabilities of the Gaussian are well tabulated. Indeed, this approximation proves quite useful for predicting the Capon (and Bartlett) threshold SNR directly in closed form.

5. A METHOD OF DIRECT THRESHOLD SNR APPROXIMATION: A SINGLE PLANEWAVE SIGNAL IN WHITE NOISE

The method of threshold SNR prediction presented in Sections 4.1–4.2 requires an initial prediction of the MSE curve, from which a subsequent estimate of the threshold SNR can be easily inferred. The predicted MSE curve is useful, as it extends the measure of parameter accuracy of the Capon (and Bartlett) algorithm well into the threshold region. It is desired, however, in this section to consider direct calculation of the threshold SNR that does not require an initial MSE prediction. This will be done for the canonical case of a single planewave signal in white noise.

Steinhardt and Bretherton [48] derived a closed form expression for the threshold SNR of ML estimation of the frequency of a sinusoid in AWGN. The simple analytic forms of the outlier probabilities and the asymptotic MSE expression (given by the CRB) made such a calculation tractable. Since such niceties are not available for the Capon algorithm, the approach taken herein will build upon the premise that *the MSE consists solely of local error contributions when the search algorithm obtains its maximum from the local interval containing the unique global maximum of the underlying ambiguity function with near probability 1.* The threshold SNR, or equivalently the smallest SNR at which this local error domination occurs, will be approximated by using the pairwise error probability associated with the most significant contender to the true global maximum; namely, the location of the largest false peak of the ambiguity function.

Let the location of the global maximum of the ambiguity function $\psi_{Capon}(\theta)$ be given by $\theta_{GM} = \theta_1$, and let the location of the largest competing local maximum (location of the highest sidelobe level) be given by $\theta_{LS} = \theta_2$. The true data covariance is clearly given by $\mathbf{R} = \sigma^2\mathbf{I} + \sigma_S^2\mathbf{v}(\theta_1)\mathbf{v}^H(\theta_1)$. For simplicity of notation, define the following variables

$$x = \sigma_S^2/\sigma^2, \;\; v_1 = ||\mathbf{v}(\theta_1)||^2, \;\; v_2 = ||\mathbf{v}(\theta_2)||^2, \;\; v_{12} = \left|\mathbf{v}^H(\theta_2)\mathbf{v}(\theta_1)\right|^2, \;\; \zeta = 1/\sigma^2. \tag{41}$$

Using the matrix inversion lemma, it is straightforward to show that the parameters of step 2 of Section 4.2 can be written in the form

$$P_{\pm}(1) = \frac{1}{2}\left[\frac{\zeta}{x + \dfrac{1}{v_1}} \pm \zeta v_2 \mp \frac{\zeta v_{12}}{x + v_1}\right], \;\; I_{12}(1) = \frac{\zeta^2 v_{12}}{(1 + x v_1)^2}. \tag{42}$$

The ratio $l_\lambda(1)$ is clearly SNR dependent and defines the argument of the F distribution in (30) and the complementary error function in (39) that determines the probability of an outlier. Thus, the smallest SNR at which local error domination occurs can be inferred by finding the value of $l_\lambda(1)$ necessary for "near enough" to zero error probability. The needed proximity to zero error probability is in general a fairly complicated function of (i) the ambiguity function and its several derivatives evaluated at the true source location, and (ii) the mathematical form of the error probability itself. *Empirical analysis of uniform linear arrays (ULAs) indicates, however, that for the large sample case the error probability when evaluated at the threshold SNR is approximately that obtained about four standard deviations out in the tails of the Gaussian approximation (39).* Denote the threshold value of the m standard deviation tail by α that is approximately given by

(38). Define the variables

$$\xi \triangleq \left[\frac{1+\alpha}{1-\alpha}\right]^2, \quad \psi \triangleq \frac{\xi+1}{\xi-1}, \quad c_\phi^2 \triangleq \frac{v_{12}}{v_1 v_2}, \quad s_\phi^2 \triangleq 1-c_\phi^2, \quad \text{and} \quad ||\mathbf{v}(\theta_k)||^2 = \gamma, \quad \text{for } k=1,2 \tag{43}$$

where c_ϕ^2 is the geometric cosine [18] and it is assumed that the scanning vectors are of equal norm. It can be shown [with (42) and elementary algebra] that satisfying the constraint $l_\lambda(1) = \alpha(4, L-N+2)$ requires obtaining the correct real root of the following quartic equation in the SNR variable x:

$$x^4 + ax^3 + bx^2 + cx + d = 0 \tag{44}$$

where the coefficients of the quartic are given by the following equations:

$$\begin{aligned} a &= 2\gamma s_\phi^2 + \frac{2}{\gamma}(1-\psi) \\ b &= \frac{4c_\phi^2}{\gamma^2(\xi-1)} + \gamma^2 s_\phi^4 - 2c_\phi^2 + 2(1-\psi)\left(\frac{1}{\gamma^2} + 1 + s_\phi^2\right) \\ c &= \frac{8c_\phi^2}{\gamma(\xi-1)} + 2\left[\frac{1}{\gamma}\left(1+s_\phi^2\right) + \gamma s_\phi^4\right] - 2\psi\left[s_\phi^2\left(\gamma + \frac{1}{\gamma}\right) + \frac{1}{\gamma}\right] \\ d &= \frac{4c_\phi^2}{\xi-1} + c_\phi^4 + 2s_\phi^2(1-\psi). \end{aligned} \tag{45}$$

One can argue that at least one of the roots is guaranteed to be real and non-negative, yielding the desired threshold SNR by the intermediate-value theorem of elementary calculus when applied to the continuous F distribution of (30), or its continuous large sample approximation (39). The closed form solution to the quartic equation is known [56, 22]. The common approach is to convert the quartic to a subsidiary or depressed cubic:

$$\begin{gathered} y^3 + py^2 + qy + r = 0; \\ \text{where } \; p = b; \;\; q = ac - 4d; \;\; r = a^2 d + c^2 - 4bd. \end{gathered} \tag{46}$$

The known solution for the roots of a cubic equation can now be applied, from which the solution of the original quartic will then follow. Define the variables

$$u = q - p^2/3; \;\; v = r - pq/3 + 2(p/3)^3; \;\; D = 4(u/3)^3 + v^2. \tag{47}$$

One of the roots of the subsidiary cubic[16] is given by the following equation

$$Y = \begin{cases} (u/3)[2/(\sqrt{D}+v)]^{(1/3)} - [(\sqrt{D}+v)/2]^{(1/3)} - p/3, & D > 0; \\ \\ 2\sqrt{(-u/3)} \times \cos\left\{\frac{1}{3}\cos^{-1}\left[\frac{-v}{2(-u/3)^{(3/2)}}\right]\right\} - p/3, & D \le 0 \end{cases} \tag{48}$$

[16]There are obviously three roots to the subsidiary cubic, and in theory it doesn't matter which solution is used to obtain the final solutions to the quartic equation. Thus, the root possessing the simplest analytic form was chosen for this presentation.

where the form of the solution depends on the sign of the discriminant D. Defining the variables

$$g = (a/2) - \sqrt{(a/2)^2 - b - Y}; h = -(Y/2) - \sqrt{(Y/2)^2 - d}, \tag{49}$$

the desired real non-negative root of the original quartic that yields the desired threshold SNR of the Capon algorithm is given by

$$\boxed{\mathrm{SNR}_{TH}^{Capon}\left(c_\phi^2, \gamma, L, N\right) \simeq -(g/2) + \sqrt{(g/2)^2 - h}.} \tag{50}$$

Applying the same approach to the Bartlett algorithm results in the quadratic equation $\tilde{A}x^2 + \tilde{B}x + \tilde{C} = 0$, whose solution yields the desired threshold SNR. The coefficients are easily shown to be

$$\tilde{A} = \gamma^4(\xi - 1)s_\phi^4, \;\; \tilde{B} = -4\gamma^3 s_\phi^2, \;\; \tilde{C} = -4\gamma^2 s_\phi^2. \tag{51}$$

The desired threshold SNR for the Bartlett algorithm uses tail threshold $\alpha(4, L)$ and is given by the quadratic formula:

$$\boxed{\mathrm{SNR}_{TH}^{Bartlett}\left(c_\phi^2, \gamma, L, N\right) \simeq \frac{2}{\gamma s_\phi^2(\xi - 1)}\left[1 + \sqrt{1 + s_\phi^2(\xi - 1)}\right].} \tag{52}$$

While the expression for the Capon threshold SNR could benefit from further asymptotic simplification, the Bartlett threshold SNR expression is rather intuitive. Note that the Bartlett threshold SNR is inversely proportional to the steering vector norm γ. This makes sense because the norm directly impacts the element level SNR; in fact, one could assume unit norm and absorb γ into the element level SNR. Larger γ leads to high element level SNRs, and thus a lower threshold value can be tolerated. Smaller γ leads to low element level SNRs, and thus a higher threshold value is needed. It is also reasonable to interpret γ as a measure of the effective array gain. Note further that the Bartlett threshold SNR is also inversely proportional to the geometric sine variable s_ϕ^2. If the steering vector for the largest sidelobe ambiguity direction is strongly correlated with the steering vector of the true signal direction, then the competing sidelobe level will be high and s_ϕ^2 will be small. As s_ϕ^2 becomes small, the Bartlett threshold SNR expression predicts that a much higher threshold SNR value is necessary to overcome the influence of the competing sidelobe.

The utility and accuracy of these results is demonstrated in Section 9.

6. A MEASURE OF THE PROBABILITY OF RESOLUTION FOR THE CAPON AND BARTLETT ALGORITHMS

Empirical analyses (presented in Section 9) corroborate the success of the adaptation of MIE to the Capon and Bartlett algorithms presented in Section 4 for well separated sources. When sources are not well separated, but are closely spaced, then empirical based MSE curves tend to depart in form from the typical composite curve illustrated in Figure 1. MIE as described in Section 4 will not predict these observed nontypical MSE curves, because it does not account for the impact of unresolved sources on the ambiguity function (at low enough SNRs unresolved sources lead to a single peak of the ambiguity function), and it does not account for intersource error contributions to the MSE, that can occur even after signals are well resolved.

A useful measure of the probability of resolution, however, can be defined that provides good prediction of the SNR at which sources can be resolved by the Capon algorithm (and Bartlett, although the usual Fourier/Rayleigh limit suffices for this conventional approach), that in turn serves as a lower bound on the threshold SNR [25]. Appendix A provides the derivation of the exact cdf and pdf for the following ratio of power spectral estimates:

$$F_{\Delta}(\theta_a,\theta_b)=\frac{P_{Capon}(\theta_a)}{P_{Capon}(\theta_b)}=\frac{\mathbf{v}^H(\theta_b)\widehat{\mathbf{R}}^{-1}\mathbf{v}(\theta_b)}{\mathbf{v}^H(\theta_a)\widehat{\mathbf{R}}^{-1}\mathbf{v}(\theta_a)};\;\; \tilde{F}_{\tilde{\Delta}}(\theta_a,\theta_b)\stackrel{\triangle}{=}\frac{P_{Bartlett}(\theta_a)}{P_{Bartlett}(\theta_b)}=\frac{\mathbf{v}^H(\theta_a)\widehat{\mathbf{R}}\mathbf{v}(\theta_a)}{\mathbf{v}^H(\theta_b)\widehat{\mathbf{R}}\mathbf{v}(\theta_b)}. \quad (53)$$

The derived cdf and pdf hold for any arbitrary hpd data covariance $\mathbf{R}$. For a two closely spaced sources scenario of the form

$$\mathbf{R}=\mathbf{R}_N+\sigma^2_{S_a}\mathbf{v}(\theta_0)\mathbf{v}^H(\theta_0)+\sigma^2_{S_b}\mathbf{v}(\theta_0+\delta\theta)\mathbf{v}^H(\theta_0+\delta\theta), \quad (54)$$

define parameter θ_{MP} as the parameter value for the source with the smallest power out of the ambiguity function, *i.e.*,

$$\theta_{MP}\stackrel{\triangle}{=}\arg\min_{\theta_0,\theta_0+\delta\theta}\psi_{Capon}(\theta). \quad (55)$$

A two-point measure of the Capon probability of resolution can be defined as

$$\begin{aligned} P^{Capon}_{res}(\theta_0,\theta_0+\delta\theta) &\stackrel{\triangle}{=} \Pr\left[P_{Capon}\left(\theta_0+\frac{\delta\theta}{2}\right)\le\rho\cdot P_{Capon}(\theta_{MP})\right] \\ &= \Pr\left[F_{\Delta}\left(\theta_0+\frac{\delta\theta}{2},\theta_{MP}\right)\le\rho\right], \end{aligned} \quad (56)$$

where it is assumed that $0\le\rho\le 1$ is a parameter related to confidence (probabilities actually hold for all non-negative ρ). The parameter ρ essentially defines the desired "dip" in the Capon power spectrum between two closely spaced sources. For example, if $\sigma^2_{S_a}=\sigma^2_{S_b}$ and $\rho=0.5$, then $P^{Capon}_{res}(\theta_0,\theta_0+\delta\theta)$ is the probability that the dip in $P_{Capon}(\theta)$ midway between these two sources is at least 3 dB less than the peak of either source. Similar measures of resolution have been proposed in [18, 25, 50, 72, 61, 47]. The algorithm for computing the Capon two-point probability of resolution is as follows:

1. Choose the desired covariance parameter $\mathbf{R}$ as in (54) and parameters in equations (28)–(29) with $F = \rho$ to obtain $P_{\pm}(\rho)$, $I_{ab}(\rho)$, $\mathcal{S}_{\lambda}(\rho)$, and $l_{\lambda}(\rho)$ with $\theta_a = \theta_0 + \delta\theta/2$ and $\theta_b = \theta_{MP}$.

2. The desired two-point probability of resolution is given by

$$\boxed{P_{res}^{Capon}(\theta_0, \theta_0 + \delta\theta) \;=\; 0.5 \cdot \{1 - \mathcal{S}_{\lambda}(\rho)\} + \mathcal{S}_{\lambda}(\rho) \cdot \mathcal{F}\left[l_{\lambda}(\rho), L - N + 2\right].} \tag{57}$$

This probability of resolution in the large sample case can be well approximated as

$$\boxed{P_{res}^{Capon}(\theta_0, \theta_0 + \delta\theta) \simeq 0.5 \cdot \{1 - \mathcal{S}_{\lambda}(\rho)\} + \mathcal{S}_{\lambda}(\rho) \cdot \mathcal{Q}\left(\frac{\dfrac{1}{1 + l_{\lambda}(\rho)} - \dfrac{1}{2}}{\sqrt{\dfrac{L - N + 3}{2[2(L - N + 2) + 1]} - \dfrac{1}{4}}}\right).} \tag{58}$$

The Bartlett probability of resolution is obtained from a similar formulation:

$$\begin{aligned} P_{res}^{Bartlett}(\theta_0, \theta_0 + \delta\theta) &\stackrel{\triangle}{=} \Pr\left[P_{Bartlett}\left(\theta_0 + \frac{\delta\theta}{2}\right) \leq \rho \cdot P_{Bartlett}(\theta_{MP})\right] \\ &= \Pr\left[\tilde{F}_{\tilde{\Delta}}\left(\theta_0 + \frac{\delta\theta}{2}, \theta_{MP}\right) \leq \rho\right]. \end{aligned} \tag{59}$$

The algorithm for computing the Bartlett probability of resolution is very similar to that for computing the Capon probability of resolution with small parameter changes:

1. Choose the desired covariance parameter $\mathbf{R}$ as in (54) and parameters in equations (28)–(29) with $F = \rho$ to obtain $P_{\pm}(\rho)$, $I_{ab}(\rho)$, $\mathcal{S}_{\lambda}(\rho)$, and $l_{\lambda}(\rho)$ with $\theta_a = \theta_{MP}$ and $\theta_b = \theta_0 + \delta\theta/2$ and $\mathbf{R}^{-1}$ replaced by $\mathbf{R}$.

2. The desired two-point probability of resolution is given by

$$\boxed{P_{res}^{Bartlett}(\theta_0, \theta_0 + \delta\theta) \;=\; 0.5 \cdot \{1 - \mathcal{S}_{\lambda}(\rho)\} + \mathcal{S}_{\lambda}(\rho) \cdot \mathcal{F}\left[l_{\lambda}(\rho), L\right].} \tag{60}$$

This probability of resolution in the large sample case can be well approximated as

$$\boxed{P_{res}^{Bartlett}(\theta_0, \theta_0 + \delta\theta) \simeq 0.5 \cdot \{1 - \mathcal{S}_{\lambda}(\rho)\} + \mathcal{S}_{\lambda}(\rho) \cdot \mathcal{Q}\left(\frac{\dfrac{1}{1 + l_{\lambda}(\rho)} - \dfrac{1}{2}}{\sqrt{\dfrac{L + 1}{2(2L + 1)} - \dfrac{1}{4}}}\right).} \tag{61}$$

The numerical results of Section 9 will demonstrate the utility of these measures for predicting the SNRs at which closely spaced sources become resolvable by the Capon or Bartlett method. This resolution SNR also provides a lower bound for the threshold SNR above which the large sample MSE performance predictions of VB and others apply when closely spaced sources are present.

7. DIRECT CLOSED FORM CALCULATION OF THE CAPON RESOLUTION/DETECTION SNR: TWO EQUAL POWER SIGNALS IN WHITE NOISE

The goal of this section is to provide a method for computing the Capon resolution SNR directly that does not require an initial calculation of the probability of resolution curves. This can be accomplished in a manner similar to that used for direct approximation of the threshold SNR described in Section 5.

Let the desired probability of resolution be given by P_d, *e.g.*, if a 90% likelihood of a 3 dB dip ($\rho = 0.5$) occurring between two spectral peaks is desired, then $P_d = 0.90$. This desired resolution probability implies a necessary threshold value for the ratio $l_\lambda(\rho)$. For small sample support L, or in particular small values of $L-N+2$, one must numerically invert the F-distribution given in (57) to obtained the needed threshold $\tilde{\alpha}$. Such inversions are commonplace in adaptive detection analysis, as they provide the required threshold values for detection statistics to maintain a specified probability of false alarm [27, 26, 49]. For large values of $L - N + 2$ (approximately greater than 40), however, a simple inversion is possible using the error function. Recall that the probability is determined by the tails of the complex F distribution, *i.e.*, a calculation of the form $\Pr\left[F_{J,J} \leq \tilde{\alpha}(\epsilon; J)\right] = \epsilon$. Using the large sample approximation of the F distribution discussed in Section 5 and presented for the probability of resolution in equation (58) of Section 6, it is easy to show that the desired tail threshold is well approximated by inverting the error function to obtain:

$$\tilde{\alpha}(\epsilon; J) \simeq \left[\frac{1}{2} + \left(\sqrt{\frac{J+1}{2J+1} - \frac{1}{2}}\right) \mathrm{erfc}^{-1}(2\epsilon)\right]^{-1} - 1. \tag{62}$$

Define the following variables

$$\epsilon = 0.5 \cdot [1 - S_\lambda(\rho)] + S_\lambda(\rho) \cdot P_d, \quad \tilde{\alpha} = \tilde{\alpha}\left(\epsilon; L - N + 2\right), \quad \tilde{\xi} = \left[\frac{\tilde{\alpha} + 1}{\tilde{\alpha} - 1}\right]^2 \tag{63}$$

and let the data covariance for two equal power closely spaced sources in white noise be defined as

$$\mathbf{R} = \sigma^2 \mathbf{I} + \sigma_S^2 \mathbf{v}(\theta_1)\mathbf{v}^H(\theta_1) + \sigma_S^2 \mathbf{v}(\theta_2)\mathbf{v}^H(\theta_2) \tag{64}$$

where clearly the signal directions are given by $\theta_1 = \theta_0$ and $\theta_2 = \theta_0 + \delta\theta$. Let the midpoint angle be denoted by $\theta_3 = \theta_0 + \delta\theta/2$, and define also the following variables

$$\begin{gathered} x = \sigma_S^2/\sigma^2, \quad \zeta = 1/\sigma^2, v_1 = ||\mathbf{v}(\theta_1)||^2, \quad v_2 = ||\mathbf{v}(\theta_2)||^2, \quad v_3 = ||\mathbf{v}(\theta_3)||^2, \\ v_{12} = \mathbf{v}^H(\theta_1)\mathbf{v}(\theta_2), \quad v_{13} = \mathbf{v}^H(\theta_1)\mathbf{v}(\theta_3), \quad v_{23} = \mathbf{v}^H(\theta_2)\mathbf{v}(\theta_3) \end{gathered} \tag{65}$$

[note that v_{12} is defined differently here than in (41)]. Setting $l_\lambda(\rho) = \tilde{\alpha}$ and solving for the SNR variable indicated by x, it can be shown [with elementary algebra] that the desired resolution SNR is obtained as a root of the following quartic equation:

$$x^4 + \tilde{a}x^3 + \tilde{b}x^2 + \tilde{c}x + \tilde{d} = 0 \tag{66}$$

where the coefficients are given by the following ratios

$$\tilde{a} = B/A, \;\; \tilde{b} = C/A, \;\; \tilde{c} = D/A, \;\; \tilde{d} = E/A \tag{67}$$

that are defined in terms of the following variables

$$\begin{array}{rcl} A & = & \tilde{\xi} A_-^2 - A_+^2 + 4\left|A_I\right|^2 \rho \\ B & = & 2\tilde{\xi} A_- B_- - 2A_+ B_+ + 8\rho \mathrm{Re}\left(A_I B_I^*\right) \\ C & = & 2\tilde{\xi} A_- C_- + B_-^2 - \left(2A_+ C_+ + B_+^2\right) + 4\rho\left[2\mathrm{Re}\left(A_I C_I^*\right) + \left|B_I\right|^2\right] \\ D & = & 2\tilde{\xi} B_- C_- - 2B_+ C_+ + 8\rho \mathrm{Re}\left(B_I C_I^*\right) \\ E & = & \tilde{\xi} C_-^2 - C_+^2 + 4\rho\left|C_I\right|^2 . \end{array} \tag{68}$$

These coefficients are expressed in terms of further coefficients defined as follows:

$$A_\pm = \left(1 - \frac{\left|v_{12}\right|^2}{v_1 v_2}\right)\left(v_1 \pm \rho v_3\right) - v_1 + \frac{\left|v_{12}\right|^2}{v_2} \mp \rho \frac{\left|v_{13}\right|^2}{v_1} \pm 2\mathrm{Re}\left(\frac{v_{13}^* v_{12} v_{23}}{v_1 v_2} x^2\right) \mp \rho \frac{\left|v_{23}\right|^2}{v_2} \tag{69}$$

$$B_\pm = \left(\frac{1}{v_1} + \frac{1}{v_2}\right)\left(v_1 \pm \rho v_3\right) - \frac{v_1}{v_2} - \frac{\left|v_{12}\right|^2}{v_1 v_2} \mp \rho \frac{\left|v_{13}\right|^2}{v_1 v_2} \mp \rho \frac{\left|v_{23}\right|^2}{v_1 v_2}, \;\; C_\pm = \frac{\left(v_1 \pm \rho v_3\right)}{v_1 v_2} \tag{70}$$

$$A_I = v_{13}\left(1 - \frac{\left|v_{12}\right|^2}{v_1 v_2}\right) - v_{13} + \frac{v_{13}\left|v_{12}\right|^2}{v_1 v_2}, \;\; B_I = v_{13}\left(\frac{1}{v_1} + \frac{1}{v_2}\right) - \frac{v_{13}}{v_2} - \frac{v_{12} v_{23}}{v_1 v_2}, \;\; C_I = \frac{v_{13}}{v_1 v_2}. \tag{71}$$

The roots of (66) can be obtained using the algorithm described by (46)–(49) from Section 5 swapping (a, b, c, d) with $(\tilde{a}, \tilde{b}, \tilde{c}, \tilde{d})$. The desired real non-negative root of the original quartic that yields the desired resolution SNR of the Capon algorithm for confidence level P_d is given by

$$\boxed{\mathrm{SNR}_{res}^{Capon}\left(v_1, v_2, v_3, v_{12}, v_{13}, v_{23}, L, N, \rho, P_d\right) = -(g/2) + \sqrt{(g/2)^2 - h}.} \tag{72}$$

Although this expression could likewise benefit from an asymptotic simplification [a simple exercise left to the ambitious], it is exact and found to be quite useful for system parameter trade studies and design.

8. SIGNAL MODEL MISMATCH EFFECTS: MSE PREDICTION AND RESOLUTION

The scanning vectors $\mathbf{v}(\theta)$ used to form the Capon spectra $P_{Capon}(\theta)$ are chosen by the user and are therefore subject to errors. The array responses of the signals present in the data, as described by the true underlying covariance parameter $\mathbf{R}$, are likely to differ from the scanning vectors chosen by the user. This difference is historically referred to as signal model mismatch [18], and its presence often limits achievable performance. Accounting for its impact is of particular interest for high-resolution approaches, since signals that do not fall on the scanning search manifold will suffer some degree of suppression by construction[17] [see (3)]. In this section, a strategy for accounting for mismatch in MSE prediction is presented for a single signal in white noise. Extension to colored noise [30] and multiple signals is transparent.

Let the true data covariance be given by $\mathbf{R} = \sigma^2\mathbf{I} + \sigma_S^2\mathbf{d}\mathbf{d}^H$, where the true signal array response is given by $\mathbf{d}$, yet the scanning vectors chosen by the user are given by $\mathbf{v}(\theta)$. It will be assumed that although mismatch is present, the ambiguity function $\psi_{Capon}(\theta) = 1/\mathbf{v}^H(\theta)\mathbf{R}^{-1}\mathbf{v}(\theta)$ remains multimodal and has a unique global maximum in the search domain of interest, the location of which shall be denoted by θ_{GM}. Define the conditioning event $\mathcal{B} = \{$ Global maximum of ambiguity function is at θ_{GM} $\}$. Let the locations of all other local maxima of the ambiguity function within the signal parameter domain of interest when evaluated at a sufficiently large SNR[18] (large enough that the global maximum is evident and located at θ_{GM}) be given by the finite set $\tilde{\mathcal{M}} = \{\theta \,|\, \theta_1, \theta_2, \ldots, \theta_{M-1}\}$. MSE is defined relative to some assumed "true" location of the signal. Let that assumed true location be denoted θ_T. Note that the VB asymptotic local error MSE predictions [57] hold for arbitrary data covariance matrices $\mathbf{R}$. Thus, the asymptotic MSE prediction $\sigma^2_{VB}(\theta_T)$ holds in the presence of signal model mismatch, and no new theory need be developed in the regime of high SNR values for which these predictions hold. The Capon asymptotic local error MSE of the estimate $\widehat{\theta}$ in the presence of mismatch is given by

$$\sigma^2_{VB}(\theta_T) = E\left\{\left(\widehat{\theta} - \theta_T\right)^2\right\} = \left[E\left\{\widehat{\theta} - \theta_T\right\}\right]^2 + E\left\{\left(\widehat{\theta} - \theta_{GM}\right)^2\right\} \tag{73}$$

where the asymptotic bias can be written

$$E\left\{\widehat{\theta} - \theta_T\right\} = E\left\{\widehat{\theta} - \theta_{GM}\right\} + (\theta_{GM} - \theta_T)\,. \tag{74}$$

Regarding the threshold region of MSE performance, the lesson learned in Section 4.1 is that *the correct weights governing the transition of MSE performance from the no information region to*

[17] While it is common practice to diagonally load the estimated data covariance to robustify the Capon beamformer to the deleterious effects of mismatch errors [19, 61, 23], the impact of such regularization shall not be considered herein. Such an analyses is currently underway [42]. It is noteworthy, however, to state herein that the asymptotic MSE performance for a diagonally loaded Capon estimator has been observed to be bounded by that predicted for the unloaded Capon estimator [57], and that predicted for the unloaded Bartlett estimator [21]. It is perhaps straightforward to construct a proof of these bounds based solely on continuity.

[18] For the DOA estimation problem, the location of these maxima is weakly dependent on SNR, but in general this dependence can be significant and should be accounted for (see [30], for example).

the asymptotic region are those given by the interval error probabilities relative to the local interval of the global maximum of the ambiguity function. Thus, the total MSE for this Capon parameter estimate can be approximated by

$$E\left\{\left(\widehat{\theta}-\theta_T\right)^2\middle|\,\mathcal{B}\right\}\simeq\left[1-\sum_{m=1}^{M-1}p\left(\widehat{\theta}=\theta_m\middle|\,\mathcal{B}\right)\right]\cdot\sigma_{VB}^2(\theta_T)+\sum_{m=1}^{M-1}p\left(\widehat{\theta}=\theta_m\middle|\,\mathcal{B}\right)(\theta_m-\theta_T)^2 \quad (75)$$

where the interval error probabilities are approximated by the dominant pairwise error probability of the UB sum:

$$\boxed{p\left(\widehat{\theta}=\theta_m\middle|\,\mathcal{B}\right)\simeq\Pr\left[P_{Capon}(\theta_m)>P_{Capon}(\theta_{GM})|\,\mathcal{B}\right].} \quad (76)$$

Note that the estimation error is with respect to the assumed true target angle θ_T, but the error probabilities are with respect to the location of the true global maximum of the ambiguity function θ_{GM}. Equations (73)–(76) represent the first generalization of MIE MSE prediction to encompass signal model mismatch. These equations provide accurate predictions of mismatch performance and have been recently applied with success to fairly complex high multipath environments where mismatch is often inevitable [30]. A recent analysis has lead to a lower bound on MSE performance when signal mismatch is present within a Bayesian estimation context [67, 70]. The approach presented in this section, although applied to the Capon estimator, is likewise applicable to other nonlinear estimation schemes including the Bartlett algorithm and ML estimation.

Regarding resolution in the presence of mismatch, the two-point measure of the probability of resolution derived in Section 6 holds for all choices of scanning vectors $\mathbf{v}(\theta)$ and hpd covariance matrices $\mathbf{R}$. Thus, no modification or new theory need be developed to handle the impact of signal model mismatch on the resolution of the Capon algorithm.

9. NUMERICAL RESULTS

9.1 Single Broadside Signal in White Noise

Consider a DOA estimation scenario involving a single planewave source in AWGN resulting in a set of signal bearing snapshots $\mathbf{x}(l) \sim \mathcal{CN}[\mathbf{0}, \mathbf{I}+\sigma_S^2 \mathbf{v}(\theta_T)\mathbf{v}^H(\theta_T)]$, $l = 1, 2, \ldots, L$, for an $N = 18$ element uniform linear array (ULA) with slightly less than lambda over two element spacings. The array has a 3 dB beamwidth of 7.2 degrees, and the desired target signal is arbitrarily placed at $\theta_T = 90$ degrees (array broadside). The signal parameter search space of interest is defined to be $\theta \in [60°, 120°]$. The signal parameter to be estimated is clearly the scalar angle of arrival $\theta = \theta_T$. The resulting Monte Carlo simulation-based MSE performance, the Cramér-Rao Bound (CRB), and the MIE-based MSE predictions as a function of the array element level SNR are shown in Figure 3 for the sample support cases of $L = 1.5N, 2N$, and $3N$. The VB asymptotic local error MSE prediction is illustrated for the $L = 2N$ case for comparison. Note that the VB prediction is only valid above the estimation threshold SNR. The MIE MSE prediction is remarkably accurate well into the estimation threshold region, as it continues with accurate prediction where the VB MSE predictions begin to become inaccurate at low SNRs. Note that UB approximation begins to over-predict the MSE in the no information region. Thus, it is hard limited to the variance of a uniform distribution. It is known that the Capon estimator is not asymptotically (SNR$\rightarrow \infty$) efficient for fixed L, such that increasing the SNR does not bring its MSE performance closer to the CRB [61]. This nonefficiency is likewise manifest in these performance curves. [MATLAB code is provided in Appendix D for the benefit of the interested reader, that will reproduce the MSE prediction of this example.]

Figure 3 also illustrates the accuracy of the direct closed form approximation of the threshold SNR given by equation (50). The threshold SNRs indicated by the solid vertical lines use a value of α based on the tails of equation (30) (approximately 5×10^{-5} error probability), whereas the dashed vertical lines use a value of α derived from the tails of the large sample approximation (39) four standard deviations out. The threshold SNR based on (39) becomes more accurate as L increases. Figure 5 further illustrates the utility of this direct calculation by plotting the Capon threshold SNR as a function of the peak sidelobe level c_ϕ^2 and the norm of the array responses γ. Smaller norms and larger sidelobe levels result in higher threshold SNR points with the stronger dependence being on the norm parameter γ. The second plot in Figure 5 shows the impact of increased sample support on the resulting threshold SNR point; reduced finite sample effects result in smaller threshold SNRs, with the stronger dependence being the height of the peak sidelobe level c_ϕ^2.

Figure 4 shows the analogous MSE predictions and Monte Carlo results obtained from processing the same data through the conventional Bartlett algorithm. The MIE-based MSE predictions are very accurate well into the threshold region. Note that for this case of a single planewave signal in AWGN that this conventional beamforming approach results in an efficient estimate of the DOA at high SNRs. It can be shown that the Bartlett algorithm in fact yields the ML estimate in this case [3, 13]. The losses in parameter accuracy seen by the Capon algorithm relative to the CRB in this case are adaptive training losses. Clearly, if there is only a single signal present in a white noise environment, then there is no need to adapt (*i.e.*, there is no interference to cancel). Since the

Capon algorithm unnecessarily attempts to adapt in this benign environment, there is some loss in performance. These losses, however, become gains in the presence of colored noise, or multiple signals. Note also from Figure 4 the remarkable accuracy of the direct threshold SNR calculation of (52). The utility of this direct threshold SNR approximation is further illustrated in Figure 6 where it is plotted versus sidelobe level, sample support, and steering vector norm; in contrast with Figure 5, the Bartlett algorithm is the preferred choice in this case since both optimal accuracy is achieved at high SNRs, and the threshold SNR values are lower.

9.2 Two Signals in White Noise

Next consider the same scenario as in Section 9.1, but with an additional source of equal power included in the environment at 70 degrees. The Capon algorithm MSE performance of both signal parameter estimates is illustrated in Figure 7, and the Bartlett algorithm MSE performance in Figure 8. The MIE predictions remain quite accurate well into the threshold region in both cases. This example also provides a good illustration of the benefit of adaptive processing. The two signals have sidelobe energy that is permitted to interfere with the mainlobe energy of the other signal when using the conventional Bartlett algorithm. This interference introduces a bias (a small one in this case) in DOA estimates at high SNRs that cannot be overcome by larger signal strength. The source of this bias can be traced to the locations of the peaks of the ambiguity function relative to the true signal locations. This is illustrated in Figure 9, where close examination reveals the difference in these locations, and Figure 10 shows the MSE curve of one signal at high SNRs leveling out at the bias. The adaptive Capon algorithm on the other hand places nulls in signal directions it is not steered to. This adaptive nulling minimizes the impact of one signal on the DOA estimation of another. The benefit of this adaptivity is illustrated in Figure 7 as larger signal strength results in improved accuracy. It is noteworthy that the Bartlett algorithm provides better accuracy at the low SNRs in the threshold region, whereas the Capon algorithm MSE performance eventually equals and surpass that of the Bartlett at high SNRs. While neither the Bartlett nor the Capon algorithm are efficient in this case, increased signal strength results in improved parameter estimation accuracy for the Capon algorithm.

9.3 Mismatch: Tilted Minimum Redundancy Linear Array

Section 8 presented a strategy for accounting for mismatch in MSE predictions. As an illustration, consider an $N = 4$ element minimum redundancy linear array (MRLA) [61] that has much higher sidelobes (ambiguities) than a fully populated 7-element ULA (see conventional beampatterns in Figure 11). Mismatch can be introduced by tilting this array, yet processing the data as if the array were not tilted. The adaptation of MIE described in Section 8 can account for this mismatch as illustrated in Figure 12, where several tilt angles have been considered. Note that the MSE predictions accurately capture both the global errors due to the high ambiguities (threshold region), as well as the asymptotic bias resulting from mismatch.

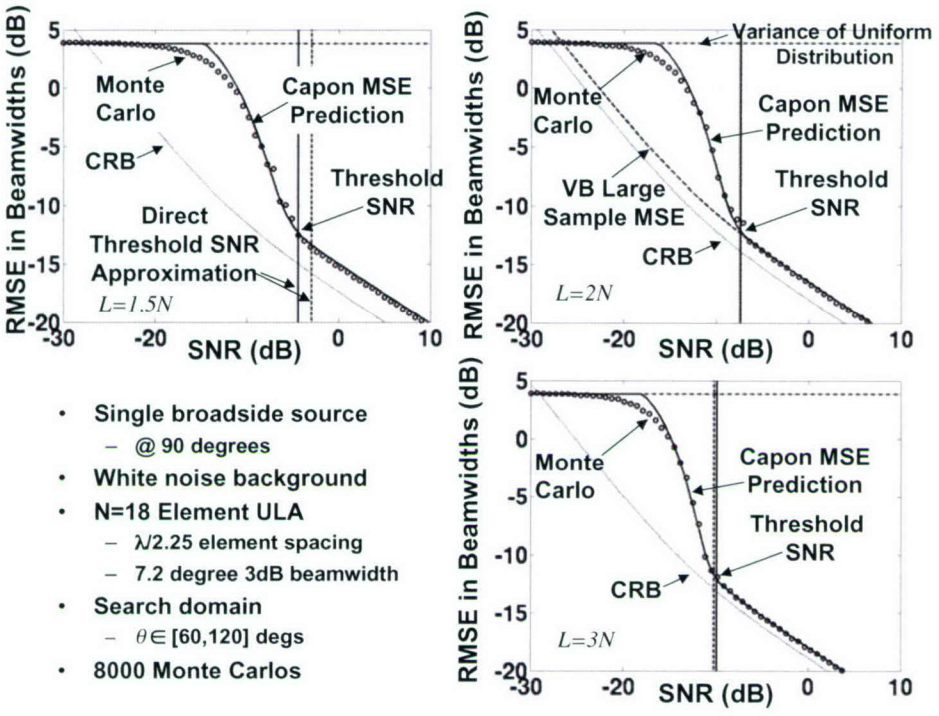

Figure 3. Single source Capon MSE performance, $\theta_1 = \theta_T = 90°$, $L = 1.5N, 2N, 3N$.

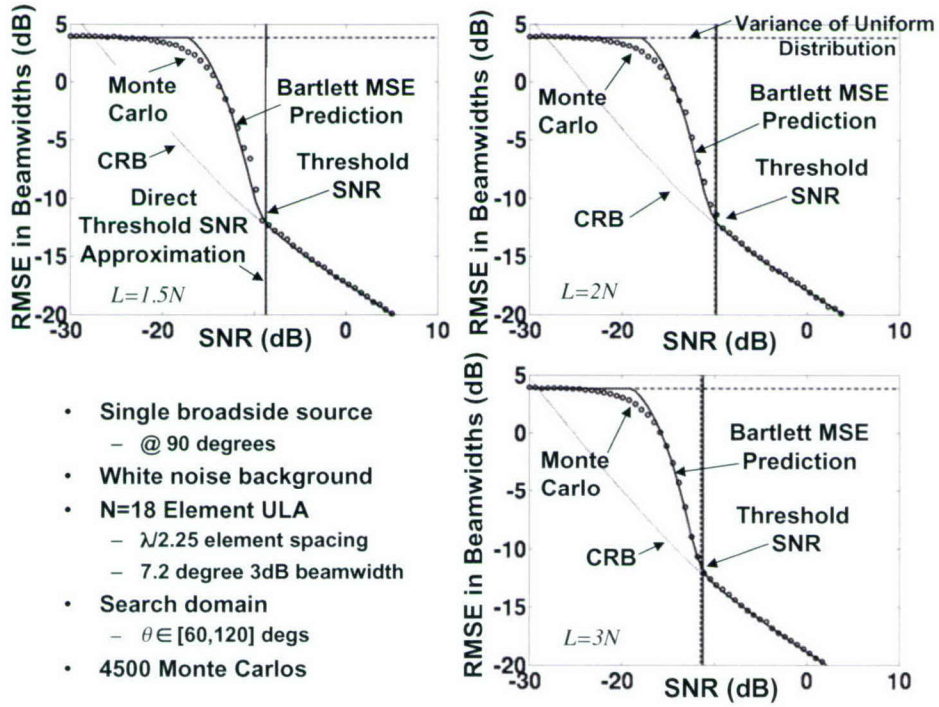

Figure 4. Single source Bartlett MSE performance, $\theta_1 = \theta_T = 90°$, $L = 1.5N, 2N, 3N$.

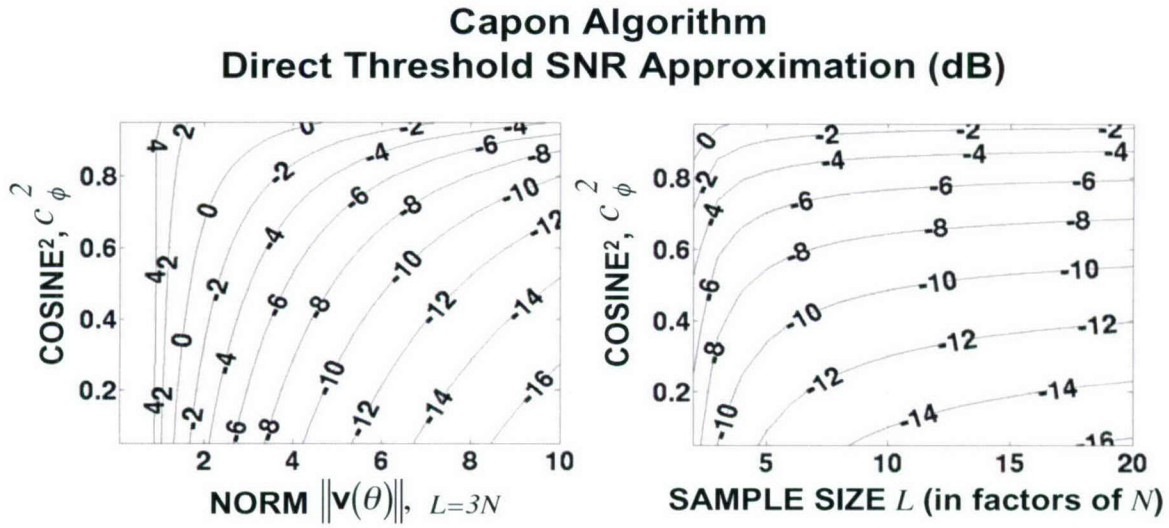

Figure 5. Capon threshold SNR for single source, $N = 18$ element ULA, and $\theta_1 = \theta_T = 90°$.

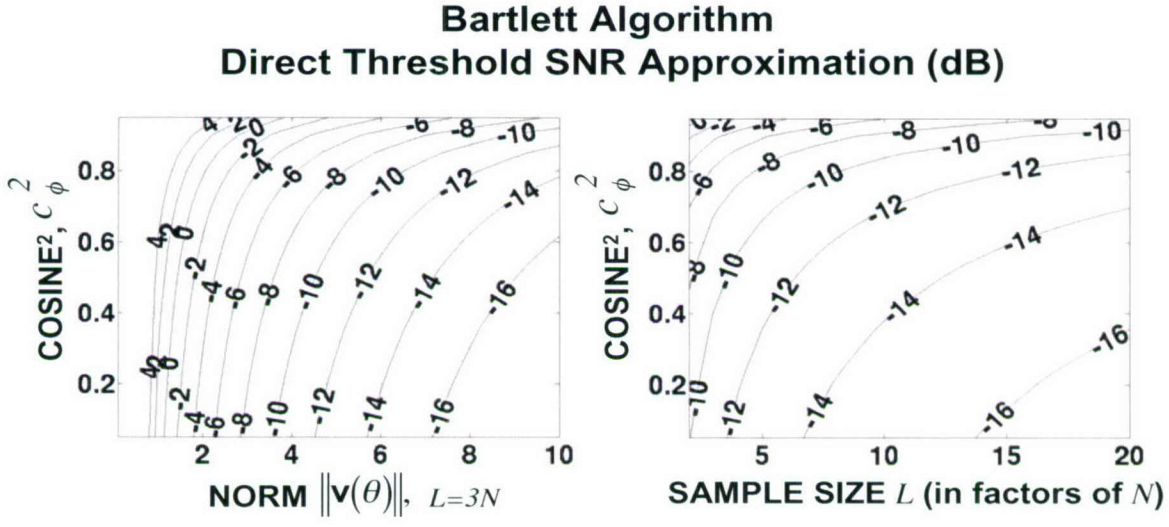

Figure 6. Bartlett threshold SNR for single source, $N = 18$ element ULA, and $\theta_1 = \theta_T = 90°$.

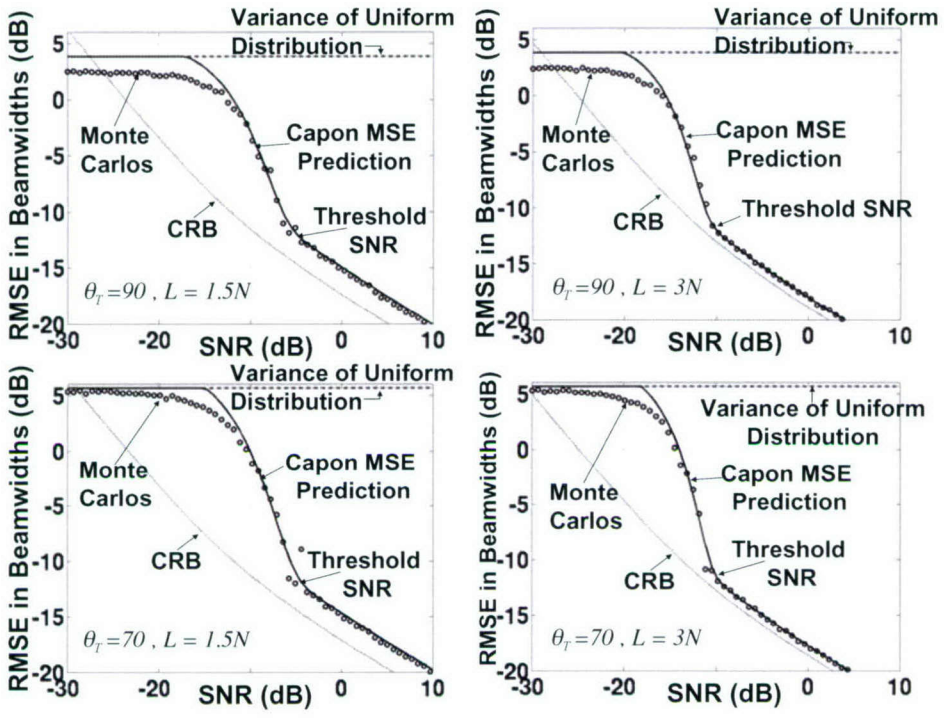

Figure 7. Two-source Capon MSE performance, 1500 Monte Carlo, $\theta_1 = 90°$, $\theta_2 = 70°$, $L = 1.5N, 3N$.

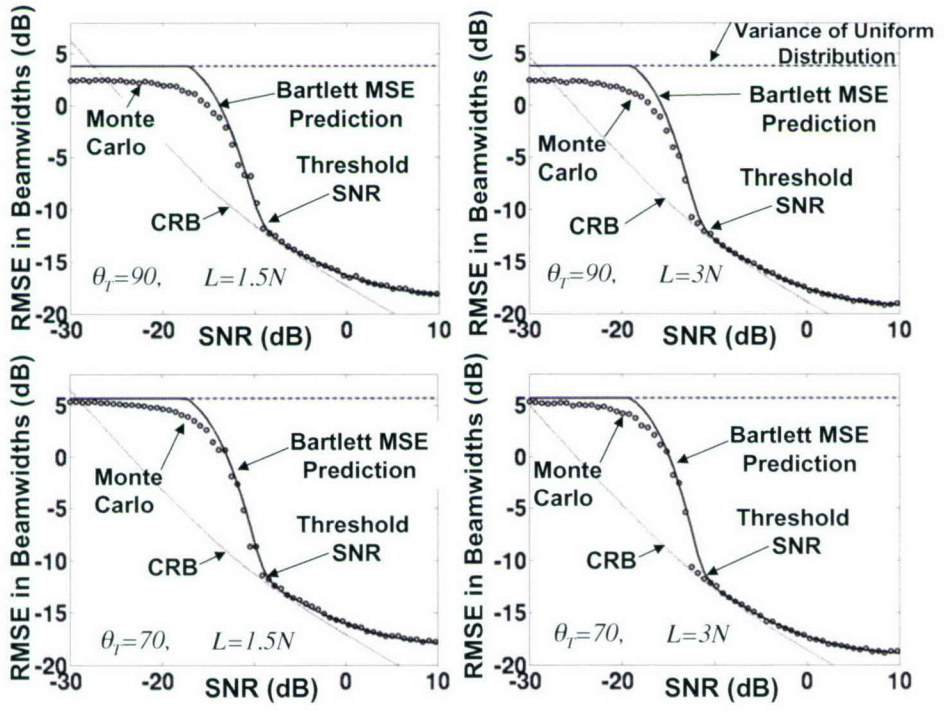

Figure 8. Two-source Bartlett MSE performance, 1500 Monte Carlo, $\theta_1 = 90°$, $\theta_2 = 70°$, $L = 1.5N, 3N$.

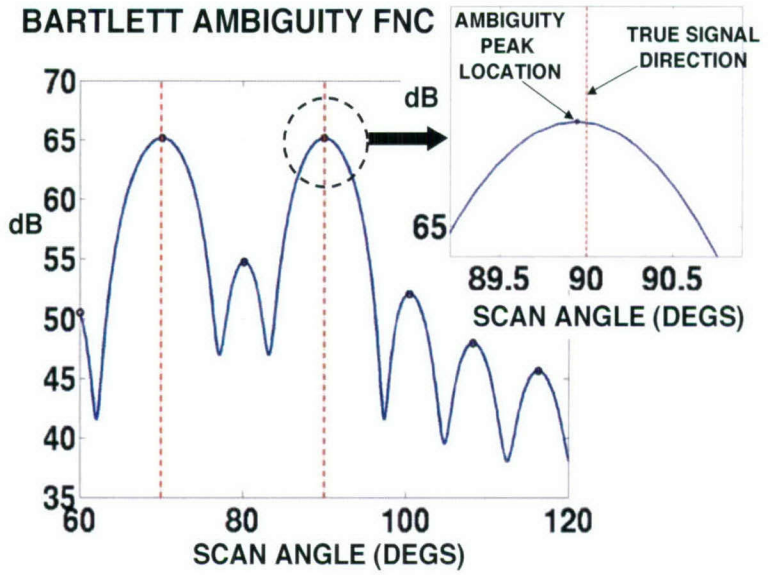

Figure 9. Bartlett ambiguity function at high SNR showing bias origin, $N = 18$ element ULA, $L = 1.5N$ snapshots.

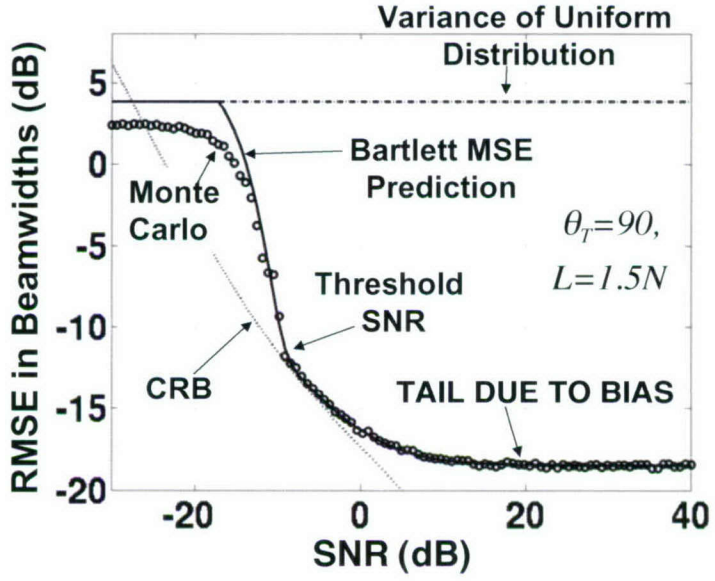

Figure 10. MSE of Bartlett DOA estimate for $N = 18$ element ULA, showing tail due to bias.

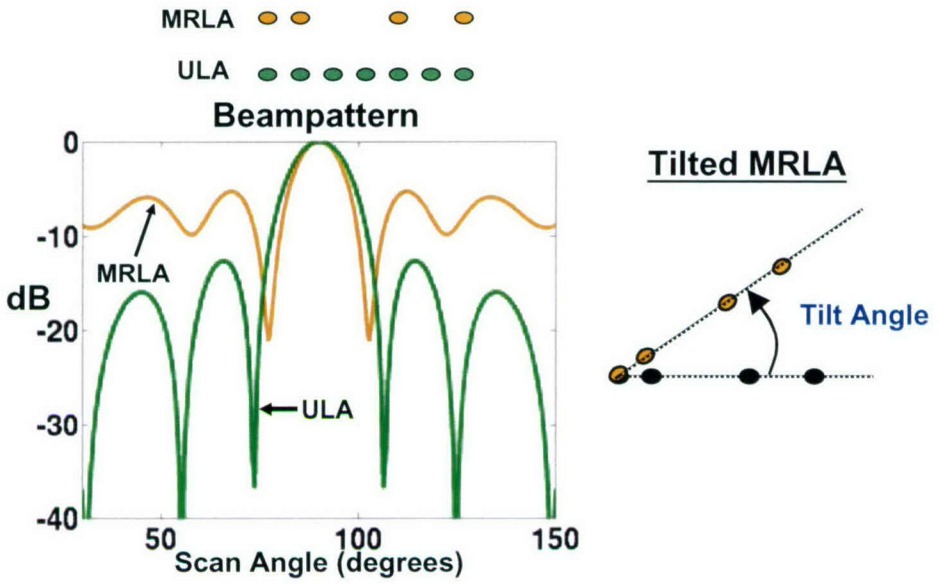

Figure 11. 4-element minimum redundancy linear array: high ambiguities relative to fully populated 7-element ULA.

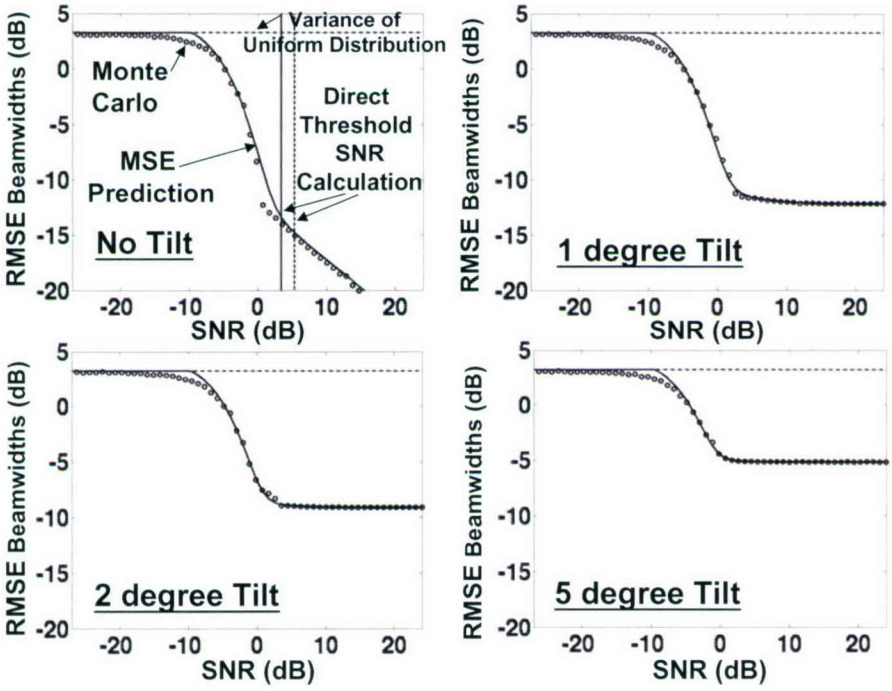

Figure 12. Mismatch example: MSE for tilted MRLA with signal at broadside and $L = 3N$, 1500 Monte Carlo.

9.4 Capon Algorithm Probability of Resolution

The two-point measure of the Capon probability of resolution proposed in Section 6 allows one to predict the SNRs required for a dip in the estimated power spectrum of a specified level to appear between closely spaced sources with high confidence. Consider the $N = 18$ element ULA of the example in Section 9.2, and choose a sample support of $L = 3N$. It is of interest to consider resolution performance as the position of the additional source of equal power varies. The resulting probabilities of resolution for both the Capon and Bartlett algorithm derived in Section 6 are plotted in the upper right of Figure 13 as a function of the angle separation for varied choices of element-level SNR. The superiority of the Capon method is clearly illustrated as resolving power increases with SNR; in contrast, the conventional Bartlett method cannot exceed the Fourier/Rayleigh limit no matter how strong the signals. This is reflected in the Bartlett probability of resolution as all curves are so close they appear as one, only achieving good resolution at separations of a beamwidth or greater. Note that as the signals become arbitrarily close, the two-point probability of resolution must migrate back to 0.5 as the two signals become indistinguishable.

As the next example, let the additional source of equal power be placed at 93 degrees, *i.e.*, at less than half a beamwidth separation. Let the nominal ULA array sensor positions $\mathbf{z}_n$ be independently perturbed by zero mean spherically symmetric Gaussian noise, such that the true array sensor positions are given by $\mathbf{z}_n + \mathbf{e}_n$, where $\mathbf{e}_n \sim \mathcal{N}_3(\mathbf{0}, \mathbf{I}_3\sigma^2_{RMS})$. The lower left and right of Figure 13 show a plot of the Capon probability of resolution as a function of the element level SNR with $L = 2N$ spatial snapshots. Two forms of mismatch are considered: (i) deterministic, and (ii) stochastic. The lower left plot was generated by simply using a single realization of a perturbed array as the root MSE of the perturbations is steadily increased (different perturbations were used for each value of σ^2_{RMS}). The lower right plot represents the resolution observed as one averages over an ensemble of perturbation realizations. Note that the location of the SNR at which resolving occurs appears to be relatively constant as a function of the perturbation level; namely, the maximal resolution is achieved at an element SNR of approximately 15 dB (about 40 dB array SNR). SNR in excess of this value is essentially wasteful. As more mismatch is introduced, the asymptotic likelihood of resolution decreases. The dip in P^{Capon}_{res} before its eventual rise as SNR is varied is simply due to the fact that the underlying Capon ambiguity function has a single peak midway between the two sources for low SNR values (sources are unresolved), as illustrated in the upper left of Figure 13. It is only when the source SNRs exceed that necessary for resolution that two distinct peaks appear at the source locations, with a dip in between. Since the two-points used for the probability of resolution calculation are chosen such that one is at one of the source locations and the other midway between the two sources, a dip occurs before the rise.

Lastly, consider the same array configuration illuminated by two equal power sources. It is desired to determine the SNR required for these sources such that a realization of the Capon spectrum will have a dip (of any level, *i.e.*, $\rho = 1$) between the two signal DOAs with a 90% likelihood, *i.e.*, $P^{Capon}_{res}(\theta_0, \theta_0 + \delta\theta) = 0.9$. This resolution SNR can be determined from the probability of resolution curves obtained from (57). One can likewise make use of the direct calculation provided by (72). Figure 14 plots this resolution SNR as a function of both angle separation $\delta\theta$ and sample support L. Clearly, angle separation is the primary determinant for this resolution SNR. Increasing sample support provides the largest gains when the signals are appreciably separated, thus driving

down the large variance of the adaptive sidelobes [26, 40, 41]. This is evidenced in Figure 14 by the larger swings of the -5 dB and -10 dB contours as L is increased. As the signal separation decreases, these swings are barely noticeable as finite sample effects are less important because the SNRs required for resolution are so large that they dominate the convergence of the adaptive nulls of the Capon processor. Reference [41] explores the statistics of adaptive nulling, and demonstrates that while convergence is impacted by finite sample effects, it is also inversely proportional to signal strength. Hence, only a few training samples of a very strong interferer are required for adequate null formation, whereas many samples are required to drive down the quiescent sidelobes of the adaptive beamformer. These characteristics of adaptive beamforming are well known and serve as catalysts for the study of robust beamforming methods [19, 23].

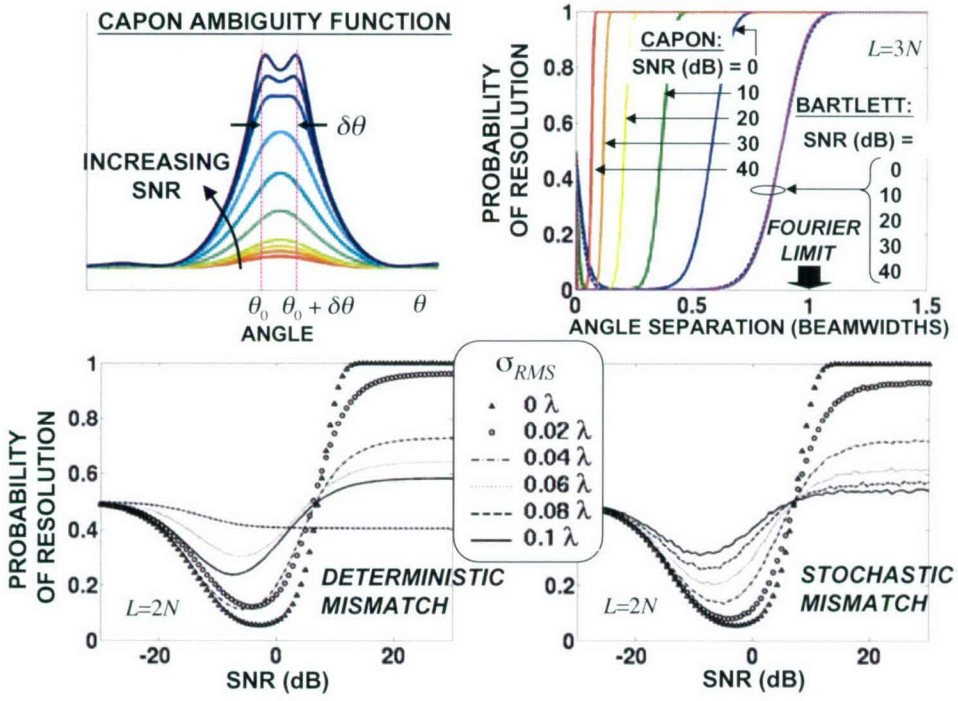

Figure 13. Capon and Bartlett probability of resolution for $N = 18$ element ULA.

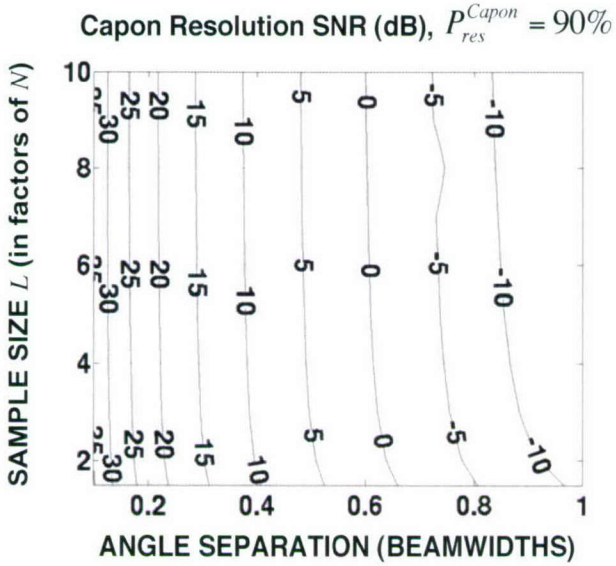

Figure 14. Direct calculation of Capon resolution SNR, $P_{res}^{Capon} = 0.9$.

10. CONCLUSIONS

The method of interval errors (MIE) has been successfully adapted and extended to the Capon-MVDR algorithm and the Bartlett algorithm, providing remarkably accurate prediction of the MSE threshold SNRs for the DOA estimation of an arbitrary number of well separated sources. These SNRs are predicted via simple finite sum expressions for the pairwise error probabilities, involving no numerical integration, and circumventing the need for many time-consuming Monte Carlo simulations. Simple large sample approximations for these error probabilities based on the well-tabulated complementary error function were derived. Closed form approximations of the threshold SNR points of both the Capon and Bartlett algorithms were derived for the large sample canonical case of a single planewave signal in white noise. A new two-point measure of the Capon algorithm probability of resolution was proposed that accurately predicts the SNRs necessary for mutual source resolvability for sources of arbitrary closeness. For convenience, a direct inversion of these resolution probabilities yielding the required resolution/detection SNR was provided for the canonical case of two equal power signals in white noise. This direct inversion simplifies system parameter trade studies. Both the threshold region MSE predictions and resolution probabilities account for colored noise, finite sample effects, and signal model mismatch, and thus, represent valuable design and analysis tools for any system employing the Capon and/or Bartlett algorithm.

APPENDIX A
DERIVATION OF PAIRWISE ERROR PROBABILITIES FOR THE CAPON AND BARTLETT ALGORITHMS

The analysis presented in this report has assumed that each of the K signals of interest possess a single parameter of interest θ_k. Several applications involve signals that possess multiple parameters each, *i.e.*, $\boldsymbol{\theta}_k = [\alpha_{k,1}, \alpha_{k,2}, \ldots, \alpha_{k,A}]^T$ (see [21, 24]). The following derivation is valid for such a case. This is emphasized by the chosen notation.

The desired pairwise error probabilities are defined by the following

$$\begin{aligned} P_e^{Capon}(\boldsymbol{\theta}_a|\boldsymbol{\theta}_b) &= \Pr\left[P_{Capon}(\boldsymbol{\theta}_a) > P_{Capon}(\boldsymbol{\theta}_b)|\,\mathcal{A}\right] \\ P_e^{Bartlett}(\boldsymbol{\theta}_a|\boldsymbol{\theta}_b) &= \Pr\left[P_{Bartlett}(\boldsymbol{\theta}_a) > P_{Bartlett}(\boldsymbol{\theta}_b)|\,\mathcal{A}\right]. \end{aligned} \tag{A-1}$$

The conditioning event $\mathcal{A}$ is satisfied via the appropriate choice of the data covariance $\mathbf{R}$. The following derivations are valid, however, for any arbitrary $\mathbf{R}$; hence, the conditioning notation is omitted. The analysis in [37] requires that the pdf of the ratio F_Δ be derived where

$$F_\Delta \triangleq \frac{\mathbf{v}^H(\boldsymbol{\theta}_b)\widehat{\mathbf{R}}^{-1}\mathbf{v}(\boldsymbol{\theta}_b)}{\mathbf{v}^H(\boldsymbol{\theta}_a)\widehat{\mathbf{R}}^{-1}\mathbf{v}(\boldsymbol{\theta}_a)} \text{ and } \tilde{F}_{\tilde{\Delta}} \triangleq \frac{\mathbf{v}^H(\boldsymbol{\theta}_a)\widehat{\mathbf{R}}\mathbf{v}(\boldsymbol{\theta}_a)}{\mathbf{v}^H(\boldsymbol{\theta}_b)\widehat{\mathbf{R}}\mathbf{v}(\boldsymbol{\theta}_b)}. \tag{A-2}$$

Both of these random variables are non-negative with probability 1, and hence are defined over the domain of non-positive real numbers. Note that the corresponding cdfs are given by

$$\begin{aligned} \Pr\left(F_\Delta \le F\right) &= \Pr\left[\mathbf{v}^H(\boldsymbol{\theta}_b)\widehat{\mathbf{R}}^{-1}\mathbf{v}(\boldsymbol{\theta}_b) - F\cdot\mathbf{v}^H(\boldsymbol{\theta}_a)\widehat{\mathbf{R}}^{-1}\mathbf{v}(\boldsymbol{\theta}_a) \le 0\right] \\ \Pr\left(\tilde{F}_{\tilde{\Delta}} \le \tilde{F}\right) &= \Pr\left[\mathbf{v}^H(\boldsymbol{\theta}_a)\widehat{\mathbf{R}}\mathbf{v}(\boldsymbol{\theta}_a) - \tilde{F}\cdot\mathbf{v}^H(\boldsymbol{\theta}_b)\widehat{\mathbf{R}}\mathbf{v}(\boldsymbol{\theta}_b) \le 0\right]. \end{aligned} \tag{A-3}$$

The desired pairwise error probabilities can be written in terms of these cdfs:

$$P_e^{Capon}(\boldsymbol{\theta}_a|\boldsymbol{\theta}_b) = 1 - \Pr\left(F_\Delta \le 1\right) \text{ and } P_e^{Bartlett}(\boldsymbol{\theta}_a|\boldsymbol{\theta}_b) = 1 - \Pr\left(\tilde{F}_{\tilde{\Delta}} \le 1\right). \tag{A-4}$$

Thus, the goal of this section is to first derive the cdfs of F_Δ and $\tilde{F}_{\tilde{\Delta}}$ from which both the desired pairwise error probabilities follow, and the pdfs of these random variables via differentiation. This analysis draws heavily upon the techniques described in Section 3-5 of [49], involving whitening, orthogonal rotations, use of matrix lemmas, and complex Gaussian-related statistics (as summarized in Appendix C). One such complex Gaussian-related statistic is the complex central F-statistic, obtained from the ratio of two complex central chi-squared statistics, *i.e.*, $\chi_J^2/\chi_B^2 \stackrel{d}{=} F_{J,B}$ with pdf given by[19]

$$P_{F_{J,B}}(F) = \frac{(J+B-1)!}{(J-1)!(B-1)!}\frac{F^{J-1}}{(1+F)^{(J+B)}}, \quad F \ge 0. \tag{A-5}$$

[19] If random variable A has the same pdf as random variable B, then they are said to be equal in distribution, and this is denoted by $A \stackrel{d}{=} B$.

This statistic will be useful in the developments to follow. The cdfs and pdfs of F_Δ and $\tilde{F}_{\tilde{\Delta}}$ will be derived independently in sequence. Let the $N \times L$ data matrix and associated $N \times N$ un-normalized estimated data covariance from which the estimated signal parameters shall be derived be given, respectively, by

$$\mathbf{X} = [\mathbf{x}(1)|\mathbf{x}(2)|\cdots|\mathbf{x}(L)] \text{ and } \widehat{\mathbf{R}} = \mathbf{X}\mathbf{X}^H. \tag{A-6}$$

A.1 Capon Algorithm

Note that the data matrix $\mathbf{X}$ can be represented as a linearly transformed white data matrix $\mathbf{Z}$ that is invariant to any unitary rotation $\mathbf{Q}$, leading to an equivalent stochastic representation for the estimated data covariance matrix:

$$\mathbf{X} \stackrel{d}{=} \mathbf{R}^{1/2}\mathbf{Q}^H\mathbf{Z} \Longrightarrow \widehat{\mathbf{R}}^{-1} = \left(\mathbf{X}\mathbf{X}^H\right)^{-1} \stackrel{d}{=} \mathbf{R}^{-1/2}\mathbf{Q}^H\left(\mathbf{Z}\mathbf{Z}^H\right)^{-1}\mathbf{Q}\mathbf{R}^{-1/2}. \tag{A-7}$$

Let $\mathbf{V} = [\mathbf{v}(\boldsymbol{\theta}_a)|\mathbf{v}(\boldsymbol{\theta}_b)]$, and choose the unitary rotation $\mathbf{Q}$ such that

$$\mathbf{Q}\mathbf{R}^{-1/2}\mathbf{V} = \begin{bmatrix} \boldsymbol{\Delta}_{2\times 2} \\ \mathbf{0}_{(N-2)\times 2} \end{bmatrix} \text{ and let } \boldsymbol{\Delta} = [\boldsymbol{\delta}_a|\boldsymbol{\delta}_b]. \tag{A-8}$$

Note from (A-8) that

$$\boldsymbol{\Delta}^H\boldsymbol{\Delta} = \mathbf{V}^H\mathbf{R}^{-1}\mathbf{V} = \begin{bmatrix} \mathbf{v}^H(\boldsymbol{\theta}_a)\mathbf{R}^{-1}\mathbf{v}(\boldsymbol{\theta}_a) & \mathbf{v}^H(\boldsymbol{\theta}_a)\mathbf{R}^{-1}\mathbf{v}(\boldsymbol{\theta}_b) \\ \mathbf{v}^H(\boldsymbol{\theta}_b)\mathbf{R}^{-1}\mathbf{v}(\boldsymbol{\theta}_a) & \mathbf{v}^H(\boldsymbol{\theta}_b)\mathbf{R}^{-1}\mathbf{v}(\boldsymbol{\theta}_b) \end{bmatrix} = \begin{bmatrix} ||\boldsymbol{\delta}_a||^2 & \boldsymbol{\delta}_a^H\boldsymbol{\delta}_b \\ \boldsymbol{\delta}_b^H\boldsymbol{\delta}_a & ||\boldsymbol{\delta}_b||^2 \end{bmatrix}. \tag{A-9}$$

Partition the white data matrix such that

$$\mathbf{Z} = \begin{bmatrix} \left[\mathbf{Z}_1^H\right]_{2\times L} \\ \left[\mathbf{Z}_2^H\right]_{(N-2)\times L} \end{bmatrix}. \tag{A-10}$$

Using well known matrix inversion lemmas for partitioned matrices, note that the inverse of the whitened sample covariance matrix can be written as

$$\left(\mathbf{Z}\mathbf{Z}^H\right)^{-1} = \begin{bmatrix} \boldsymbol{\Theta}_{2\times 2}^{-1} & \star \\ \star & \star \end{bmatrix} \text{ where } \boldsymbol{\Theta} = \mathbf{Z}_1^H\left[\mathbf{I}_L - \mathbf{Z}_2\left(\mathbf{Z}_2^H\mathbf{Z}_2\right)^{-1}\mathbf{Z}_2^H\right]\mathbf{Z}_1. \tag{A-11}$$

Note that $\boldsymbol{\Theta}$ is white complex Wishart distributed with $L - N + 2$ degrees of freedom [34], denoted by $\boldsymbol{\Theta} \sim \mathcal{CW}(\mathbf{I}_2, L - N + 2)$. Combining this matrix partition with (A-8), it follows that

$$\mathbf{v}^H(\boldsymbol{\theta}_k)\widehat{\mathbf{R}}^{-1}\mathbf{v}(\boldsymbol{\theta}_k) \stackrel{d}{=} \mathbf{v}^H(\boldsymbol{\theta}_k)\mathbf{R}^{-1/2}\mathbf{Q}^H(\mathbf{Z}\mathbf{Z}^H)^{-1}\mathbf{Q}\mathbf{R}^{-1/2}\mathbf{v}(\boldsymbol{\theta}_k) \stackrel{d}{=} \boldsymbol{\delta}_k^H\boldsymbol{\Theta}^{-1}\boldsymbol{\delta}_k \tag{A-12}$$

for $k = a, b$. Thus, the first equation in (A-3) can be written as

$$\begin{aligned} \Pr\left(F_\Delta \le F\right) &= \Pr\left(\boldsymbol{\delta}_b^H\boldsymbol{\Theta}^{-1}\boldsymbol{\delta}_b - F\cdot\boldsymbol{\delta}_a^H\boldsymbol{\Theta}^{-1}\boldsymbol{\delta}_a \le 0\right) \\ &= \Pr\left\{\mathrm{tr}\left[\boldsymbol{\Theta}^{-1}\left(\boldsymbol{\delta}_b\boldsymbol{\delta}_b^H - F\cdot\boldsymbol{\delta}_a\boldsymbol{\delta}_a^H\right)\right] \le 0\right\} \\ &= \Pr\left\{\mathrm{tr}\left[\boldsymbol{\Theta}^{-1}\left(\mathbf{Q}_F\boldsymbol{\Lambda}(F)\mathbf{Q}_F^H\right)\right] \le 0\right\} \\ &= \Pr\left\{\mathrm{tr}\left[\boldsymbol{\Theta}^{-1}\boldsymbol{\Lambda}(F)\right] \le 0\right\}, \end{aligned} \tag{A-13}$$

The last equality in (A-13) follows from the invariance of complex white Gaussian data to unitary rotations [34, 49]. Define the following variables for $\mathbf{\Theta}$:

$$\mathbf{\Theta} = \begin{bmatrix} \theta_{1,1} & \theta_{1,2} \\ \theta_{2,1} & \theta_{2,2} \end{bmatrix} \Longrightarrow \mathbf{\Theta}^{-1} = \begin{bmatrix} \theta^{1,1} & \theta^{1,2} \\ \theta^{2,1} & \theta^{2,2} \end{bmatrix} = \frac{1}{|\mathbf{\Theta}|} \cdot \begin{bmatrix} \theta_{2,2} & -\theta_{1,2} \\ -\theta_{2,1} & \theta_{1,1} \end{bmatrix}. \tag{A-14}$$

From (A-13) it follows that

$$\begin{aligned} \Pr\left(F_\Delta \leq F\right) &= \Pr\left[\theta^{1,1}\lambda_1(F) + \theta^{2,2}\lambda_2(F) \leq 0\right] \\ &= \begin{cases} \Pr\left[\dfrac{\theta^{1,1}}{\theta^{2,2}} \leq \dfrac{-\lambda_2(F)}{\lambda_1(F)}\right], & \text{sign}[\lambda_1(F)] = 1 \\ \Pr\left[\dfrac{\theta^{1,1}}{\theta^{2,2}} > \dfrac{-\lambda_2(F)}{\lambda_1(F)}\right], & \text{sign}[\lambda_1(F)] = -1. \end{cases} \end{aligned} \tag{A-15}$$

From matrix inversion lemma in (A-14) note that

$$\frac{\theta^{1,1}}{\theta^{2,2}} = \frac{\theta_{2,2}}{\theta_{1,1}} \stackrel{d}{=} \frac{{}_1\chi^2_{L-N+2}}{{}_2\chi^2_{L-N+2}} \tag{A-16}$$

where the last equality in distribution follows from the fact that $\mathbf{\Theta} \sim \mathcal{CW}(\mathbf{I}_2, L-N+2)$. Thus, letting $l_\lambda(F) = -\lambda_2(F)/\lambda_1(F)$, it follows from the origin of (A-5) and (A-15) that

$$\Pr\left(F_\Delta \leq F\right) = 0.5 \cdot \{1 - \text{sign}\left[\lambda_1(F)\right]\} + \text{sign}[\lambda_1(F)] \int_{-\infty}^{l_\lambda(F)} P_{F_{L-N+2,L-N+2}}(a)da. \tag{A-17}$$

Differentiating (A-17), the desired pdf of F_Δ is obtained:

$$P_{F_\Delta}(F;\mathbf{\Delta}) = \begin{cases} \text{sign}[\lambda_1(F)] \cdot P_{F_{L-N+2,L-N+2}}\left[l_\lambda(F)\right] \cdot \dfrac{d}{dF} l_\lambda(F), & F \geq 0 \\ 0, & \text{otherwise} \end{cases} \tag{A-18}$$

where

$$\frac{d}{dF} l_\lambda(F) = \frac{-1}{\lambda_1(F)} \cdot \frac{d}{dF}\lambda_2(F) + \frac{\lambda_2(F)}{[\lambda_1(F)]^2} \cdot \frac{d}{dF}\lambda_1(F). \tag{A-19}$$

Exact closed form expressions for the eigenvalues $\lambda_n(F)$, $n = 1, 2$ and their derivatives are derived in Appendix B. Expressing these eigenvalues in terms of the original system parameters $\mathbf{v}(\boldsymbol{\theta}_a), \mathbf{v}(\boldsymbol{\theta}_b)$, and $\mathbf{R}$ is accomplished with (A-9) yielding their ratio as expressed in (29). The cdf can be written compactly as

$$\Pr\left(F_\Delta \leq F\right) = 0.5 \cdot \{1 - \text{sign}\left[\lambda_1(F)\right]\} + \text{sign}[\lambda_1(F)] \cdot \mathcal{F}[l_\lambda(F), L-N+2] \tag{A-20}$$

from which the pairwise error probabilities easily follow. ■

A.2 Bartlett Algorithm

Note that the data matrix $\mathbf{X}$ can be represented as a linearly transformed white data matrix $\mathbf{Z}$ that is invariant to any unitary rotation $\tilde{\mathbf{Q}}$, leading to an equivalent stochastic representation for the estimated data covariance matrix:

$$\mathbf{X} \stackrel{d}{=} \mathbf{R}^{1/2}\tilde{\mathbf{Q}}^H\mathbf{Z} \Longrightarrow \widehat{\mathbf{R}} = \mathbf{X}\mathbf{X}^H \stackrel{d}{=} \mathbf{R}^{1/2}\tilde{\mathbf{Q}}^H\mathbf{Z}\mathbf{Z}^H\tilde{\mathbf{Q}}\mathbf{R}^{1/2}. \tag{A-21}$$

Let $\mathbf{V} = [\mathbf{v}(\boldsymbol{\theta}_a)|\mathbf{v}(\boldsymbol{\theta}_b)]$ and partition the whitened data matrix as in (A-10). Choose the unitary rotation $\tilde{\mathbf{Q}}$ such that

$$\tilde{\mathbf{Q}}\mathbf{R}^{1/2}\mathbf{V} = \begin{bmatrix} \tilde{\boldsymbol{\Delta}}_{2\times 2} \\ \mathbf{0}_{(N-2)\times 2} \end{bmatrix} \text{ and let } \tilde{\boldsymbol{\Delta}} = [\tilde{\boldsymbol{\delta}}_a|\tilde{\boldsymbol{\delta}}_b]. \tag{A-22}$$

Note from (A-22) that

$$\tilde{\boldsymbol{\Delta}}^H\tilde{\boldsymbol{\Delta}} = \mathbf{V}^H\mathbf{R}\mathbf{V} = \begin{bmatrix} \mathbf{v}^H(\boldsymbol{\theta}_a)\mathbf{R}\mathbf{v}(\boldsymbol{\theta}_a) & \mathbf{v}^H(\boldsymbol{\theta}_a)\mathbf{R}\mathbf{v}(\boldsymbol{\theta}_b) \\ \mathbf{v}^H(\boldsymbol{\theta}_b)\mathbf{R}\mathbf{v}(\boldsymbol{\theta}_a) & \mathbf{v}^H(\boldsymbol{\theta}_b)\mathbf{R}\mathbf{v}(\boldsymbol{\theta}_b) \end{bmatrix} = \begin{bmatrix} ||\tilde{\boldsymbol{\delta}}_a||^2 & \tilde{\boldsymbol{\delta}}_a^H\tilde{\boldsymbol{\delta}}_b \\ \tilde{\boldsymbol{\delta}}_b^H\tilde{\boldsymbol{\delta}}_a & ||\tilde{\boldsymbol{\delta}}_b||^2 \end{bmatrix}. \tag{A-23}$$

Note that the whitened sample covariance matrix can be written as

$$\mathbf{Z}\mathbf{Z}^H = \begin{bmatrix} \left(\mathbf{Z}_1^H\mathbf{Z}_1\right)_{2\times 2} & \star \\ \star & \star \end{bmatrix}. \tag{A-24}$$

Clearly, the matrix $\mathbf{Z}_1^H\mathbf{Z}_1$ is complex central Wishart distributed according to $\mathcal{CW}_2\left(\mathbf{I}_2, L\right)$ [34, 49]. Combining this matrix partition with (A-22), it follows that

$$\mathbf{v}^H(\boldsymbol{\theta}_k)\widehat{\mathbf{R}}\mathbf{v}(\boldsymbol{\theta}_k) \stackrel{d}{=} \mathbf{v}^H(\boldsymbol{\theta}_k)\mathbf{R}^{1/2}\tilde{\mathbf{Q}}^H\mathbf{Z}\mathbf{Z}^H\tilde{\mathbf{Q}}\mathbf{R}^{1/2}\mathbf{v}(\boldsymbol{\theta}_k) \stackrel{d}{=} \tilde{\boldsymbol{\delta}}_k^H\mathbf{Z}_1^H\mathbf{Z}_1\tilde{\boldsymbol{\delta}}_k \tag{A-25}$$

for $k = a, b$. Thus, the second equation in (A-3) can be written as

$$\begin{aligned} \Pr\left(\tilde{F}_{\tilde{\Delta}} \leq \tilde{F}\right) &= \Pr\left(\tilde{\boldsymbol{\delta}}_a^H\mathbf{Z}_1^H\mathbf{Z}_1\tilde{\boldsymbol{\delta}}_a - \tilde{F}\cdot\tilde{\boldsymbol{\delta}}_b^H\mathbf{Z}_1^H\mathbf{Z}_1\tilde{\boldsymbol{\delta}}_b \leq 0\right) \\ &= \Pr\left\{\mathrm{tr}\left[\mathbf{Z}_1^H\mathbf{Z}_1\left(\tilde{\boldsymbol{\delta}}_a\tilde{\boldsymbol{\delta}}_a^H - \tilde{F}\cdot\tilde{\boldsymbol{\delta}}_b\tilde{\boldsymbol{\delta}}_b^H\right)\right] \leq 0\right\} \\ &= \Pr\left\{\mathrm{tr}\left[\mathbf{Z}_1^H\mathbf{Z}_1\left(\tilde{\mathbf{Q}}_{\tilde{F}}\tilde{\boldsymbol{\Lambda}}(\tilde{F})\tilde{\mathbf{Q}}_{\tilde{F}}^H\right)\right] \leq 0\right\} \\ &= \Pr\left\{\mathrm{tr}\left[\mathbf{Z}_1^H\mathbf{Z}_1\tilde{\boldsymbol{\Lambda}}(\tilde{F})\right] \leq 0\right\}. \end{aligned} \tag{A-26}$$

The last equality in (A-26) follows from the invariance of complex white Gaussian data to unitary rotations [34, 49]. It follows from (A-26) that

$$\begin{aligned} \Pr\left(\tilde{F}_{\tilde{\Delta}} \leq \tilde{F}\right) &= \Pr\left[{}_1\chi_L^2\cdot\tilde{\lambda}_1(\tilde{F}) + {}_2\chi_L^2\cdot\tilde{\lambda}_2(\tilde{F}) \leq 0\right] \\ &= \Pr\begin{bmatrix} & \mathrm{sign}[\tilde{\lambda}_1(\tilde{F})] = 1 & \\ \frac{{}_1\chi_L^2}{{}_2\chi_L^2} & \leq & \frac{-\tilde{\lambda}_2(\tilde{F})}{\tilde{\lambda}_1(\tilde{F})} \\ & > & \\ & \mathrm{sign}[\tilde{\lambda}_1(\tilde{F})] = -1 & \end{bmatrix}. \end{aligned} \tag{A-27}$$

Thus, letting $\tilde{l}_{\tilde{\lambda}}(\tilde{F}) = -\tilde{\lambda}_2(\tilde{F})/\tilde{\lambda}_1(\tilde{F})$, it follows from the origin of (A-5) and (A-27) that

$$\Pr\left(\tilde{F}_{\tilde{\Delta}} \leq \tilde{F}\right) = 0.5 \cdot \left\{1 - \text{sign}\left[\tilde{\lambda}_1(\tilde{F})\right]\right\} + \text{sign}[\tilde{\lambda}_1(\tilde{F})] \int_{-\infty}^{\tilde{l}_{\tilde{\lambda}}(\tilde{F})} P_{F_{L,L}}(a)da. \tag{A-28}$$

Differentiating (A-28), the desired pdf of $\tilde{F}_{\tilde{\Delta}}$ is obtained:

$$P_{\tilde{F}_{\tilde{\Delta}}}(\tilde{F}; \tilde{\boldsymbol{\Delta}}) = \begin{cases} \text{sign}[\tilde{\lambda}_1(\tilde{F})] \cdot P_{F_{L,L}}\left[\tilde{l}_{\tilde{\lambda}}(\tilde{F})\right] \cdot \dfrac{d}{d\tilde{F}} \tilde{l}_{\tilde{\lambda}}(\tilde{F}), & \tilde{F} \geq 0 \\ 0, & \text{otherwise} \end{cases} \tag{A-29}$$

where

$$\frac{d}{d\tilde{F}} \tilde{l}_{\tilde{\lambda}}(\tilde{F}) = \frac{-1}{\tilde{\lambda}_1(\tilde{F})} \cdot \frac{d}{d\tilde{F}} \tilde{\lambda}_2(\tilde{F}) + \frac{\tilde{\lambda}_2(\tilde{F})}{[\tilde{\lambda}_1(\tilde{F})]^2} \cdot \frac{d}{d\tilde{F}} \tilde{\lambda}_1(\tilde{F}). \tag{A-30}$$

Exact closed form expressions for the eigenvalues $\tilde{\lambda}_n(F)$, $n = 1, 2$ and their derivatives are derived in Appendix B. Expressing these eigenvalues in terms of the original system parameters $\mathbf{v}(\boldsymbol{\theta}_a), \mathbf{v}(\boldsymbol{\theta}_b)$, and $\mathbf{R}$ is accomplished with (A-23). The cdf can be written compactly as

$$\Pr\left(\tilde{F}_{\tilde{\Delta}} \leq \tilde{F}\right) = 0.5 \cdot \left\{1 - \text{sign}\left[\tilde{\lambda}_1(\tilde{F})\right]\right\} + \text{sign}[\tilde{\lambda}_1(\tilde{F})] \cdot \mathcal{F}[\tilde{l}_{\tilde{\lambda}}(\tilde{F}), L] \tag{A-31}$$

from which the pairwise error probabilities easily follow. ■

APPENDIX B
EIGENVALUES OF RANK TWO MATRICES

It is desired to derive closed form expressions for the eigenvalues and their derivative with respect to F of the following parameterized rank two matrix:

$$\mathbf{A} = \mathbf{a}\mathbf{a}^H - F \cdot \mathbf{b}\mathbf{b}^H \tag{B-1}$$

where clearly $\mathbf{a}$ and $\mathbf{b}$ are linearly independent. Note that both eigenvectors must be linear combinations of these two vectors such that if $\mathbf{A}\tilde{\mathbf{v}} = \lambda\tilde{\mathbf{v}}$, then there exists some complex scalar β such that $\tilde{\mathbf{v}} = \beta \cdot \mathbf{a} + \mathbf{b}$. Satisfying both conditions requires that

$$\begin{aligned} \mathbf{A}\tilde{\mathbf{v}} &= \lambda\tilde{\mathbf{v}} \\ \left(\mathbf{a}\mathbf{a}^H - F \cdot \mathbf{b}\mathbf{b}^H\right) \cdot (\beta\mathbf{a} + \mathbf{b}) &= \lambda \cdot (\beta\mathbf{a} + \mathbf{b}). \end{aligned} \tag{B-2}$$

This leads to two relations for λ

$$\begin{aligned} \lambda &= ||\mathbf{a}||^2 + (1/\beta)\mathbf{a}^H\mathbf{b} \\ \lambda &= -\left(F\beta\mathbf{b}^H\mathbf{a} + F||\mathbf{b}||^2\right) \end{aligned} \tag{B-3}$$

that when satisfied simultaneously lead to the following quadratic equation for the scalar β

$$\beta^2 \cdot (F\mathbf{b}^H\mathbf{a}) + \beta \cdot (||\mathbf{a}||^2 + F||\mathbf{b}||^2) + (\mathbf{a}^H\mathbf{b}) = 0. \tag{B-4}$$

The quadratic formula leads to the following solutions for the eigenvalues

$$\boxed{\lambda_{1,2}(F) = \left[\frac{||\mathbf{a}||^2 - F||\mathbf{b}||^2}{2}\right] \pm \sqrt{\left[\frac{||\mathbf{a}||^2 + F||\mathbf{b}||^2}{2}\right]^2 - F|\mathbf{a}^H\mathbf{b}|^2}} \tag{B-5}$$

that can be readily differentiated to obtain

$$\boxed{\frac{d}{dF}\lambda_{1,2}(F) = \frac{-||\mathbf{b}||^2}{2} \pm \frac{\left[\frac{||\mathbf{a}||^2||\mathbf{b}||^2 + F||\mathbf{b}||^4}{4}\right] - \frac{|\mathbf{a}^H\mathbf{b}|^2}{2}}{\sqrt{\left[\frac{||\mathbf{a}||^2 + F||\mathbf{b}||^2}{2}\right]^2 - F|\mathbf{a}^H\mathbf{b}|^2}}.} \tag{B-6}$$

■

APPENDIX C
COMPLEX GAUSSIAN-BASED STATISTICS: A SUMMARY

This appendix provides a short summary of statistics related to the complex Gaussian distribution. Similar results for the real Gaussian are well known [34]. These complex analogs are derived in [27].

Let two random vectors be complex normal distributed as $\tilde{\mathbf{z}} \sim \mathcal{CN}_N(\mathbf{0}, \mathbf{I}_N)$ and $\tilde{\mathbf{z}}_\delta \sim \mathcal{CN}_N(\tilde{\mathbf{m}}, \mathbf{I}_N)$.

Proposition C.1 *The pdf of the random variable $\tilde{\rho} = ||\tilde{\mathbf{z}}||^2$ is given by a complex central chi-square of N degrees of freedom:*

$$\tilde{\rho}^{N-1} e^{-\tilde{\rho}}/(N-1)! \qquad \tilde{\rho} \geq 0. \tag{C-1}$$

This distribution is denoted by $\tilde{\rho} \sim \chi^2_N$.

Proposition C.2 *The pdf of the random variable $\tilde{\rho}_\delta = ||\tilde{\mathbf{z}}_\delta||^2$ is given by a complex noncentral chi-square of N degrees of freedom:*

$$\tilde{\rho}_\delta^{N-1} e^{-\tilde{\rho}_\delta} e^{-\delta^2} {}_0F_1(N; \delta^2\, \tilde{\rho}_\delta)/(N-1)!, \;\; \tilde{\rho}_\delta \geq 0 \tag{C-2}$$

where ${}_0F_1(\cdot)$ is a hypergeometric function [1], and the noncentrality parameter is given by $\delta^2 = ||\tilde{\mathbf{m}}||^2$. This distribution is denoted by $\tilde{\rho}_\delta \sim \chi^2_N(\delta)$.

Proposition C.3 *The pdf of the random variable $\tilde{F}_{N,M} = \chi^2_N/\chi^2_M$ where both chi-squared statistics are independent is given by*

$$\frac{(N+M-1)!}{(N-1)!(M-1)!} \frac{\tilde{F}^{N-1}}{(1+\tilde{F})^{(N+M)}}, \;\; \tilde{F} \geq 0, \tag{C-3}$$

a complex central $\tilde{F}$-distribution with N, M degrees of freedom.

Proposition C.4 *The pdf of the random variable $\tilde{F}_{N,M}(\delta) = \chi^2_N(\delta)/\chi^2_M$ where both chi-squared statistics are independent is given by*

$$\frac{(N+M-1)!}{(N-1)!(M-1)!} \frac{\tilde{F}^{N-1}}{(1+\tilde{F})^{(N+M)}} \cdot e^{-\delta^2} {}_1F_1[N+M; N; \delta^2\, \tilde{F}/(1+\tilde{F})], \;\; \tilde{F} \geq 0 \tag{C-4}$$

a complex noncentral $\tilde{F}$-distribution with N, M degrees of freedom, where ${}_1F_1(\cdot;\cdot;\cdot)$ is the confluent hypergeometric function [1]. The cumulative distribution function (cdf) for this random variable is given by

$$Pr(\tilde{F}_{N,M} \leq x) = \frac{x^N}{(1+x)^{N+M-1}} \sum_{k=0}^{M-1} \begin{pmatrix} N+M-1 \\ k+N \end{pmatrix} \cdot x^k \cdot IG_{k+1}\left(\frac{\delta^2}{1+x}\right) \tag{C-5}$$

where $IG_m(a) = e^{-a} \sum_{k=0}^{m-1} a^k/k!$ is the incomplete Gamma function. The cdf for the central complex F is the special case of $\delta = 0$.

Proposition C.5 *The pdf of the random variable* $\tilde{\beta}_{N,M} = 1/(1+\tilde{F}_{M,N})$ *is given by*

$$\frac{(N+M-1)!}{(N-1)!(M-1)!}\tilde{\beta}^{N-1}(1-\tilde{\beta})^{M-1},\ \ 0 \le \tilde{\beta} \le 1 \tag{C-6}$$

a complex central beta distribution. In addition, its cdf is given by the convenient finite sum

$$Pr(\tilde{\beta}_{N,M} \le x) = x^{N+M-1}\sum_{k=0}^{M-1}\left(\begin{array}{c} N+M-1 \\ k \end{array}\right)\cdot\left(\frac{1-x}{x}\right)^{k}. \tag{C-7}$$

Noting that $Pr(\tilde{F}_{N,M} \le x) = Pr(-1+1/\tilde{\beta}_{M,N} \le x)$, a second representation for the cdf of the central $\tilde{F}$ is possible.

Proposition C.6 *The pdf of the random variable* $\tilde{\beta}_{N,M}(\delta) = 1/(1+\tilde{F}_{M,N}(\delta))$ *is given by*

$$\frac{(N+M-1)!}{(N-1)!(M-1)!}\tilde{\beta}^{N-1}(1-\tilde{\beta})^{M-1}\cdot e^{-\delta^2}\sum_{n=0}^{N}\frac{N!(M-1)!}{(N-n)!(M-1-n)!}\frac{\left(\delta^2\right)^n}{n!}(1-\tilde{\beta})^n, \tag{C-8}$$

for $0 \le \tilde{\beta} \le 1$. *This is known as the complex noncentral beta distribution.*

Proposition C.7 *The cdf of the random variable* $\tilde{\beta}_{N,M}(\delta) = 1/(1+\tilde{F}_{M,N}(\delta))$ *is given by*

$$Pr(\tilde{\beta}_{N,M}(\delta) \le x) = 1 - x^{N+M-1}\sum_{m=M}^{N+M-1}\left(\begin{array}{c} N+M-1 \\ m \end{array}\right)\left(\frac{1-x}{x}\right)^{m} IG_{m-M+1}\left(x\cdot\delta^2\right) \tag{C-9}$$

for $x \ge 0$.

APPENDIX D
MATLAB CODE FOR CANONICAL EXAMPLE: SINGLE BROADSIDE PLANEWAVE SIGNAL IN WHITE NOISE

```
function [] = Capon_Alg_MSE;
%-------------------------------------------------------------------------
% This code computes the threshold region mean squared error (MSE) performance of
% the Direction-Of-Arrival (DOA) estimate obtained from the Capon-MVDR algorithm of
% a single planewave signal in white noise as observed on a uniform liinear array (ULA).
% This code is based upon the theoretical results to be published in the IEEE
% Transactions on Signal Processing, 2005.
%
%  Christ D. Richmond, christ@ll.mit.edu, 12/10/2004
%  MIT Lincoln Laboratory, All rights reserved
%-------------------------------------------------------------------------
% SET RUN PARAMETERS...
%----------------------
% Define GLOBAL variables
global run_params;

% Define model parameters...

run_params.N = 18; % Number of array sensors, beams, or spatial channels
run_params.d = 1/2.25; % Element separation in wavelengths
run_params.L = 3 * run_params.N; % Sample support
run_params.K = run_params.L - run_params.N + 2; % Degrees of freedom for F-distribution
                                                % of pairwise error probability
run_params.wl_dB = 0; % White noise level dB
run_params.Ang_low = 90-30; % Lower limit of search angles (degrees);
run_params.Ang_high = 90+30; % Upper limit of search angles (degrees);
run_params.Del_Ang = run_params.Ang_high - run_params.Ang_low; % Degrees
%-----------------
% MVDR / Capon Parameters...
%---------------------------
run_params.Sig_angles = [90]; % True signal direction (degrees; 90degs is broadside)
see_src_no = 1;  % Source # whose MSE is of interest, for multiple signal case
                 % [not included here]
run_params.Tgt_angs_degs =  run_params.Sig_angles;
run_params.No_sigs = length(run_params.Sig_angles);
%-------------------------------------------------------------------------
run_params.SNRs_dB = linspace(-30,15,50)-run_params.wl_dB; % Element level
                                                           % signal-to-noise
                                                           % ratio (SNR) (decibels)
run_params.SNRs = bd(run_params.SNRs_dB); % Element level SNR in power domain
run_params.ULA_BW_degs = ULA_3dB_BW(run_params.N,run_params.d); % Beamwidth for ULA (degs)
%-------------------------------------------------------------------------
% GET TRUE DATA COVARIANCES...
%-----------------------------
R_mvdr = cell(1,length(run_params.SNRs));
Ri_mvdr = cell(1,length(run_params.SNRs));
R_mvdr_sqrt = cell(1,length(run_params.SNRs));
R_mvdr_si = cell(1,length(run_params.SNRs));
```

```
49
50  for usnr = 1:length(run_params.SNRs);
51
52  % function[R,Ri]=getRvan(N,wl_dB,tht,thl_dB,d,flg);
53  [R,Ri] = getRvan(run_params.N,run_params.wl_dB,[run_params.Sig_angles], ...
54                   [run_params.SNRs_dB(usnr)*ones(1,run_params.No_sigs)],run_params.d);
55  R_mvdr{usnr} = R; Ri_mvdr{usnr} = Ri;
56
57  % function [Rsqrt,Rsqrti,DetRsqrt] = get_Rsqrt(R);
58  [Rsqrt,Rsqrti,jnk] = get_Rsqrt(R); R_mvdr_sqrt{usnr} = Rsqrt;  R_mvdr_si{usnr} = Rsqrti;
59
60  end; % for usnr = 1:length(run_params.SNRs);
61  run_params.R_mvdr = R_mvdr; run_params.Ri_mvdr = Ri_mvdr;
62  run_params.R_mvdr_sqrt = R_mvdr_sqrt; run_params.R_mvdr_si = R_mvdr_si;
63  %-------------------------------------------------------------------------
64  run_params.res_fac = 40; % Conventional beamsplit ratio for angle search
65
66  % # grid samples in angle search...
67  run_params.Nres = run_params.res_fac*ceil(180/run_params.ULA_BW_degs);
68  anggs = linspace(run_params.Ang_low,run_params.Ang_high,run_params.Nres);
69  V = van(run_params.N,anggs,run_params.d); % search angles and steering vectors
70  run_params.Vanggs = van(run_params.N,anggs,run_params.d); run_params.anggs = anggs;
71  %-------------------------------------------------------------------------
72  run_params.angsi = run_params.Sig_angles;
73  run_params.Vs = van(run_params.N,run_params.angsi,run_params.d);
74  run_params.V = van(run_params.N,run_params.anggs,run_params.d);
75  %-------------------------------------------------------------------------
76  % COMPUTE ASYMPTOTIC LOCAL ERROR MSE AND BOUNDS...
77  %-----------------------------------------------
78  % Get Cramer-Rao Bound...
79
80  % See C. D. Richmond, "Cramer-Rao Bounds: The Adaptive Array Story," Proceedings of
81  % the Adaptive Sensor Array Processing Workshop, MIT Lincoln Laboratory, March 2000.
82
83  disp(['Computing CRB Local Bounds...']);
84
85  thT = run_params.Tgt_angs_degs;
86  VT = van(run_params.N,thT,run_params.d); % True target array response
87  den_ang = zeros(length(run_params.SNRs),length(run_params.angsi));
88
89  for usnr=1:length(run_params.SNRs); u = usnr; sig_S = run_params.SNRs(usnr);
90  run_params.R = run_params.R_mvdr{usnr}; run_params.Ri = run_params.Ri_mvdr{usnr};
91  %-------------
92  D = van_p(run_params.N,thT,run_params.d);
93  dRsdw = hm( sig_S * ( D*VT' + VT*D' ) ) ; dRsdwds = hm( D*VT' + VT*D' );
94  dRsds = hm( VT*VT' );
95  Rs =  run_params.R_mvdr{usnr}; Rsi = run_params.Ri_mvdr{usnr};
96
97  F = zeros(2); F(1,1) = trace( dRsdw * Rsi * dRsdw * Rsi );
98  F(1,2) = trace( dRsdw * Rsi * dRsds * Rsi );
99  F(2,2) = trace( dRsds * Rsi * dRsds * Rsi ); F(2,1)=conj(F(1,2));
100 %-------------
101 F = run_params.L * hm( F ); J = hm( inv(F) );
102 crbw(usnr) = 1/abs( F(1,1) ); crbws(usnr) = abs( J(1,1) );
```

```
103 den_ang(usnr,:) = 1/abs( J(1,1) );
104 end; % for usnr=1:length(run_params.SNRs); u = usnr;
105
106 crb = 1./den_ang; % CRB in radians
107 %----------------------------------------
108 % Get Vaidyanathan-Buckley (VB) local error Capon MSE ...
109 % Based on C. Vaidyanathan, K. M. Buckley, ''Performance Analysis of the MVDR Spatial
110 % Spectral Estimator,'' IEEE Transactions on Signal Processing, Vol. 43, No. 6,
111 % pp. 1427--1437, June 1995.
112
113 thT = run_params.Tgt_angs_degs;
114 VT = van(run_params.N,thT,run_params.d); % True target array response
115 den_ang = zeros(length(run_params.SNRs),length(run_params.angsi));
116
117 for usnr=1:length(run_params.SNRs);
118
119 run_params.R = run_params.R_mvdr{usnr}; run_params.Ri = run_params.Ri_mvdr{usnr};
120 Rs =  run_params.R_mvdr{usnr}; Rsi = run_params.Ri_mvdr{usnr};
121 thT_true = run_params.Sig_angles(see_src_no);
122 %----------------------------------------
123 % Get asymptotic bias...
124 a = van(run_params.N,thT_true,run_params.d);
125 ap = van_p(run_params.N,thT_true,run_params.d);
126 app = van_p2(run_params.N,thT_true,run_params.d);
127 Ri = run_params.Ri_mvdr{usnr};
128
129 thT_asymp = - real( ap'*Ri*a ) / real( ap'*Ri*ap + a'*Ri*app ) + thT_true;
130 Asymp_Bias = thT_asymp - thT_true; % Only accurate when bias is small...
131 %----------------------------------------
132 % Evaluate at ASYMPTOTIC MSE of angle estimates...
133 a = van(run_params.N,thT_asymp,run_params.d);
134 ap = van_p(run_params.N,thT_asymp,run_params.d);
135 app = van_p2(run_params.N,thT_asymp,run_params.d);
136 ap3 = van_p3(run_params.N,thT_asymp,run_params.d);
137
138 % use notation of VB paper for convenience...
139 L = run_params.L; N = run_params.L; K = run_params.N;
140
141 fpp = 2 * real( ap'*Ri*ap + a'*Ri*app ); B = ap*a' + a*ap';
142 fp3 = 2 * real( 3 * ap'*Ri*app + a'*Ri*ap3 );
143 ED2 = (2 * (N- K) / ( (N-K-1)*(N-K+1) ) ) * real( a'*Ri * B * Ri * ap ) / ( fpp^2 );
144 ED3 = (2 * (N- K) / ( (N-K-1)*(N-K+1) ) ) * real( a'*Ri * B * Ri * app ) / ( fpp^2 );
145 AddBias = ED3 - fp3 * ED2 / ( 2 * fpp );
146
147 % Evaluate using BOTH
148 Bias = Asymp_Bias + AddBias; den_ang(usnr,:) = 1/(Bias^2 + ED2 ); % 1/(VB MSE) in 1/radians
149 end; % for usnr=1:length(run_params.SNRs);
150 %-------------------------------------------------------------------------
151 % COMPUTE GLOBAL ERRORS USING METHOD OF INTERVAL ERRORS (MIE)...
152 %-------------------------------------------------------------
153 disp(['Determining location of local maxima/peaks/sidelobes...']);
154
155 peak_SLL_idx = cell(length(run_params.angsi),1);
156 peak_SLL_angs = cell(length(run_params.angsi),1);
```

```
157 peak_SLL_V = cell(length(run_params.angsi),1);
158 peak_SLL_vals = cell(length(run_params.angsi),1);
159
160 ridx = length(run_params.SNRs_dB);
161 %-------------------------------------------------------------------------
162 mx_dim = 0; usnr = length(run_params.SNRs); ua = see_src_no;
163 Vo = run_params.V; Ri = run_params.Ri_mvdr{usnr};
164 t_mvdr = 1./sum( conj( Vo ) .* ( Ri*Vo ) , 1 ); tMVDR_dB = db10( t_mvdr );
165
166 f_ambig0 = figure; plot( run_params.anggs, tMVDR_dB );
167 xlabel('Search Angle (degrees)'); ylabel('SNR (dB)');
168 title('MVDR Ambiguity Function'); vln(run_params.Sig_angles,'r-.');
169
170 irm_idx = find(imregionalmax(tMVDR_dB));
171
172 % Throw out maxima due to true signals...
173 idx = []; for u = 1:run_params.No_sigs;
174 idx = [idx find(abs(anggs(irm_idx)-run_params.Sig_angles(u))<=run_params.ULA_BW_degs)];
175 end; % for u = 1:run_params.No_sigs;
176
177 irm_idx = irm_idx( setdiff([1:length(irm_idx)],idx) );
178 aa =  tMVDR_dB(irm_idx); [jnk,iro] = sort( aa ); iro = flipud( iro(:) ).';
179 figure(f_ambig0);
180 hold on; plot(run_params.anggs(irm_idx),tMVDR_dB(irm_idx),'ko'); hold off;
181
182 % If local max is not an ENDPOINT, then refine...
183 run_params.Ri_hat = run_params.Ri_mvdr{usnr};
184 for u_nsig = 1:length(irm_idx(iro));
185 % refine if NOT endpoint max...
186 if ( irm_idx(iro(u_nsig)) ~= 1 ) & ( irm_idx(iro(u_nsig)) ~= length(tMVDR_dB) );
187 idx = irm_idx(iro(u_nsig));
188 fh = @MVDR_fnc; % Use function handle to make visible to fminbnd (a MATLAB function);
189 a_refine(u_nsig) = ...
190 fminbnd(fh,max(run_params.Ang_low,anggs(idx)-(1/2)*run_params.ULA_BW_degs),...
191               min(anggs(idx)+(1/2)*run_params.ULA_BW_degs,run_params.Ang_high));
192
193 % Check that angle estimate refinement is small...if not, then don't use...
194 % could be a saddle point...
195 if abs( anggs(idx) - a_refine(u_nsig) ) >= (1/4)*run_params.ULA_BW_degs;
196 a_refine(u_nsig) = anggs(idx); end;
197
198 else;
199 a_refine(u_nsig) = anggs( irm_idx(iro(u_nsig)) );
200 end; % if ( irm_idx(iro(u_nsig)) ~= 1 ) & ( irm_idx(iro(u_nsig)) ~= length(tMVDR_dB) );
201
202 peak_SLL_angs{ua}(u_nsig) = a_refine(u_nsig);
203 peak_SLL_V{ua}(:,u_nsig) = van(run_params.N,peak_SLL_angs{ua}(u_nsig),run_params.d);
204
205 end; % for u_nsig = 1:length(irm_idx);
206
207 aV = peak_SLL_V{ua}; peak_SLL_vals{ua} = db10( 1./abs( sum( conj( aV ) .* (Ri*aV), 1)  ) );
208 aa = db10( 1./abs( sum( conj( aV ) .* (Ri*aV), 1)  ) );
209 if length(aa) > mx_dim; mx_dim = length(aa); end;
210 run_params.peak_SLL_angs = peak_SLL_angs; run_params.peak_SLL_V = peak_SLL_V;
```

```
peak_SLL_idx = irm_idx(iro);
%-------------------------------------------------------------------------
% BUILD MSE ERROR TERMS FOR GLOBAL ERROR CONTRIBUTIONS...
%-------------------------------------------------------------------------
disp('Building Error and mu/lambda Matrices...');
Err_Mat = zeros(1,mx_dim); Ptht_cond = zeros(1,mx_dim); ua = see_src_no;
possible_angs = peak_SLL_angs{ua};
for upa = 1:length(possible_angs);
Err_Mat(1,upa) = (pi/180)^2 * abs( run_params.angsi(ua) - possible_angs(upa) )^2; end;
%-------------------------------------------------------------------------
% COMPUTE TOTAL MSE USING MIE MSE APPROXIMATION...
%-------------------------------------------------------------------------
MF_MSE_Approx = zeros(length(run_params.SNRs),1);
Glb_MSE = zeros(length(run_params.SNRs),1);  Loc_MSE= zeros(length(run_params.SNRs),1);
t0 = clock; rand('state',sum(100*clock));
disp(['Beginning MSE Calculations...']);
% True array response
run_params.vT = van(run_params.N,run_params.Sig_angles(see_src_no),run_params.d);

for usnr = 1:length(run_params.SNRs); % Compute MSE as function of element level SNR...
Prob_Err_Mat = zeros(1,mx_dim);
for upa = 1:length(possible_angs); % Errors
% function [Pe] = Pe_Capon(R,va,vb,L);
Prob_Err_Mat(1,upa) = ...
Pe_Capon(run_params.Ri_mvdr{usnr},peak_SLL_V{ua}(:,upa),run_params.vT,run_params.L);
end; % for upa = 1:length(possible_angs);

MF_MSE_Approx(usnr) = ...
(1./den_ang(usnr)).' .* (1-min(1,sum(Prob_Err_Mat,2)))+sum( Err_Mat .* Prob_Err_Mat, 2 );
amidon(t0,usnr,length(run_params.SNRs));
end; % for usnr = 1:length(run_params.SNRs);

run_params.MF_MSE_Approx = MF_MSE_Approx; MF_MSE_Approx0 = MF_MSE_Approx;
%-------------------------------------------------------------------------
% Clip MSE so that it maxes out at MSE of UNIFORMLY distirbuted estimate...

BW_degs = run_params.ULA_BW_degs;

xx = linspace(run_params.Ang_low,run_params.Ang_high,1000);
fxx = ( 1/( xx(end) - xx(1) ) ) * ones(size(xx));
varx = trapz( xx, fxx .* (xx - run_params.Sig_angles(see_src_no)).^2 );
unif_mse = varx * (pi/180)^2;

for u=1:length(MF_MSE_Approx);
MF_MSE_Approx(u) = min(MF_MSE_Approx(u),unif_mse); % Clipping...
end; % for u=1:length(MF_MSE_Approx);
%-----------------------------
% PLOT FINAL RESULTS...
figure;
plot(run_params.SNRs_dB,db10( sqrt( (180/pi)^2 *( MF_MSE_Approx )*...
(1/run_params.ULA_BW_degs)^2 ) ),'r-');
hold on;
plot(run_params.SNRs_dB,db10( sqrt( (180/pi)^2 *( crb )*...
(1/run_params.ULA_BW_degs)^2 ) ),'k:');
```

```
hold off;
hold on;
plot(run_params.SNRs_dB,db10( sqrt( (180/pi)^2 *( 1./den_ang )*...
(1/run_params.ULA_BW_degs)^2 ) ),'g--');
hold off;
title('Capon Algorithm Threshold Region MSE Prediction');
xlabel('Element Level SNR (dB)'); ylabel('Root MSE in Beamwidths (dB)')

% Direct threshold SNR approximation for Capon algorithm...
[jnk,ioi] = max( abs( bd( peak_SLL_vals{1} ) ) );
v1 = run_params.vT; v2 = peak_SLL_V{1}(:,ioi); a12 = abs( v1'*v2 )^2;
a1 = abs(v1'*v1); a2 = abs(v2'*v2); co = a12/a1/a2; gam = a1;
[Est_Thg] = Capon_ThSNR_II_dB(run_params.N,co,run_params.L,run_params.N);
vln(db10(Est_Thg),'k-.'); axis([-30 10 -20 5]);
legend('MIE MSE','CRB','VB MSE','Approx. SNR_TH')
return;
%-------------------------------------------------------------------------
% ALL SUBFUNCTIONS....
%-------------------------------------------------------------------------
function [Pe] = Pe_Capon(Ri,va,vb,L);

% function [Pe] = Pe_Capon(Ri,va,vb,L);
%
% This code implements the algorithm for computing the pairwise error probability for
% the Capon algorithm presented in IEEE T-SP paper by C. D. Richmond, to appear 2005.
%
% INPUTS:
% -------
%  Ri - Inverse of true data covariance matrix
% va - Array response for error/outlier sidelobe direction
%      (location of local max of ambiguity fnc)
% vb - Array response for true signal
% L - Number of data samples (spatial snapshots) used in covariance estimation
%
% OUTPUT:
% -------
% Pe - Pairwise error probability of Capon algorirth:
%      Pe = Prob[ P_Capon(tht_a) > P_Capon(tht_b) ]
%
% Author: Christ D. Richmond
% Date: 8/18/04

N = length(va); K = L - N + 2; F = 1;
pa = abs( va'*Ri*va ); pb = abs( vb'*Ri*vb ); Iab = F * abs( va'*Ri*vb )^2;
Pp = (pb + F * pa)/2; Pm = (pb - F * pa)/2; D = sqrt( Pp^2 - Iab );
l = -( Pm + D ) / (Pm - D); S = sign(Pm - D);
if K <= 40;
Pe = 0.5 * (1 + S) - S * cumF(K,K,0,l);
else;
sigb = sqrt( (K+1)/(2 * (2*K + 1 ) ) - (0.5)^2 );
arg_ef = ( 1/(1+l) - 0.5 )/( sigb * sqrt(2) );
Pe = 0.5 * (1 + S) - S * 0.5 * erfc(arg_ef);
end; % if K <= 40;

```

```
return;
%----------------------------------------------------------------------
function [Th] = Capon_ThSNR_II_dB(gam,co,L,N,eta);

% function [Th] = Capon_ThSNR_dB(gam,co,L,N);
%
% This function implements the direct computation of an approximation for
% the threshold SNR of the Capon algorithm for the fundamental and canonical case of
% a single planewave source in white noise.  The approximation is valid in the
% large sample case, i.e. approximately L >= 2N.
%
% INPUTS:
% -------
% gam - Norm of array responses (equal norm is assumed).  Note that gam = # sensors
%       for usual Vandermonde steering vectors.
% co - Geometric cosine between true signal array response and array response for
%      direction of highest sidelobe of Capon ambiguity function.
% L - Sample support of estimated data covariance
% N - number of sensors in array
%
% OUTPUT:
% ------
% Th - Capon threshold SNR (in power domain, not in decibels)
%
% Author: Christ D. Richmond
% Date: 8/18/2004
%----------------------------------------------------------------------
M = L - N + 2; n_std = 4;
if nargin < 5;
eta = - ( 1 - n_std * sqrt( 1/( 2*M + 1 ) ) ) / ( 1 + n_std * sqrt( 1/( 2*M + 1 ) ) );
end; % if nargin < 5;
%----------------------------------------------------------------------
xi = ( (1-eta)/(1+eta) )^2; em = (xi - 1); ep = (xi + 1); psi = ep/em; so = 1-co;
%----------------------------------------------------------------------
% coefficients of quartic...
a = 2*gam*so + (2/gam)*(1-psi);
b = (4*co/gam/gam/em) + 2*( (gam*gam * so*so / 2) - co) + 2*(1-psi)*( 1/gam/gam + 1+so );
c = (8*co/gam/em) + 2*( (1+so)/gam + gam*so*so ) - 2*psi*( so*(gam+1/gam) + 1/gam);
d = 4*co/em + co^2 + 2*so*(1-psi);
%----------------------------------------------------------------------
% Apply solution to quartic equation...
p = b; q = (a*c - 4*d); r = (a^2 * d + c^2 - 4*b*d); u = q - p^2 / 3;
v = r - p*q/3 + 2*p^3/27;

j0 = 4*(u/3)^3 + v^2; % Discriminant

if j0 > 0;

w = sqrt( j0 ); % y = ( (w - v)/2 )^(1/3) - (u/3)*(2/(w-v))^(1/3) - p/3;
y = (u/3)*(2/(w+v))^(1/3) - ((w+v)/2)^(1/3) - p/3;

elseif j0 <= 0;

s = sqrt( (-u/3) ); t = -v/(2*s^3); k = acos(t)/3;
```

```
ck = cos(k); sk = sin(k);
yrts = real( [ 2 *s*ck - p/3; s * (-ck + sqrt(3) * sk ) - p/3; ...
             s * (-ck - sqrt(3) * sk ) - p/3] );

y = yrts(1); % All roots appear to work...

end; % if j0 > 0;

e2 = a^2/4 - b - y;  e = sqrt(e2); f2 = (y.^2)*(1/4) - d;
f = sqrt(f2); ef = a*y*(1/4) + c/2;
G = a/2 + e; g = a/2 -e; H = -y./2 + f; h = -y./2 - f;
frts = [ ( -G + sqrt( G^2 - 4*H ) )/2; ( -G - sqrt( G^2 - 4*H ) )/2;
( -g + sqrt( g^2 - 4*h ) )/2 ; ( -g - sqrt( g^2 - 4*h ) )/2];
Th = frts(3); % Root leading to desired solution
return;
%-------------------------------------------------------------------------
function[x]=bd(y); x = 10.^(y./10); return;
%-------------------------------------------------------------------------
function[y]=db10(x); y = 10*log10( abs(x) ); return;
%-------------------------------------------------------------------------
function [H] = hm( A ); H = ( A + A' ) * (1/2); return;
%-------------------------------------------------------------------------
function [out] = ULA_3dB_BW(N,d);

% function [out] = ULA_3dB_BW(N,d);
%
% Computes beamwidth for uniform linear array.
%
% N - number of elements
% d - element separation in wavelengths
%
L = N*d; out = (180/pi) *  (1 ./ L); return;
%-------------------------------------------------------------------------
function[v]=van(N,ang,elem,flg)

% function[v]=van(N,ang,elem)
%
% This function computes simple vandermonde steering vectors.
%
% N - Number of elements
% ang - Look direction in degs: 0 deg endfire; 90 deg broadside
%       180 opposite endfire
% elem - Element spacing in wavelenths
% flg - Flag to make array center the phase reference

if nargin < 4; v = exp(j*2*pi*elem*[0:N-1]'*cos(ang(:)'*pi/180));
else; v = exp(j*2*pi*elem*([0:N-1]' - (N-1)/2 )*cos(ang(:)'*pi/180)); end;
%-------------------------------------------------------------------------
function[v]=van_p(N,ang,elem,flg)

% function[v]=van_p(N,ang,elem,flg)
%
% This function computes the first derivative of vandermonde steering vectors
%
```

```
427 % N - Number of elements
428 % ang - Look direction in degs: 0 deg endfire; 90 deg broadside
429 %       180 opposite endfire
430 % elem - Element spacing in wavelenths
431
432 if nargin < 4;
433 C = -j*2*pi*elem*[0:N-1]'*sin(ang(:)'*pi/180);
434 v = C .* exp(j*2*pi*elem*[0:N-1]'*cos(ang(:)'*pi/180));
435 else;
436 C = -j*2*pi*elem*([0:N-1]' - (N-1)/2 )*sin(ang(:)'*pi/180);
437 v = C .* exp(j*2*pi*elem*([0:N-1]' - (N-1)/2 )*cos(ang(:)'*pi/180));
438 end;
439 return;
440 %---------------------------------------------------------------------------
441 function[v]=van_p2(N,ang,elem,flg)
442
443 % function[v]=van_p2(N,ang,elem,flg)
444 %
445 % This function computes the second derivative of vandermonde steering vectors.
446 %
447 % N - Number of elements
448 % ang - Look direction in degs: 0 deg endfire; 90 deg broadside
449 %       180 opposite endfire
450 % elem - Element spacing in wavelenths
451
452 if nargin < 4;
453
454 % v = exp(j*2*pi*elem*[0:N-1]'*cos(ang(:)'*pi/180));
455
456 Cs = -j*2*pi*elem*[0:N-1]'*sin(ang(:)'*pi/180);
457 Cc = -j*2*pi*elem*[0:N-1]'*cos(ang(:)'*pi/180);
458 v = [Cc + Cs .* Cs] .* exp(j*2*pi*elem*[0:N-1]'*cos(ang(:)'*pi/180));
459 else;
460 Cs = -j*2*pi*elem*([0:N-1]' - (N-1)/2 )*sin(ang(:)'*pi/180);
461 Cc = -j*2*pi*elem*([0:N-1]' - (N-1)/2 )*cos(ang(:)'*pi/180);
462 v = [Cc + Cs .* Cs]  .* exp(j*2*pi*elem*([0:N-1]' - (N-1)/2 )*cos(ang(:)'*pi/180));
463 end;
464 return;
465 %---------------------------------------------------------------------------
466 function[v]=van_p3(N,ang,elem,flg)
467
468 % function[v]=van_p3(N,ang,elem,flg)
469 %
470 % This function computes the third derivative of vandermonde steering vectors.
471 %
472 % N - Number of elements
473 % ang - Look direction in degs: 0 deg endfire; 90 deg broadside
474 %       180 opposite endfire
475 % elem - Element spacing in wavelenths
476
477 if nargin < 4;
478 Cs = -j*2*pi*elem*[0:N-1]'*sin(ang(:)'*pi/180);
479 Cc = -j*2*pi*elem*[0:N-1]'*cos(ang(:)'*pi/180);
480 eo = exp(j*2*pi*elem*[0:N-1]'*cos(ang(:)'*pi/180));
```

```
v = ( -Cs + Cc.*Cs + 2*Cs.*Cc + Cs.^3 ) .* eo;
else;
Cs = -j*2*pi*elem*([0:N-1]' - (N-1)/2 )*sin(ang(:)'*pi/180);
Cc = -j*2*pi*elem*([0:N-1]' - (N-1)/2 )*cos(ang(:)'*pi/180);
eo = exp(j*2*pi*elem*([0:N-1]' - (N-1)/2 )*cos(ang(:)'*pi/180));
v = ( -Cs + Cc.*Cs + 2*Cs.*Cc + Cs.^3 ) .* eo;
end;
return;
%-----------------------------------------------------------------------
function[R,Ri]=getRvan(N,wl_dB,tht,thl_dB,d,flg);

% function[R,Ri]=getRvan(N,wl_dB,tht,thl_dB,d,flg);
%
% This function computes the data covariance for simple mutually
% incoherent planewave signals in white noise.
%
% N - No. of elements
% wl_dB - noise floor level in dB
% tht - vector containing jammer directions
% thl_dB - vector containing jammer-to-noise levels in dB
% d - Element spacing in wavelenths
% flg - Flag to make array center the phase reference; otherwise,
%       it's the first element

R = eye(N)*( 10^(wl_dB/10) ) ;
if nargin > 2 & ( length(tht)~=0 & length(thl_dB)~=0 );
%function[v]=van(N,ang,elem)
if exist('flg'); V = van(N,tht,d,flg); else; V = van(N,tht,d); end;
if length(V)>0; R = R + V*diag( 10.^( ( thl_dB + wl_dB) / 10) )*V';
R = hm( R ); end;
end; % if nargin > 2 & ( length(tht)~=0 & length(thl_dB)~=0 );

if nargin > 3 & (length(tht)~=0 & length(thl_dB)~=0);
Ri = 10^( -wl_dB/10 )*( eye(N) - ...
                hm( V * hm( inv( V'*V+...
                 10^(wl_dB/10)*diag( 10.^( -( thl_dB + wl_dB) / 10) )   ) )*V' ) );
elseif nargin > 3 & ( length(tht)==0 | length(thl_dB)==0 ); ;
Ri = 10^( -wl_dB/10 )* eye(N) ;
elseif nargin == 2; Ri = 10^( -wl_dB/10 )* eye(N) ;
end;
return;
%-----------------------------------------------------------------------
function [Rsqrt,Rsqrti,DetRsqrt] = get_Rsqrt(R);

% function [Rsqrt,Rsqrti,DetRsqrt] = get_Rsqrt(R);
%
% This code uses the eigen-decomposition to obtain a symmetric matrix
% square root.
%
% Author: Christ D. Richmond
% Date: 11/24/04

[Qr,Ir] = eig(R);  Ird = diag(Ir); ir_idx = find(Ird); Iir = Ird;
Iir(ir_idx) = sqrt( 1./Ird(ir_idx) );
```

```
Rsqrt = hm( Qr * diag( sqrt( Ird(ir_idx) ) ) * Qr' );
Rsqrti = hm( Qr * diag( Iir ) * Qr' );
DetRsqrt = prod( Ird ); % Determinant
return;
%------------------------------------------------------------------------
function[]=vln(vll,varargin);

% function[]=vln(vll,varargin);
%
% This plotting function plots vertical lines at locations indicated by vector vll.
%
% vll - vertical line locations
%
% Author: Christ D. Richmond
%
figure(gcf); ax = axis; hold on;
for u = 1:length(vll); vo = vll(u); xx = vo*[1 1]; yy = ax(3:4);
plot(xx,yy,varargin{:}); end; hold off;
%------------------------------------------------------------------------
function [out] = MVDR_fnc(param_val);

% function [out] = MVDR_fnc(param_val);
%
% The MVDR / Capon Spectral Estimator parameterized as a function of
% the unknown signal parameters (angle)
%
% Author: Christ D. Richmond

global run_params

% function[v]=van(N,ang,elem,flg);
v_a = van(run_params.N, param_val,run_params.d); V = run_params.Ri_hat * v_a;
den = ( abs( sum( conj( v_a ) .* V, 1 ) ) );
out = den; % Written upside down because matlab search routine finds "MINIMA"
%------------------------------------------------------------------------
function[F] = cumF(N,M,d,x)

% function[F] = cumF(N,M,d,x)
%
% This function computes the cumulative distribution function for the complex central F.
%
% N and M are deg of freed. for complex non-central F_{N,M}(d)
% d ( = delta^2 of thesis p.50) is non-centrality parameter
% x value at which to evaluate the cdf of F_{N,M}(d)
%
% Author: Christ D. Richmond
%

idxo = find( x==0 ); % idx = setdiff(1:length(x),idx);
x(idxo) = 1; % anything but zero...

s=0; for k=0:M-1; s = s + bcf2(N+M-1,k+N)*(x).^k.*Gam(d*1./(1+x),k+1); end;
F =  exp( N * log(x) - (N+M-1) * log(1 + x)  + log(s) ); F(idxo) = 0;

```

```
589 function[g]=Gam(y,m); g = 1-gammainc(y,m); return;
590 function [y] = bcf2(n,k);
591 for u=1:length(k);
592 y(u) = exp( gammaln(n+1) - gammaln(k(u)+1) - gammaln((n-k(u))+1) );
593 end; return;
594 %-------------------------------------------------------------------------
595 function[perc]=amidon(t0,iter,total);
596
597 tnew = clock; startmin = 60*t0(4) + t0(5) + t0(6)/60;
598 pastmin = 60*tnew(4) + tnew(5) + tnew(6)/60;
599 sofarmin = pastmin - startmin; min_iter = sofarmin/iter;
600 min_left = min_iter * ( total - iter );
601 disp([num2str(100*iter/total) '% done; ' num2str(min_left) ' Minutes, or ' ...
602 num2str(min_left/60)  ' Hours, or ' num2str(min_left/60/24) ' Days left']);
603 %-------------------------------------------------------------------------
```

ACRONYMS

AWGN	Additive White Gaussian Noise
CBF	Conventional Beamforming
cdf	Cumulative Distribution Function
CRB	Cramér-Rao Bound
DFT	Discrete Fourier Transform
DOA	Direction-of-Arrival
FFT	Fast Fourier Transform
FM	Frequency Modulation
HN	Hawkes-Nehorai asymptotic local error MSE prediction of Bartlett algorithm
hpd	hermitian positive definite
IE	Interval Errors
KW	Kaveh and Wang
MFP	Matched Field Processing
MIE	Method of Interval Errors
ML	Maximum Likelihood
MSE	Mean Squared Error
MUSIC	MUltiple SIgnal Classification
MVDR	Minimum Variance Distortionless Response (adaptive beamformer)
NIE	No Interval Errors
OSF	Objective Search Function
PCM	Pulse Code Modulation
pdf	Probability Density Function
RB	Rife and Boorstyn
SNR	Signal-to-Noise Ratio
SVD	Singular Value Decomposition
TKV	Tufts, Kot, and Vaccaro

ACRONYMS CONTINUED

UB	Union Bound
ULA	Uniform Linear Array
VB	Vaidyanathan-Buckley asymptotic local error MSE prediction of Capon algorithm
WWB	Weiss-Weinstein Bound
ZZB	Ziv-Zakai Bound

REFERENCES

[1] M. Abramovich and I. A. Stegun, Editors, *Handbook of Mathematical Functions*, Dover Publishing Co. Inc. New York, 1972.

[2] F. Athley, "Threshold Region Performance of Deterministic Maximum Likelihood DOA Estimation of Multiple Sources," *Proceedings of the Thirty-Sixth Asilomar Conference on Signals, Systems and Computers*," Vol. 2, pp. 1283–1287, November 2002.

[3] F. Athley, *Space Time Parameter Estimation in Radar Array Processing*, Ph.D. Dissertation, Chalmers University of Technology, Gothenburg, Sweden, June 2003.

[4] A. J. Barabell, J. Capon, D. F. Delong, J. R. Johnson, and K. Senne, "Performance Comparison of Superresolution Array Processing Algorithms," Project Report TST–72, Lincoln Laboratory, MIT, 1984.

[5] J. R. Barry, E. A. Lee, and D. G. Messerschmitt, *Digital Communication*, 3rd Edition, Kluwer Academic Publishers, 2004.

[6] M. S. Bartlett, "Smoothing Periodograms from Time Series with Continuous Spectra," *Nature*, Vol. 161, pp. 686–687, 1948.

[7] M. S. Bartlett, "Periodogram Analysis and Continuous Spectra," *Biometrika*, Vol. 37, pp. 1–16, 1950.

[8] K. L. Bell, *Performance Bounds in Parameter Estimation with Application to Bearing Estimation*, Ph.D. Dissertation, George Mason University, Fairfax, Virginia, 1995.

[9] K. L. Bell, Y. Steinberg, Y. Ephraim, and H. L. Van Trees, "Extended Ziv-Zakai Lower Bound for Vector Parameter Estimation," *IEEE Transactions on Information Theory*, Vol. 43, No. 2, pp. 624–637, March 1997.

[10] E. Biglieri, G. Caire, and G. Taricco, "Expurgating the Union Bound to Error Probability: A Generalization of the Verdú-Shields Theorem," *Proceedings of the IEEE International Symposium on Information Theory*, p. 373, June 29–July 4, 1997.

[11] J. F. Bohme, "Array Processing," Chapter 1 in *Advances in Spectrum Analysis and Array Processing, Volume II*, S. Haykin, Editor, Prentice Hall, Englewood Cliffs, New Jersey, 1991.

[12] E. Boyer, P. Forster, and P. Larzabal, "Nonasymptotic Statistical Performance of Beamforming for Deterministic Signals," *IEEE Signal Processing Letters*, Vol. 11, No. 1, pp. 20–22, January 2004.

[13] E. Boyer, P. Forster, and P. Larzabal, "Nonasymptotic Performance Analysis of Beamforming With Stochastic Signals," *IEEE Signal Processing Letters*, Vol. 11, No. 1, pp. 23–25, January 2004.

[14] D. R. Brillinger, *Time Series Data Analysis and Theory*, Holt, Rinehart and Winston, Inc., 1975.

[15] J. Capon, "High–Resolution Frequency–Wavenumber Spectrum Analysis," *Proceedings of the IEEE*, Vol. 57, 1408–1418 (1969).

[16] J. Capon and N. R. Goodman,"Probability Distributions for Estimators of Frequency Wavenumber Spectrum," *Proceedings of the IEEE*, Vol. 58, No. 10, 1785–1786 (1970).

[17] J. Capon, "Maximum-Likelihood Spectral Estimation," in *Nonlinear Methods of Spectral Analysis, 2nd Edition*, Edited by S. Haykin, Springer, New York, 1983.

[18] H. Cox, "Resolving Power and Sensitivity to Mismatch of Optimum Array Processors," *Journal of the Acoustical Society of America*, Vol. 54, No. 3, pp. 771–785, 1973.

[19] H. Cox, R. Zeskind, and M. Owen, "Robust Adaptive Beamforming," *IEEE Transactions on Acoustics, Speech, and Signal Processing*, Vol. 35, No. 10, pp. 1365–1376, October 1987.

[20] B. Friedlander and A. J. Weiss, "The Resolution Threshold of a Direction Finding Algorithm for Diversely Polarized Arrays," *IEEE Transactions on Signal Processing*, Vol. 42, No. 7, pp. 1719–1727, July 1994.

[21] M. Hawkes and A. Nehorai, "Acoustic Vector-Sensor Beamforming and Capon Direction Estimation," *IEEE Transactions on Signal Processing*, Vol. 46, No. 9, 2291–2304, 1998.

[22] D. Herbison-Evans, "Solving Quartics and Cubics for Graphics," Online at http://linus.socs.uts.edu.au/~don/pubs/solving.html.

[23] Y. Hua, A. Gershman, and Q. Cheng, Editors, *High-Resolution and Robust Signal Processing*, Marcel Dekker, 2004.

[24] A. Jakobsson, S. Lawrence Marple, Jr., and P. Stoica, "Computationally Efficient Two-Dimensional Capon Spectrum Analysis," *IEEE Transaction on Signal Processing*, Vol. 48, No. 9, pp. 2651–2661, September 2000.

[25] M. Kaveh and H. Wang, "Threshold Properties of Narrow-Band Signal-Subspace Array Processing Methods," Chapter 5 in *Advances in Spectrum Analysis and Array Processing, Volume II*, S. Haykin, Editor, Prentice Hall, Englewood Cliffs, New Jersey, 1991.

[26] E. J. Kelly, "Performance of an Adaptive Detection Algorithm; Rejection of Unwanted Signals," *IEEE Trans. Aerosp. Electron. Syst.*, Vol. 25, No. 2, pp. 122–133, March 1989.

[27] E. J. Kelly and K. Forsythe, "Adaptive Detection and Parameter Estimation for Multidimensional Signal Models," Technical Report 848, Lincoln Laboratory, MIT (1989).

[28] R. T. Lacoss, "Data Adaptive Spectral Analysis Methods," *Geophysics*, Vol. 36, No. 4, pp. 661–675, August 1971.

[29] S. Lawrence Marple, Jr., *Digital Spectral Analysis with Applications*, Prentice-Hall, Inc., Englewood Cliffs, New Jersey, 1987.

[30] N. Lee and C. D. Richmond, "Threshold Region Performance Prediction for Adaptive Matched Field Processing Localization," *Proceedings of the Adaptive Sensor Array Processing Workshop*, MIT Lincoln Laboratory, March 2004.

[31] J. Li and P. Stoica, "An Adaptive Filtering Approach to Spectral Estimation and SAR Imaging," *IEEE Transactions on Signal Processing*, Vol. 44, No. 6, pp. 1469–1484, June 1996.

[32] M. J. Malone, "On the Threshold Effect in FM Data Systems," *IEEE Transactions on Communication Technology*, Vol. 14, No. 5, pp. 625–631, October 1966.

[33] T. L. Marzetta, "A New Interpretation of Capon's Maximum Likelihood Method of Frequency-Wavenumber Spectral Estimation," *IEEE Transactions on Acoustics, Speech, and Signal Processing*, Vol. 31, No. 2, pp. 445–449, April 1983.

[34] R. J. Muirhead, *Aspects of Multivariate Statistical Theory*, John Wiley & Sons, Inc. 1982.

[35] I. S. Reed, J. D. Mallett, and L. E. Brennan, "Rapid Convergence Rate in Adaptive Arrays," *IEEE Trans. Aerospace and Electronic Systems*, Vol. AES-10, No. 6, 853–863 (1974).

[36] I. Reuven and H. Messer, "The Use of the Barankin Bound for Determining the Threshold SNR in Estimating the Bearing of a Source in the Presence of Another," *Proceedings of the ICASSP*, Vol. 3, pp. 1645–1648, May 1995.

[37] C. D. Richmond, "Mean Squared Error and Threshold SNR Prediction of Maximum-Likelihood Signal Parameter Estimation with Estimated Colored Noise Covariances," *IEEE Transactions on Information Theory*, to appear 2005.

[38] C. D. Richmond, B. D. Van Veen, and T. Limpiti, "Mean Squared Error Performance Prediction of Linearly Constrained Minimum Variance Source Localization," *Proceedings of the 14th International Conference on Biomagnetism (Biomag)*, P4-2, pp. 581-582, August 10, 2004, Boston, MA.

[39] C. D. Richmond, "Derived PDF of Maximum-Likelihood Signal Parameter Estimator which Employs an Estimated Noise Covariance," *IEEE Transactions on Signal Processing*, Vol. 44, No. 2, pp. 305–315, February 1996.

[40] C. D. Richmond, "MVDR Adaptive Sidelobes: Extending Ruze's Formula and Providing and Exact Calculation of the Probability of Sidelobe Suppression," *Proceedings of the IEEE Sensor Array and Multi-channel (SAM) Signal Processing Workshop*, pp. 73-76, March 2000.

[41] C. D. Richmond, "Statistics of Adaptive Nulling and Use of the Generalized Eigen-Relation (GER) for Modeling Inhomogeneities in Adaptive Processing," *IEEE Transactions on Signal Processing*, Vol. 48, No. 5, May 2000, pp. 1263-1273.

[42] C. D. Richmond, R. R. Nadakuditi, and A. Edelman, "Asymptotic Mean Squared Error Performance of Diagonally Loaded Capon-MVDR Processor," submitted to *Adaptive Sensor Array Processing Workshop*, MIT Lincoln Laboratory, 2005.

[43] D. C. Rife and R. R. Boorstyn, "Single-Tone Parameter Estimation from Discrete-Time Observations," *IEEE Transactions on Information Theory*, Vol. 20, No. 5, pp. 591–598, September 1974.

[44] A. W. Rihaczek, *Principles of High-Resolution Radar*, McGraw-Hill, Inc., 1969.

[45] C. E. Shannon, "Communication in the Presence of Noise," *Proceedings of the Institute of Radio Engineers*, Vol. 37, No. 1, pp. 10–21, January 1949.

[46] W. M. Siebert, "A Radar Detection Philosophy," *IRE Transactions on Information Theory*, IT-2, pp. 204–221, September 1956.

[47] S. T. Smith, "Statistical Resolution Limits and the Complexified Cramér-Rao Bound," *IEEE Transactions on Signal Processing*, to appear 2005.

[48] A. O. Steinhardt and C. Bretherton, "Threshold in Frequency Estimation," *Proc. 1985 IEEE International Conference on Acoustics, Speech, and Signal Processing*, Tampa, FL, pp. 1273–1276, March 26-29, 1985.

[49] A. O. Steinhardt, "Adaptive Multisensor Detection and Estimation," Chapter 3 in *Adaptive Radar Detection and Estimation*, Edited by S. Haykin and A. O. Steinhardt, John Wiley & Sons, Inc., 1992.

[50] P. Stoica, V. Šimonytė, and T. Söderström, "On the Resolution Performance of Spectral Analysis," *Signal Processing*, Vol. 44, pp. 153–161, 1995.

[51] P. Stoica, P. Handel, and T. Soderstrom, "Study of Capon Method for Array Signal Processing," *Circuits Syst. Signal Processing*, Vol. 14, No. 6, pp. 749–770, 1995.

[52] P. Stoica and R. Moses, *Introduction to Spectral Analysis*, Prentice–Hall, Upper Saddle River, New Jersey, 1997.

[53] J. K. Thomas, L. L. Scharf, and D. W. Tufts, "The Probability of a Subspace Swap in the SVD," *IEEE Transaction on Signal Processing*, Vol. 43, No. 5, pp. 730–736, March 1995.

[54] D. W. Tufts, A. C. Kot, and R. J. Vaccaro, "The Analysis of Threshold Behavior of SVD-Based Algorithms," *Proceedings of the Twenty-First Asilomar Conference on Signals, Systems, and Computers*, November, 1987.

[55] D. W. Tufts, A. C. Kot, and R. J. Vaccaro, "The Threshold Effect in Signal Processing Algorithms Which Use an Estimated Subspace," Chapter 19 in *SVD and Signal Processing, II: Algorithms, Analysis, and Applications*, Edited by R. J. Vaccaro, Elsevier Science Publishers B. V. New York, 1991.

[56] H. W. Turnbull, *Theory of Equations*, Oliver and Boyd, London, Fifth Edition 1952.

[57] C. Vaidyanathan and K. M. Buckley, "Performance Analysis of the MVDR Spatial Spectral Estimator," *IEEE Transactions on Signal Processing*, Vol. 43, No. 6, pp. 1427–1437, June 1995.

[58] C. Vaidyanathan and K. M. Buckley, "Performance Analysis of the Enhanced Minimum Variance Spatial Spectrum Estimator," *IEEE Transactions on Signal Processing*, Vol. 46, No. 8, pp. 2202–2206, August 1998.

[59] H. L. Van Trees, *Detection, Estimation, and Modulation Theory Part I*, New York: Wiley, 1968.

[60] H. L. Van Trees, *Detection, Estimation, and Modulation Theory Part III: Radar-Sonar Signal Processing and Gaussian Signals in Noise*, New York: Wiley, 1968.

[61] H. L. Van Trees, *Detection, Estimation, and Modulation Theory Part IV: Optimum Array Processing*, New York: John Wiley & Sons, Inc. 2002.

[62] S. Verdú, "Maximum Likelihood Sequence Detection for Intersymbol Interference Channels: A New Upper Bound on Error Probability," *IEEE Transactions on Information Theory*, Vol. 33, No. 1, pp. 66–68, January 1987.

[63] M. Viberg and A. L. Swindlehurst, "Analysis of the Combined Effects of Finite Sample and Model Errors on Array Processing Performance," *IEEE Transactions on Signal Processing*, Vol. 42, No. 11, pp. 3073–3083, November 1994.

[64] S. Weimin, N. Jinlin, L. Guosui, and Z. Guangyi, "The Effect of Channel Mismatch on the Spatial Spectrum and Resolution Ability of MUSIC Algorithm," *Proceedings of the CIE International Conference of Radar*, pp. 96–99, October 1996.

[65] A. J. Weiss and E. Weinstein, "Fundamental Limitations in Passive Time Delay Estimation–Part I: Narrow-Band Systems," *IEEE Transactions on Acoustics, Speech, and Signal Processing*, Vol. 31, No. 2, pp. 472–486, April 1983.

[66] P. M. Woodward, *Probabililty and Information Theory, with Applications to Radar*, McGraw-Hill Book Co., Inc., New York, 1953.

[67] W. Xu, *Performance Bounds on Matched-Field Methods for Source Localization and Estimation of Ocean Environmental Parameters*, Ph.D. Dissertation, MIT, Cambridge, MA, June 2001.

[68] W. Xu, A. B. Baggeroer, and H. Schmidt, "Quantitative Ambiguity Analysis for Matched-Field Source Localization," *Proceedings of the Thirty-Sixth Asilomar Conference on Signals, Systems and Computers*," Vol. 1, pp. 448–452, November 2002.

[69] W. Xu and C. D. Richmond, "Quantitative Ambiguity Analysis for Matched-Field Source Localization under Spatially-Correlated Noise Field," *Proceedings of MTS/IEEE Oceans Conference*, San Diego, CA, September 2003.

[70] W. Xu, A. B. Baggeroer, and K. L. Bell, "A Bound on Mean-Squared Estimation Error with Background Parameter Mismatch," *IEEE Transactions on Information Theory*, Vol. 50, No. 4, pp. 621-632, April 2004.

[71] W. Xu, A. B. Baggeroer, and C. D. Richmond, "Bayesian Bounds for Matched-Field Parameter Estimation," *IEEE Transactions on Signal Processing*, Vol. 52, No. 12, December 2004, pp. 3293-3305.

[72] Q. T. Zhang, "Probability of Resolution of the MUSIC Algorithm," *IEEE Transaction on Signal Processing*, Vol. 43, No. 4, pp. 978–987, April 1995.

REPORT DOCUMENTATION PAGE

Form Approved
OMB No. 0704-0188

1. REPORT DATE *(DD-MM-YYYY)*	2. REPORT TYPE	3. DATES COVERED *(From - To)*
16 May 2005	Technical Report	

4. TITLE AND SUBTITLE

Capon and Bartlett Beamforming: Threshold Effect in Direction-of-Arrival Estimation Error and On the Probability of Resolution

5a. CONTRACT NUMBER
F19628-00-C-0002

5b. GRANT NUMBER

5c. PROGRAM ELEMENT NUMBER

6. AUTHOR(S)

C. D. Richmond

5d. PROJECT NUMBER
524

5e. TASK NUMBER
2

5f. WORK UNIT NUMBER

7. PERFORMING ORGANIZATION NAME(S) AND ADDRESS(ES)

MIT Lincoln Laboratory
244 Wood Street
Lexington, MA 02420-9108

8. PERFORMING ORGANIZATION REPORT NUMBER

TR-1101

9. SPONSORING / MONITORING AGENCY NAME(S) AND ADDRESS(ES)

Defense Advanced Research Projects Agency/ATO
3701 North Fairfax Drive
Arlington, VA 22203-1714

10. SPONSOR/MONITOR'S ACRONYM(S)

11. SPONSOR/MONITOR'S REPORT NUMBER(S)
ESC-TR-2005-055

12. DISTRIBUTION / AVAILABILITY STATEMENT

Approved for public release; distribution is unlimited.

13. SUPPLEMENTARY NOTES

14. ABSTRACT

Below a specific threshold signal-to-noise ratio (SNR), the mean squared error (MSE) performance of signal direction-of-arrival (DOA) estimates derived from the Capon algorithm degrades swiftly. Prediction of this threshold SNR point is of practical significance for robust system design and analysis. The exact pairwise error probabilities for the Capon (and Bartlett) algorithm are derived herein, given by simple finite sums involving no numerical integration, include finite sample effects, and hold for an arbitrary colored data covariance. An accurate large sample approximation of these error probabilities in terms of the well tabulated complementary error function is also provided. Via an adaptation of an interval error-based method, these error probabilities, along with the local error MSE predictions of Vaidyanathan and Buckley, facilitate accurate prediction of the Capon threshold region DOA MSE performance for an arbitrary number of well separated sources, circumventing the need for numerous Monte Carlo simulations. A large sample closed form approximation for the Capon (and Bartlett) threshold SNR is provided for uniform linear arrays. A new exact two-point measure of the Capon probability of resolution, that includes the deleterious effects of signal model mismatch, is a serendipitous by-product of this analysis that predicts the SNRs required for closely spaced sources to be mutually resolvable by the Capon algorithm. Lastly, a new general strategy is provided for obtaining accurate MSE predictions that account for signal model mismatch.

15. SUBJECT TERMS

Capon	minimum variance	threshold	resolution SNR	Wishart
Capon algorithm	MVDR	threshold SNR	mismatch	complex Wishart
beamformer	Bartlett	resolution	sensitivity	DOA
adaptive	conventional	probability of resolution	finite sample	DOA estimation

16. SECURITY CLASSIFICATION OF:			17. LIMITATION OF ABSTRACT	18. NUMBER OF PAGES	19a. NAME OF RESPONSIBLE PERSON
a. REPORT	b. ABSTRACT	c. THIS PAGE			19b. TELEPHONE NUMBER *(include area code)*
Unclassified	Unclassified	Unclassified	None	88	